DOCTORAL DISSERTATION

STRUCTURAL DETAILS OF TEXTILE REINFORCED CONCRETE

September 2020

Mechanical and Civil Engineering Division
Graduate School of Engineering, Gifu University

By

BUI SI MUOI

DOCTORAL DISSERTATION

STRUCTURAL DETAILS OF TEXTILE REINFORCED CONCRETE

September 2020

Mechanical and Civil Engineering Division
Graduate School of Engineering, Gifu University

By

BUI SI MUOI

ACKNOWLEDGEMENT

In completion of this dissertation, the author wishes to express my profound gratitude and deepest appreciation to my advisor Prof. KUNIEDA Minoru for providing invaluable support, continuous enthusiasm, and kind attention.

The works accomplished in this thesis were possible because of the contributions of a large group of people, and here I would like to take the opportunity to thank all of them. Sincere thanks are also due to all master and bachelor students in Advanced Materials Structure Laboratory, Gifu University, for helping the author in preparing and conducting experiments.

The author cannot forget to thank the Vietnamese Ministry of Training and Education for providing the scholarship to pursue the degree of Doctor of Engineering at Gifu University.

My acknowledgment will never be completed without thanking my family and friends.

ABSTRACT

Conventional reinforced concrete is one of the most commonly used building materials, yet it has historically shown disadvantages in terms of durability due to aging degradation, environmental conditions, and lack of maintenance. For this reason, new materials providing higher mechanical performance, long-term durability, as well as sustainability are becoming a major driving force for innovation in the construction industry. Over the past decade, Textile Reinforced Concrete (TRC), comprising a combination of cementitious matrix and non-corrosive multi-axial textile fabrics, has emerged as a promising novel alternative offering corrosion resistance, as well as thinner and lightweight structures. Therefore, TRC is very suitable for the production of structural and nonstructural elements, such as road and pedestrian bridges, and silos as well as façades and/or sandwich panels. Furthermore, a thin layer of TRC with very high tensile strength is possible for repair or strengthening of existing concrete structures.

The practical application of this new and valuable material is, however, hindered by the lack of standardized specifications regarding structural details including lap splice lengths, stress transfer lengths. Series of experimental works were carried out to determine these structural details. The experiments series can be categorized into four main objects:

- Understanding bond behavior between textiles and mortars
- Determining the lap splice length of TRC members
- Determining the stress transfer length between textile and rebars
- Investigating the effect of mesh size on bond behavior between textiles and mortars

For each object, proper experimental tests were conducted. The textile reinforcement mesh in this study was 2D biaxial carbon fabric. To understand bond behavior, a doubled-side pull-out test with different embedment lengths was carried out. With the help of the tensile force - crack width relationships obtained from these investigations, the respective bond stress-slip relationship of the textile reinforcement could be defined.

For determining lap splice length, specimens with different lap lengths were fabricated. In this research, two types of members, including members subjected to uniaxial tensile forces and members subjected to bending moments, were examined. A comparison between the behavior of specimens with lap splice and the control specimens with continuous textile reinforcements was made to determine the adequate lap splice length. From the results and conclusions obtained from these

experiments, the lap splice length of 300 mm was verified to be sufficient for TRC members made of high strength ordinary mortar. For TR-SHCC specimens (Textile reinforced SHCC) and TRC-LS specimens made of low strength ordinary mortar, the required must be greater than 300 mm. In addition, the specimens exhibited different failure modes, including pull-out, delamination, and mixed failure, however, the rupture of yarns was not reported. It showed that the combination of the textile and examined mortars was unable to exploit the full capacity of textile.

The fundamental requirements of strength and robustness of TRC structures cannot be met unless the tensile reinforcing bars at each critical section are sufficiently anchored on both sides of the critical section. The anchorage on each side of a critical section must ensure that the bar force is fully transferred to surrounding concrete and rebars through the bond. Four-point bending tests were conducted to investigate flexural behavior and failure modes of the anchorage zone within a pure moment area. Similar conclusions were also drawn for the case of determining the stress transfer length of TRC members. The stress transfer length of 300 mm was adequate for high strength ordinary mortar but insufficient in the case of SHCC.

As mentioned above, TRC having high strength, great corrosion resistance, and durability showed a promising application on repair and strengthening the RC structures. Eighteen RC beams were fabricated and strengthened by FRP and different types of textiles. The comparison of enhancing the bending capacity of RC beams indicated the effectiveness of strengthening materials. In addition, the results revealed the effect of mesh size on the bond behavior between textile and mortar.

Keywords: Textile Reinforced Concrete (TRC), Structural Details, Bond Behavior, Lap Splice Length, Stress Transfer Length.

TABLE OF CONTENTS

LIST OF TABLES

CHAPTER 5

CHAPTER 6

LIST OF FIGURES

CHAPTER 7

CHAPTER 1

INTRODUCTION

1.1. Introduction and Problem Statement

Reinforced concrete (RC) is considered as one of the most important construction materials. However, in addition to the advantage of mechanical behavior and low-cost fabrication, a major disadvantage of the use of steel as a reinforcing material is its sensitivity to corrosion in the aging concrete. For this reason, the reinforcement corrosion, despite the partially large concrete covers, often not be permanently prevented. The result is a reduction or a loss of the load-bearing capacity of the reinforced concrete structures with a consequent reduction of the service life.

Because of this problem, new materials providing higher mechanical performance, long-term durability as well as sustainability are becoming a major driving force for innovation in the construction industry. In addition to materials like stainless steel or natural fibers, research is increasingly focusing on industrial fiber materials, such as Alkali-Resistant (AR) glass, aramid, or carbon. Such high-performance fibers are already successfully used in aircraft and automobile construction for the manufacture of extremely light, high load-bearing, and

corrosion-resistant structures. The development of new and sustainable composite materials has promoted the use of these fibers for the construction industry. The mesh-like textiles with high performance and corrosion resistant fibers made of AR glass or carbon are incorporated into concrete structures to reinforce (Figure 1.1). This procedure makes it possible to produce extremely thin, and highly load-bearing textile concrete layers, which can be used both for new individual members as well as for the repair and upgrading of existing concrete structures.

a) Casting TRC

b) Harden TRC

Figure 1.1 – TRC member

a) TRC bridges
(TU Chemnitz, Germany)

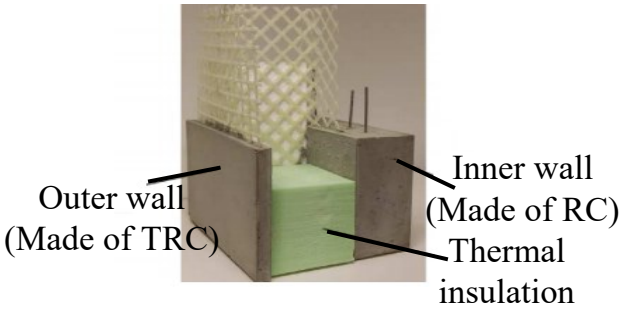

b) Sandwich wall with thin facing

c) Silo using TRC
(Naila, Germany)

d) Strengthening by TRC
(Naila, Germany)

Figure 1.2 – Applications of TRC

Over the past decade, Textile Reinforced Concrete, encompassing a combination of cementitious matrix and multi-axial carbon textile fabrics, has emerged as a promising novel alternative to traditional construction material (Brameshuber, 2006). The innovative attributes offered by TRC spans over a wide range, including favorable mechanical performance, high corrosion resistance, and longer life service [Hegger (2008)]. Therefore, TRC is very suitable for the production of structural and nonstructural elements, such as road and pedestrian bridges, and silos as well as façades and/or sandwich panels (Figure 1.2). Furthermore, a thin layer of TRC with very high tensile strength is possible for repairing or strengthening existing concrete structures [Ortlepp et al. (2009) and Ortlepp et al. (2011)].

The initial research on the development of TRC has been carried out since 1999 in two Collaborative Research Centres (CRC): CRC 532 at RWTH Aachen and CRC 528 at the Technische Universit¨ at Dresden. As part of the extensive experimental and theoretical research on the load-bearing behavior of TRC, it was possible to demonstrate that this composite material was very well suited for the manufacture and reinforcement of structural members subject to tensile, bending, shear, and torsion forces. Developed calculation models confirm the results of the experimental investigations and enable the dimensioning of the components [Jesse & Curbach (2004), Weiland et al.(2009), and Ortlepp, Schladitz & Curbach (2011)].

A significant amount of experimental investigations have characterized the tensile behavior of TRC members. They differ primarily in the shape and dimensions of specimens. Three shapes, including rectangular parallelepiped, dumbbell, and bone were identified (Figure 1.3). The rectangular parallelepiped is the most commonly used due to simple implementation. The dumbbell can overcome the effects of the differentiated shrinkage between the sides of the plate by the use of a vertical mold. However, the disadvantage is the difficulty of perfectly positioning the perforated plate [Contamine, Si Larbi & Hamelin (2011)]. The bone-shaped specimens were lesser used because of the expensive molds and particular care in implementation. The results of the tensile test showed the efficient bridge of textile fabrics on the cracks that develop under loading and carry the increasing applied loads, leading to strain-hardening behavior with multiple cracking. This typical behavior was mentioned in various investigations [Brameshuber (2006), Mesticou et al. (2017), and Kong et al. (2017)].

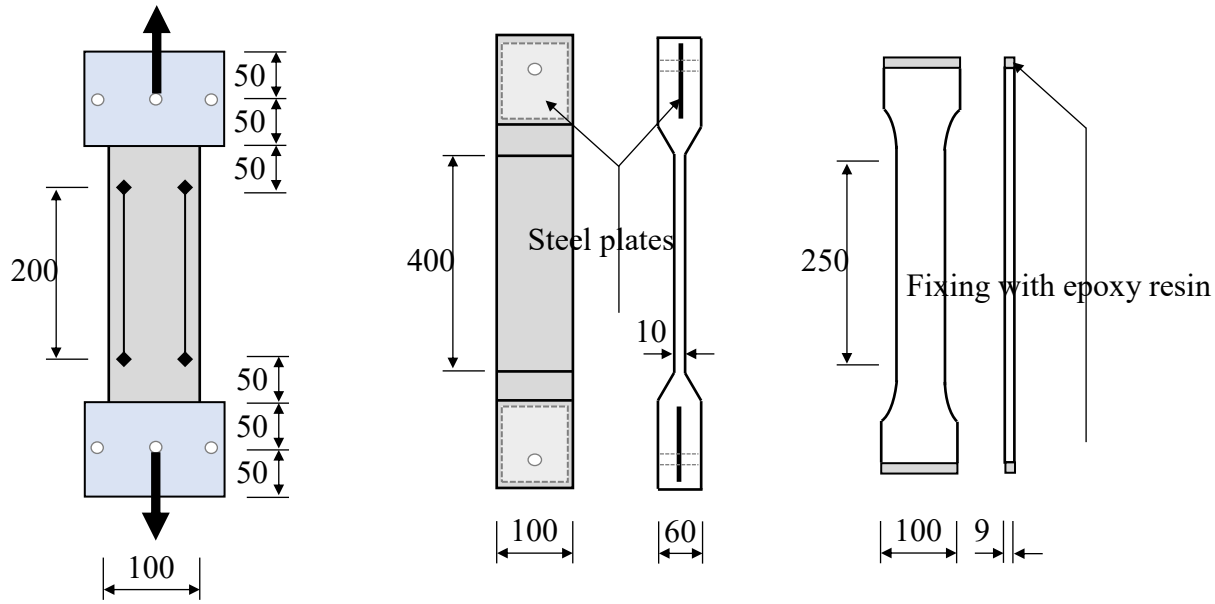

a) Rectangular parallelepiped specimen

b) Dumbell specimen

c) Boned-shape specimen

Figure 1.3 – Different shapes of specimens used for tensile test

The safe transmission of the forces between textile and mortar is required for the functionality of composite materials. Therefore, the determination of bond behavior between textile and mortar is the fundamental problem to understand the global behavior of TRC members as well as to determine structural details, including lap splice length and anchorage length. Several test setups for the examination of the bond characteristics of filament yarns embedded in a concrete matrix are already known from the literature. The two most common methods are one-sided pull-out tests [Banholzer (2006)] and a double-sided pull-out test [Lorenz & Ortlepp (2010)]. The direct results of the tests are tensile force-crack width/displacement relationship, therefore analytical solutions needed to determine a bond stress-slip relationship. Zastrau & Richter (2003) proposed a solution approach to determine the bond stress-slip relationship based upon the multilinear, segmentally closed solutions of the bond differential equation. Lorenz & Ortlepp (2010) developed the approach of Richter to establish equations of anchorage lengths and lap splice lengths.

Several experimental investigations were carried out to determine structural details, however, most of the researches was conducted with members subjected to uniaxial tensile forces. Lorenz & Ortlepp (2010) investigated comparative experimental examination of the required end anchorage lengths of textile

reinforced specimens regarding the prevention of a pull-out failure within the textile layer. The examined anchorage lengths varied between 20 and 175 mm. Two different failure mechanisms were examined. While at anchorage lengths of ≤ 125 mm and maximally anchorable yarn tensile forces smaller than the ultimate yarn tensile force, a yarn pull-out could be observed, anchorage lengths of ≥ 145 mm led to a yarn breakage on all examined specimens. Therefore, to avoid pull-out failure and exploiting the tensile bearing capacity to the fullest, the required development length can be determined at 145 mm. Ortlepp (2018) proposed an efficient adaptive test method for anchorage length in TRC. The clamping length at the upper end of the specimen was made equal to or greater than that of the glued anchorage to ensure that pullout failure. The bond length at the glued end of the specimen varied from 0 to 200 mm. It means that variable anchorage lengths were examined for each specimen. The results showed a required anchorage length of 80 mm for reference textiles. The application of an epoxy resin coating leads to the reduction of the development length. Adding sand to the epoxy resin coating reduced the development length further on. Overall, reductions of the development lengths of 50 to 60% were achieved in comparison with the unmodified reference textile because of the bond-improving measures.

To determine the overlap length of TRC members, Lorenz and Ortlepp (2011) performed tensile tests by using specimens with symmetrical and asymmetrical reinforcement arrangements. A pull-out failure occurred with overlap lengths of less than or equal 125 mm, a failure of yarn rupture was observed for overlap lengths of 150 mm. The test results also showed that the required values for development length and overlap length are equal. Donnini et al. (2019) investigated the tensile behavior of glass fabric reinforced cementitious matrix with fabrics' overlap. The test showed different failure modes depending on the configuration of fabric reinforcement. In the case of short overlap length (100 mm), the formation of longitudinal cracks led to a slippage of fabrics along with the overlay interface. For longer overlap lengths (150 and 200 mm), the breakage of the yarns was observed.

For composite materials like TRC, the required length for the full stress transmission between textile and mortar as well as between textile layers is an issue. These cannot be avoided in the practical application of textile concrete. At present, there are no comprehensive and coherent studies on detail, particularly regarding anchorage length and lap splice length of members subjected to bending moment.

1.2. Objective and Scope of Study

As described in the previous section, lack of design specifications and research on structural details of TRC becomes an issue to overcome. This dissertation aims to understand composite behavior, determine lap splice length, and stress transfer length of TRC members.

To achieve these objectives, this dissertation addressed the following relevant issues:

(1) Understanding bond behavior between textile fabric and mortar based on the pull-out test.
(2) To determine lap splice length of TRC members subjected to tensile forces
(3) To determine lap splice length of TRC members subjected to bending moment.
(4) To determine the stress transfer length between textile and rebars of members subjected to bending moment.
(5) To investigate the effect of textile configuration on composite behavior between textile and mortar.

1.3. Outline of This Research Work

The framework of the dissertation is shown in Figure 1.4. The dissertation can be divided into three main parts. The first part introduces the materials used for experiments as well as the typical tensile behavior of textile reinforced concrete. Part two is the main part of the dissertation. In particular, structural details of TRC, including bond behavior, stress transfer length, and lap splice length was considered and determined. Three types of mortar, including high and low strength normal mortal, and Strain Hardening Cementitious Composite in combination (SHCC) with textile were examined and compared (denoted as TRC, TRC-LS and TR-SHCC). Part three shows applications using textile reinforced concrete on strengthening reinforced concrete beams. Based on the effectiveness of strengthening, evaluation, and comparison of the effect of the mesh size on the composite between textile and mortar were carried out.

The organization of this dissertation from chapter 2 to chapter 7 is as follows:

Chapter 2 provides an introduction of materials that made up textile reinforced concrete, including textile fabric, two types of mortar: normal mortar and SHCC. Investigation of typical tensile behavior of TRC and TR-SHCC were also described.

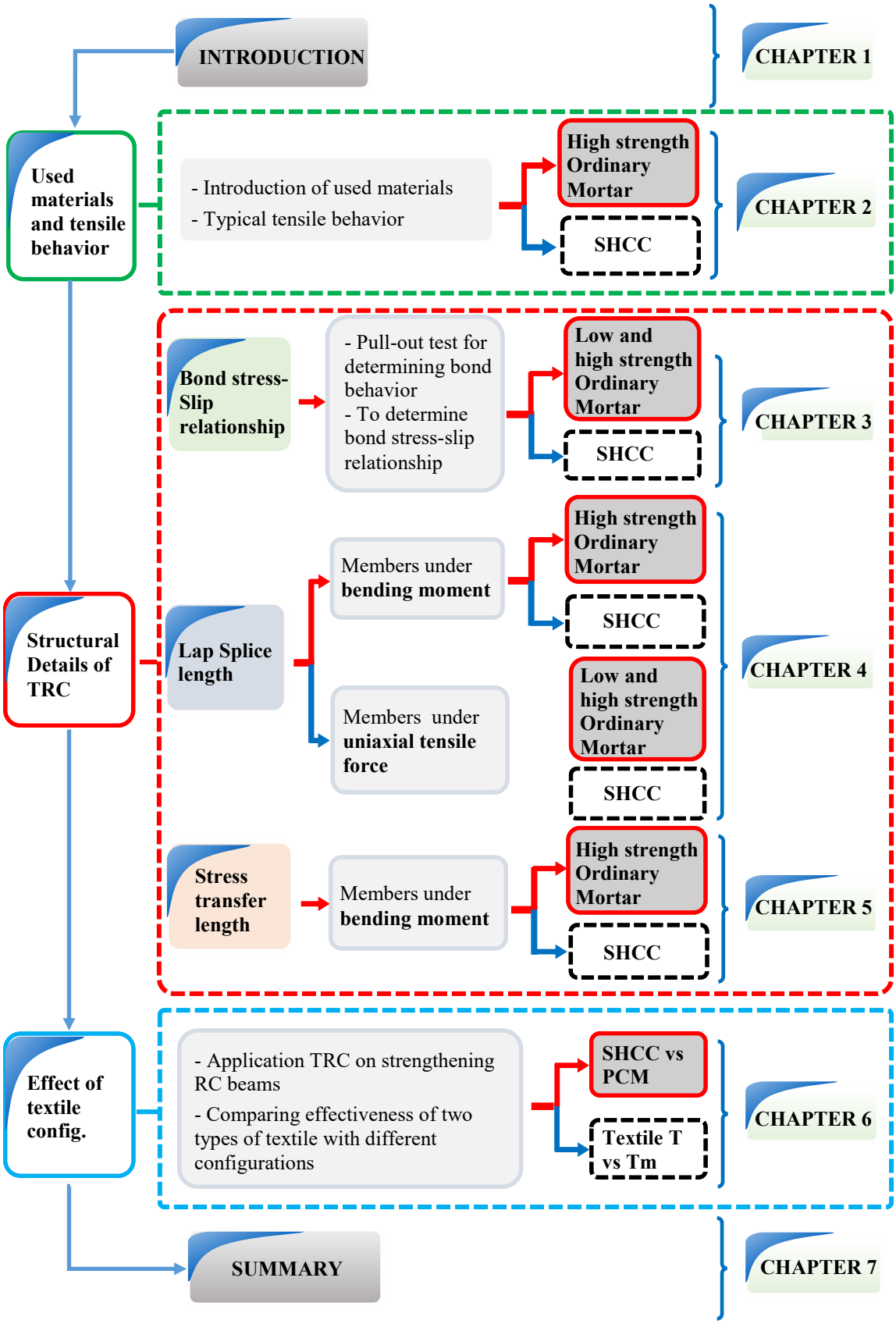

Figure 1.4 – Dissertation framework

Chapter 3 shows an investigation of bond behavior between textile fabric and mortar. The test setup of a doubled-side tensile test was described. Tests with different embedded lengths were conducted to characterize bond behavior of textile roving as well as obtain a representative trend of pull-out behavior. In addition, a bond stress-slip relationship was determined.

Chapter 4 shows a fundamental study on determining the lap splice length of TRC members. This study aims to investigate the failure behavior of TRC members with lap splice, and therefore providing knowledge for further research on determining overlap length. Two types of members were examined, including members subjected to uniaxial tensile force and members under bending moment.

In chapter 5, flexural behavior, failure modes of TRC beams with different stress transfer length was examined. Results of the test provided knowledge on determining the stress transfer length of TRC members subjected to bending moment.

Chapter 6 investigated the application of textile reinforced concrete on strengthening concrete structures. Concrete beams were strengthened by different configurations of carbon textile. For comparison, an FRP grid was also used as a reinforcement. A total of eighteen RC beams were fabricated, strengthened, and tested in four-point bending till failure. Based on the results of the test, the behavior and performance of retrofitted RC beams were revealed, including flexural capacity, bending stiffness as well as crack pattern, failure mechanisms, and failure modes. The effectiveness of beams strengthened by the textiles revealed the effect of mesh size on composite behavior between textile and mortar.

Chapter 7 provides conclusions and a summary of the results found in this study in addition to suggestions for further research needs.

CHAPTER 2

TYPICAL TENSILE RESPONSE OF TEXTILE REINFORCED CONCRETE

2.1. Introduction and Background

Textile Reinforced Concrete (TRC) exhibits strain-hardening characteristics, and therefore well suited for applications that may involve large energy absorption, high strain capacity, fatigue, and impact resistance; or for structures in seismic regions where high ductility is desired or reduction of conventional reinforcement is needed. The design and implementation of these systems require applications that go beyond the elastic response and in the strain-hardening range. This range is attributed to multiple cracking under tensile stresses and the post-crack response that exceeds the first crack stress over a wide strain range. When they used as reinforcement for concrete structures, TRCs primarily loaded under tension, even for the shear reinforcement of reinforced concrete beams [Contamine, Si Larbi, & Hamelin (2013)]. The uniaxial tension test captures the various modes of failure that take place in a TRC specimen. By using this method, one can obtain a tensile force-displacement response as well as gain insight into nonlinear modes of behavior such as distributed cracking, fiber debonding, and pullout mechanisms. Tension testing commonly conducted using a grip system to allow for the

deformation of the specimen. Thus, the uniaxial tensile test has been used in this study to understand tensile response; then towards systematic exploitation of the stress-strain response of the TRC.

2.2. Materials

2.2.1. General

TRC is a composite material made with a continuous textile fabric that is incorporated into a cementitious matrix consisting of a Portland cement binder and small-size aggregates [Brameshuber (2006, 2010); Curbach and Heeger (1998)]. A primary advantage of TRC is the continuity of the yarns providing high efficiency and reliability, which is useful for structural and semi-structural applications. This advantage is enhanced when considering the flexibility in producing textile fabrics that can be tailored for structural performance, static and impact, by optimization of the use of high-performance yarns, such as carbon, and control of their orientation. Besides, the penetration of cement paste into fabric openings and the areas between the yarns is essential in providing sufficient bonding between filaments and matrix. It is a necessary consideration for fabric reinforcements in light of the particulate nature of the cement paste, the viscosity of which is not as low as that typical of polymer materials. Thus, the design of textile fabric for cement-based composites are complicated, taking into consideration a range of parameters such as yarn orientation, yarn shape, the opening of bundle filaments, and yarn tightening effects, as well as fabric geometry and density [Curbach et al. (2006)].

2.2.2. Textile

The textile reinforcement mesh in this study was 2D biaxial fabric with an equal quantity of fiber rovings in two orthogonal directions [0°/90°] (Figure 2.2). The textile fabrics consisted of two types of carbon yarns, the longitudinal yarn (warp yarn) and the transverse yarn (weft yarn). The mesh size was 10 mm and 8.5 mm in warp and weft directions, respectively. At the intersection, knitting threads used to hold the rovings together in a stable manner. The individual rovings that make up a textile reinforcement are called yarns and consist of numerous very thin, endlessly long singular fibers, the so-called filaments. The roving is, therefore, a strand of fine filaments running in parallel. The number of filaments is typically between

1000 and 24000, and the diameter of which is only about a hundredth of a millimeter. This structure of yarns inhibits the even penetration of the fine aggregates between the filaments. The inner filaments, as a result, have less contact with the cementitious matrix, depending on the size of the fill-in zone. The fill-in zone is the depth at which adhesive load transfer can take place between the filaments and the matrix. As well, the inner region, so-called core, is defined as filaments having less contact with the matrix, but assuming that frictional load transfer between the filaments is possible (Hartig et al., 2008). To solve the problem, the yarns are impregnated with a secondary coating layer (Styrene-butadiene rubber), which has the task of distributing the tensile loads acting as evenly as possible on all filaments. It is thought that the load-carrying behavior could be enhanced through such material adjustments. Impregnation, therefore, plays a decisive role and consequently also embodies an essential part of textile concrete reinforcement. Figure 2.1 indicates the importance of impregnation on the load-bearing capacity of the textile reinforcement. The right picture shows a fully impregnated yarn, whereas the left one shows a yarn without impregnation, each with the associated stress distribution as it results in the load case. It can seem that not only the outer but also all the filaments absorb significant stresses with impregnation because the impregnation passes the loads onwards.

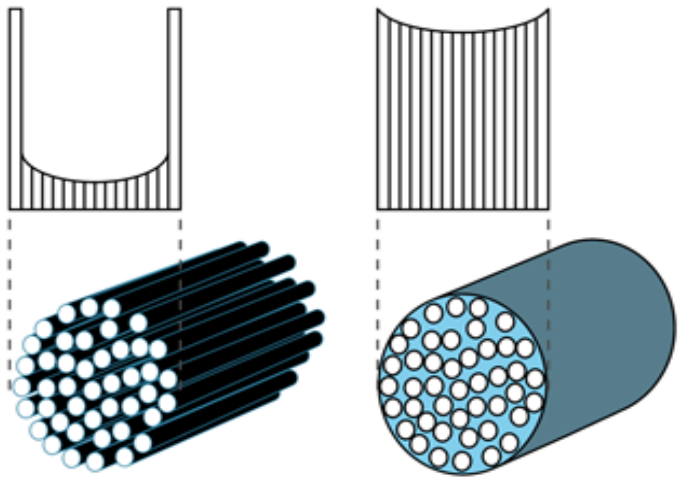

a) yarn without impregnation

b) yarn with fully impregnation

Figure 2.1 – Stress distribution within yarns

Properties of roving including the cross-sectional area of individual roving, the distance between two adjacent rovings, and mechanical properties are shown in Table 2.1.

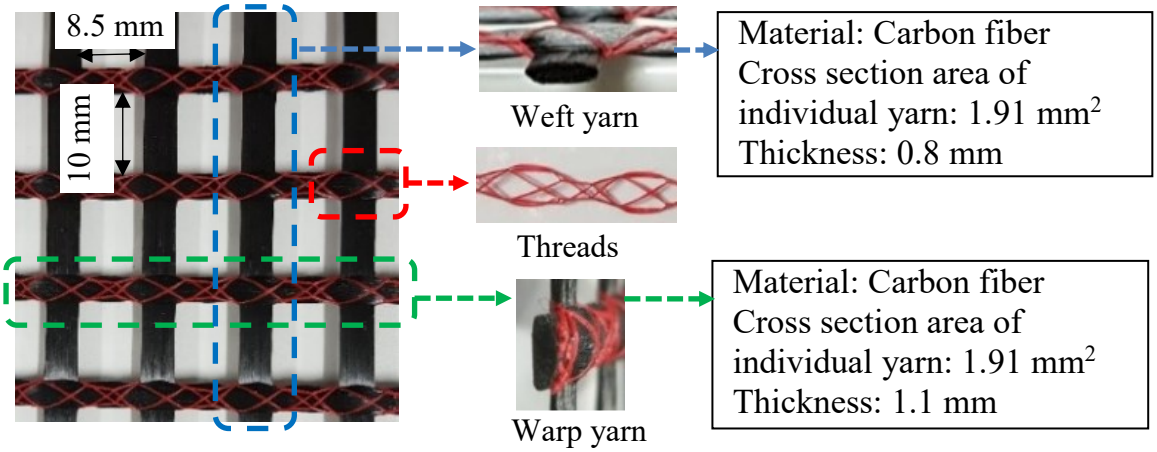

Figure 2.2 – Used textile fabric

Table 2.1 – Properties of roving

Type of yarn	Cross-sectional area (mm^2)	Rovings distance (mm)	Tensile strength (N/mm^2)	Elastic modulus (N/mm^2)
Warp/weft	1.91	12.5	1700	$140\text{-}200\times10^3$

Tensile tests for single yarns conducted to verify the mechanical properties of textile reinforcement. At first, single yarns were removed from the textile fabric. Afterward, the ends of these yarns combined with an expansion agent were put into steel tubes. The length of these tubes was 10 cm to ensure sufficient anchoring to prevent slipping of the yarns. Steel tubes were mounted on a hydraulic actuator and clamped by wedge grip shown in Figure 2.3. Two Displacement Transducers (DT) were used to measure global displacement. Two other strain gauges were attached in the middle of yarn to record strain. Figure 2.4 illustrated the average stress-strain relationship obtained from the tests. The comparison of experimentally determined tensile strength with the corresponding information provided by the manufacturer showed good agreement.

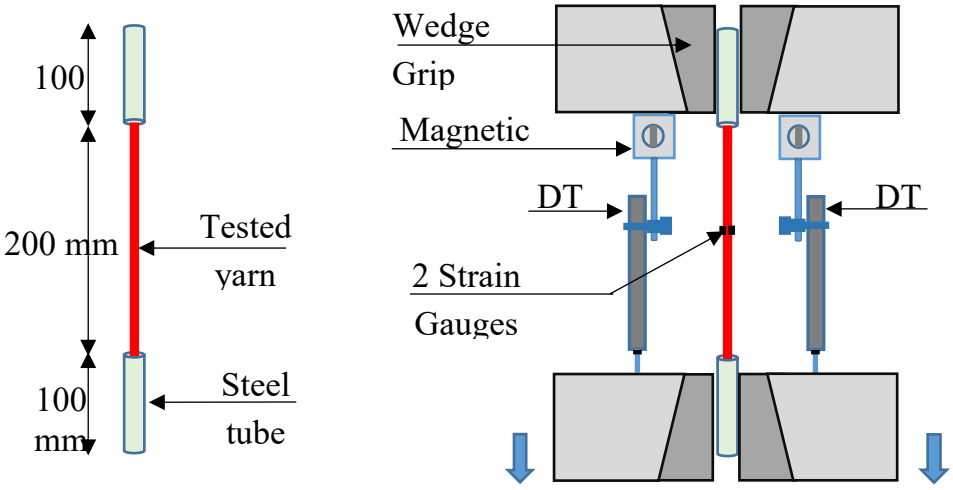

Figure 2.3 – Test setup of tensile test to determine mechanical properties of single yarn

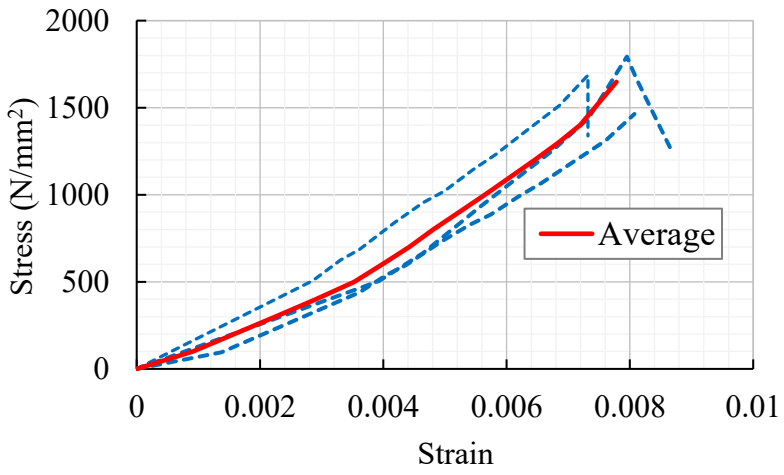

Figure 2.4 – Stress-strain relationship of single yarn

2.2.3. High Strength Ordinary Mortar

The cementitious matrix in TRC differs from that typically used in conventional steel-reinforced concrete. The mortar used for TRC must meet specialized demands regarding production processes, mechanical properties of binders, and durability of the textile reinforcements. Typically, to ensure the sufficient penetration of mortar into the textile, the mortar must have highly flowable fresh property. This particular property is achieved by using small aggregates, high binder contents, adding pozzolanic additives, and superplasticizer. Besides, the W/B ratio is 0.25. It leads to a more homogeneous and finer structure compared to ordinary concrete. The examined specimens were fabricated of mortar according to the mix proportions

described in Table 2.2. The physical and mechanical properties of mortar are compiled in Table 2.3.

Figure 2.5 – Flow test to determine flow diameter of mortar

Table 2.2 – Composition of high strength ordinary mortar

Composition	Mass rate (-)	Quantity (kg/m^3)
High early strength cement	3.00	518
Fly ash	1.00	173
Sand	8.00	1380
Water	1.00	173
Super plasticizer	0.04	7

Table 2.3 – Physical and mechanical properties of the mortar

Characteristics	Value
Density (kg/m^3)	2335
Compressive strength (N/mm^2)	75.3
Tensile strength (N/mm^2)	7.8
Elastic modulus (N/mm^2)	36500

2.2.4. Low Strength Ordinary Mortar

In addition to high strength ordinary mortar, another ordinary mortar with lower strength was also examined (named low strength ordinary mortar). This mortar consists of sand (S), cement (C), and water (W). The W/C and C/S ratios of the mortar are 0.5 and 2.0 respectively. Table 2.5 described the mechanical properties of low strength ordinary mortar.

Table 2.4 – Mechanical properties of low strength ordinary mortar

Characteristics	Value
Compressive strength (N/mm^2)	36.5
Tensile strength (N/mm^2)	3.6

2.2.5. Strain Hardening Cementitious Composite (SHCC)

The high-performance mortar used in this study was Strain Hardening Cementitious Composites (SHCC). Pre-mixed mortars were prepared at the factory, then mixing with water on site. W/C ratio was 0.4, and a superplasticizer was added to maintain the proper workability. The fibers used in the mix were high modulus polyvinyl alcohol (PVA) fibers, with a length of 8 mm and a diameter of 0.04 mm. The volume fraction of fiber was 1.7%. Standard tests, including tensile tests (Figure 2.6) and compression tests, were conducted to determine the mechanical properties of SHCC. The mechanical characteristics of the SHCC are compiled in Table 2.4.

Figure 2.6 – Test setup and crack pattern of SHCC specimen

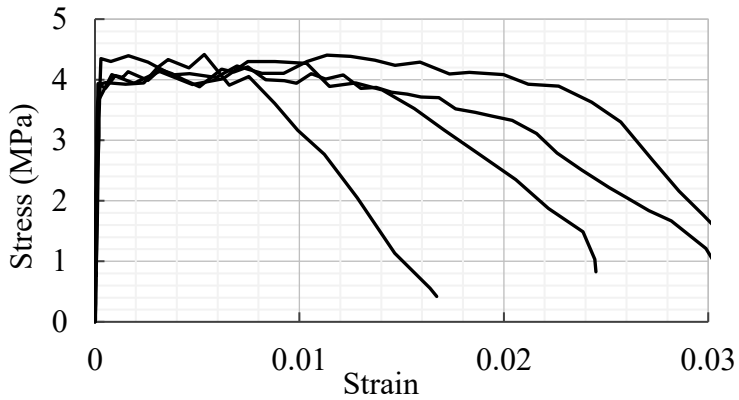

Figure 2.7 – Stress-strain relationship of SHCC

Table 2.5 – Mechanical properties of SHCC

Characteristics	Value
Compressive strength (N/mm^2)	40.5
Tensile strength (N/mm^2)	4.2

2.3. Preparations of Specimens and Test Setup

The specimens were produced in lamination manner within formworks, resulting in large-format textile-reinforced concrete slabs with a dimension of 1000×1000×15mm (Figure 2.8). The textile layer and mortar layers were placed in the formwork alternately with a mortar layer in its bottom and top. At first, a layer of mortar of 7 mm was cast into the formwork. Then, the textile fabric placed on the top of the mortar. To fix the position of textile fabric and ensure the cover thickness, spacers with a depth of 7 mm were used. Afterward, the remaining mortar layer with a thickness of 8 mm cast into the formwork. All specimens were cured in a temperature room for 14 days. After the curing period, the slabs were cut into small rectangular pieces with proper dimensions (Figure 2.9a). For the convenience, TRC, TR-SHCC, and TRC-LS referred to the combination of the textile with high strength ordinary mortar, SHCC, and low strength ordinary mortar, respectively.

Specimens were clamped by wedge grips. The load was transferred from the testing machine to the mortar through the compressive stress normal to steel plates which were directly bonded to the mortar surface. With such configuration, the load applied to mortar more evenly, therefore an excess of compressive strength of the specimens can be avoided. Tests were conducted under displacement control by using a hydraulic actuator with a load-bearing capacity of 50 kN. Two Displacement Transducers (DT) were employed on both specimen surfaces to measure displacements.

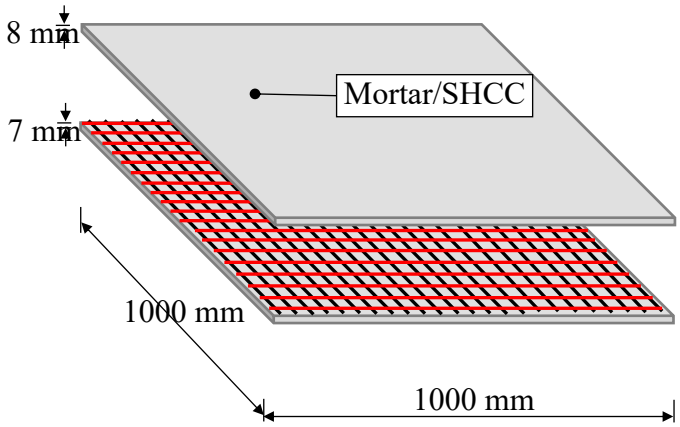

Figure 2.8 – TRC slab used for the tests

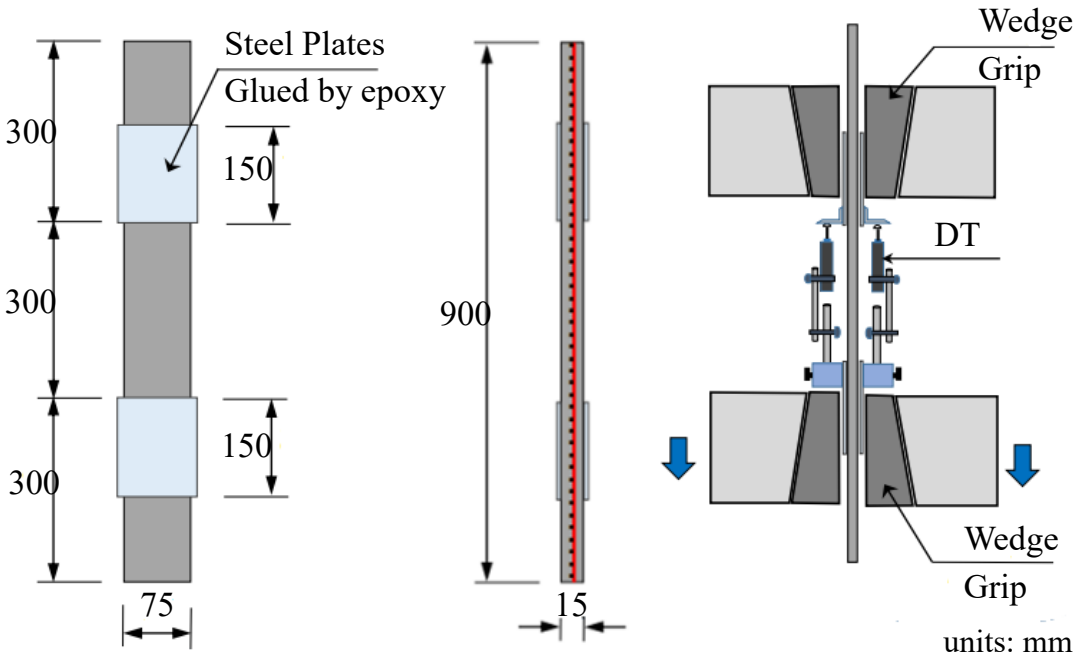

a) Specimen configuration b) Test setup

Figure 2.9 – Specimen configuration and test setup

2.4. Results and Discussion

2.4.1. High Strength Ordinary Mortar Case

Figure 2.10 demonstrates the tensile force-displacement relationship. There are four states for TRC: State I (uncracked concrete), State IIA (crack formation), State IIB (crack stabilization), and State III (failure state). State I corresponds to the

elastic state of the uncracked TRC member, where the stiffness is entirely a function of the concrete matrix. First cracking takes place once the tensile strength of concrete is reached, which following initiates the tensile stresses in the textile reinforcement within the cracked region. Multiple crack formation follows with a minimal increase in load, defined as State IIA. The crack formation eventually stabilizes in State IIB. Lastly, the failure of TRC occurs when the delamination between textile and mortar occurred and expanded (see Figure 2.11). The tensile stress of the yarns at the point of failure load could be determined by dividing failure load by numbers of yarn and cross-section area of individual yarn. The average tensile stress of the yarns was 1550 N/mm2, came close to reaching their tensile strength (1700 N/mm2). It indicates a good and promising combination between examined mortar and the textile.

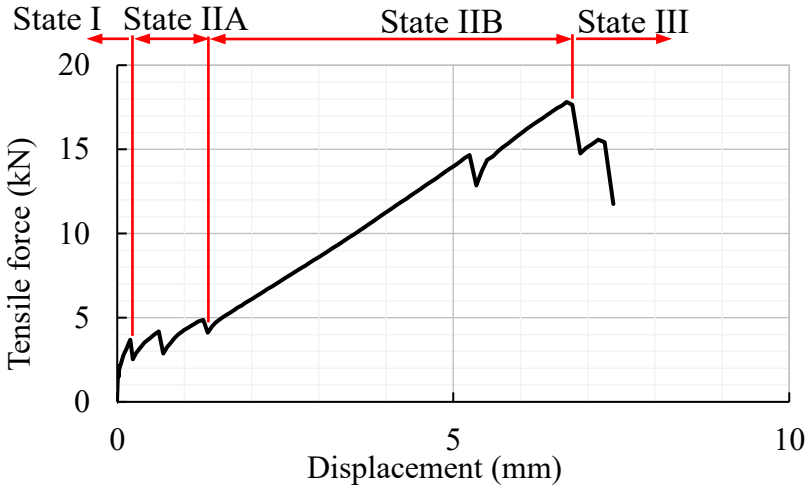

Figure 2.10 – Typical tensile force-displacement relationship of TRC specimens made of high strength ordinary mortar

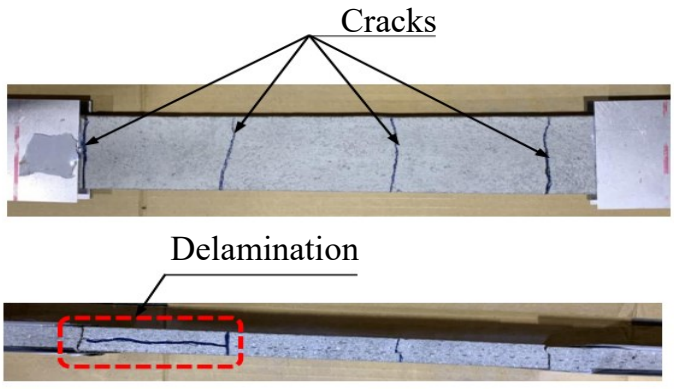

Figure 2.11 – Crack pattern of TRC member

2.4.2. Low Strength Ordinary Mortar Case

As shown in Figures 2.12 and 2.13, the pre-peak regime of specimens made of low and high strength ordinary mortar is quite similar. After initial matrix cracking, increases in the tensile load result in the formation of new cracks, and their spacing is dependent on the stress transfer between textile and matrix as quantified by the pull-out behavior and bond strength. The multiple-cracking stage terminates when all the additional loading is carried by the reinforcement and no further cracks occur in the matrix. Based on crack patterns, it can see that the high strength ordinary mortar exhibits better bond strength and stress transfer than low strength ordinary mortar as combined with the textile. Besides, the average peak load in the case of low strength ordinary mortar is 9.2 kN, much lower than the load-bearing capacity of high strength ordinary mortar cases. In terms of failure mode, specimens made of low strength ordinary mortar failed by debonding between textile and matrix, whereas delamination occurred in the case of specimens made of high strength ordinary mortar.

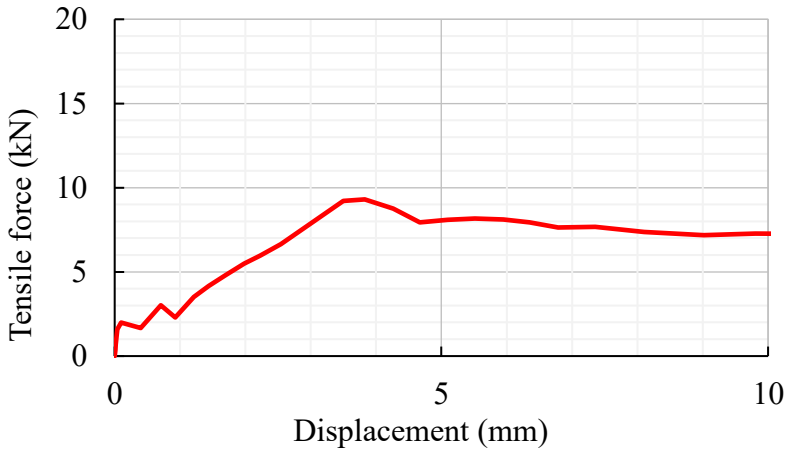

Figure 2.12 – Typical tensile force-displacement relationship of TRC-LS specimens made of low strength ordinary mortar

Figure 2.13 – Crack pattern of TRC-LS specimens made of low strength ordinary mortar

2.4.3. Tensile Behavior of TR-SHCC Specimens

Figure 2.14 illustrated the typical tensile force-displacement relationship of TR-SHCC specimens. Generally, this relationship could be divided into four states, which was similar to the behavior of TRC and TRC-LS specimens. However, there were minor differences in the number of cracks and crack width of TR-SHCC specimens. As illustrated in Figure 2.15, a great number of cracks, particularly fine cracks, were observed in state IIA. The difference may come from the strain hardening behavior, in particular the crack bridging characteristics of SHCC. Besides, the peak load of the TR-SHCC specimen was 13.1 kN that was much lower than that of the high strength ordinary mortar case. The reason may be the weak bonding between textile and SHCC, which led to the low composite of TR-SHCC specimens (see section 3.3.2). However, in the post-peak stage, TR-SHCC specimens were able to sustain the high level of loading as deformation increased, indicating that TR-SHCC exhibited better behavior of ductility and robustness in comparison with specimens made of high strength ordinary mortar. Compared with TRC-LS specimens, TR-SHCC specimens provide a quite higher load-bearing capacity. The reason for this might be the influence of weak bond strength between the textile and low strength ordinary mortar, which leads to a premature bonding failure in TRC-LS specimens.

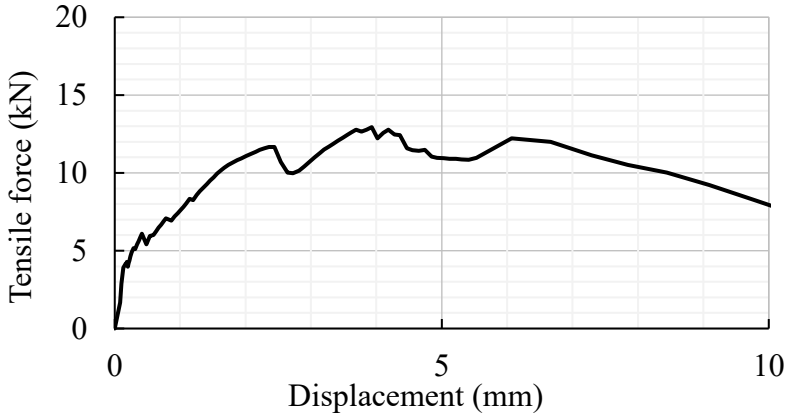

Figure 2.14 – Typical tensile force-displacement relationship of TR-SHCC specimens

Figure 2.15 – Crack pattern of TR-SHCC specimens

2.5. Summary

In this chapter, a brief introduction of the components of textile reinforced concrete was shown. Textile could be used to reinforce high strength ordinary mortar (denoted as TRC), SHCC (denoted as TR-SHCC), and low strength ordinary mortar (referred to as TRC-LS). An investigation of the typical tensile behavior of the combination between the textile and examined matrix was also carried out. The strain hardening behavior of textile reinforced concrete, including four distinct states, was clarified. Besides, the results showed that TRC specimens exhibited the highest peak load, whereas the load-bearing capacity of TRC-LS is the smallest. In the case of SHCC, TR-SHCC displayed better ductility and a higher level of loading in the post-peak stage. In the next chapters, the structural details of TRC and TR-SHCC would be investigated and determined.

CHAPTER 3

BOND BEHAVIOR BETWEEN TEXTILE AND CEMENT COMPOSITES

3.1. Introduction and Background

In fiber composite materials, such as TRC, bond behavior between the textile yarns and the cementitious matrix is a principal factor influencing the global structural behavior [Zastrau et al. (2008)]. For that reason, the determination of bond behavior is essential for accordingly understanding the behavior of TRC and providing input data for numerical models. The so-called pull-out test was a widely accepted experimental technique to determine the bond behavior between textile reinforcement and the surrounding mortar. Depending on the failure mechanism and the sample geometry, the experimental setups described in the literature simplified into one-sided and two-sided pull-out tests.

For one-sided pull-out tests, as shown in Figure 3.1, proposed by Banholzer (2006) as well as by Peled & Bentur (2006), the investigated yarns were embedded on one side in the concrete matrix. At the opposite end, the anchorage was done using appropriate mechanical clamping devices or by pouring the multifilament yarn into an epoxy resin block. A disadvantage of this method was the capillary

phenomenon, which may induce the penetration of epoxy resin into the interior of embedded length and led to an adverse effect on the result of the test.

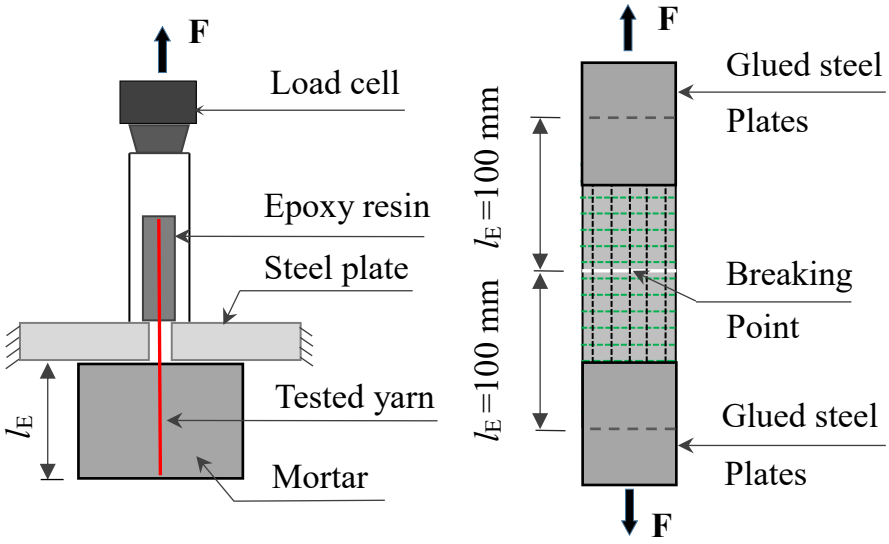

a) Test setup by Banholzer b) Test setup by Butler

Figure 3.1 – Setups of pull-out test proposed by Banholzer (2006) and Butler (2010)

In contrast, in two-sided pull-out tests by Butler (2010), Kang & Brameshuber (2006), and Krüger (2004), the tested yarns were fully embedded into the surrounding fine concrete, and the force was transmitted to the yarn through the bond with the matrix. During the pull-out test, the tensile force F and the associated crack opening w were measured in the area of predetermined breaking point. For symmetrical two-sided pull-out tests (Figure 3.1b) described by Butler (2010), the anchorage lengths of both sides of specimen got the same value of 100 mm, which led to a simply assuming that the slip of yarns at one side equaled half of crack opening w at predetermined breaking point. Whereas, numerous investigations showed that the sufficient embedded length should be smaller than 100 mm. Generally, when the end anchorage length is higher than 100 mm, the fracture failure of tested yarn occurs rather than pull-out failure, particularly for the yarns impregnated by coating materials. By contrast, the two-sided test mentioned by Krüger (2006) had asymmetrical anchorage lengths, see Figure 3.2a. On one side of the specimen, the selection of a short end anchoring length l_E of 20 mm ensured the pull-out failure of investigated yarn. On the opposite side, the anchoring of the tested yarn in the fine concrete matrix could be ensured by a final anchoring length

of 140 mm. As a result of the complete embedding in the surrounding fine concrete, a direct introduction of force into the multifilament yarn was possible via the bond with the matrix. However, the drawback of the test was the clamping devices, which induced directly lateral pressure onto the surrounding mortar of examined yarn..

For systematic and reliable testing of randomly configured textile reinforcement structure as well as for an improved and correct evaluation of the pull-out test, further development of the experimental setup is necessary. Based on the research by Krüger (2004), Lorenz and Ortlepp (2012) developed a new technique to gain an understanding of bond behavior between textile reinforcement and mortar. For eliminating the effect of clamping devices, saw cuts were created to separate the testing area from clamping areas. Therefore, the anchorage lengths limited by the distance between breaking point and saw cut. Accordingly, in the literature, numerous researches proved the accuracy and validity of this configuration.

The setup of the pull-out test in this publication referred to the principle approaches of the research proposed by Lorenz and Ortlepp (2012). This study aimed at evaluating the bond behavior of the textile reinforcement and cement matrix in TRC. Tests with different embedded lengths were conducted to characterize failure modes of textile roving as well as obtain a representative trend of pull-out behavior.

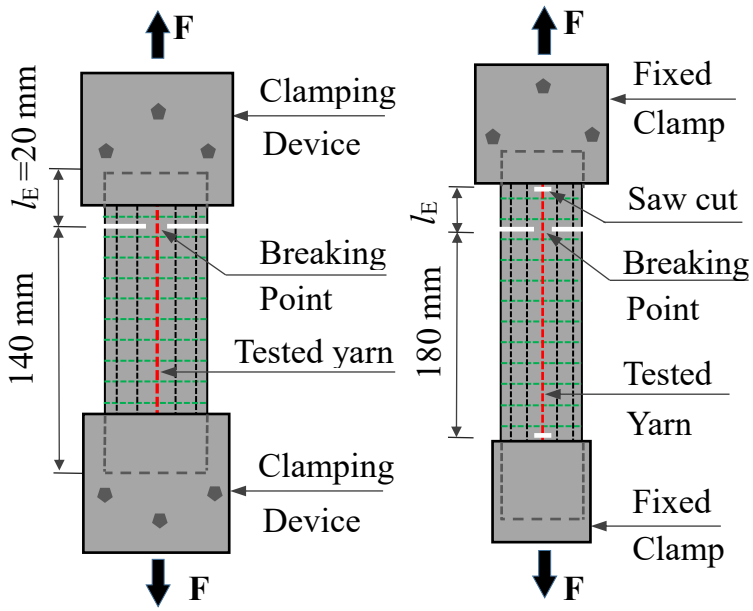

a) Test setup by Krüger b) Test setup by Lorenz

Figure 3.2 – Setups of pull-out test proposed by Krüger (2004), and Lorenz (2012)

3.2. Test Program

3.2.1. Materials

The properties of textile reinforcement, as well as the composition of ordinary mortar and SHCC, were mentioned in section 2.2. Tables 3.1, 3.2, and 3.3 described the mechanical properties of high strength ordinary mortar, SHCC, and low strength ordinary mortar, respectively.

Table 3.1 – Mechanical properties of high strength ordinary mortar

Characteristics	Value
Compressive strength (N/mm^2)	75.3
Tensile strength (N/mm^2)	7.8
Elastic modulus (N/mm^2)	36500

Table 3.2 – Mechanical properties of SHCC

Characteristics	Value
Compressive strength (N/mm^2)	40.5
Tensile strength (N/mm^2)	4.2

Table 3.3 – Mechanical properties of low strength ordinary mortar

Characteristics	Value
Compressive strength (N/mm^2)	36.5
Tensile strength (N/mm^2)	3.6

3.2.2. Specimen Preparation

The TRC specimens were produced by a hand lamination process in steel formworks resulting in large-format textile-reinforced concrete slabs with a dimension of 1000x1000x15 mm. The slabs contained only one layer of textile reinforcement. The textile layer and mortar layers were placed in the formwork alternately with a mortar layer in its bottom and top. The reinforcement layers were arranged symmetrically to the thickness and set parallel to the slab surface. After the curing period, the slabs were cut into small rectangular specimens with proper dimensions. With this configuration, all investigated specimens in the test came from the same batch of mortar. As a result, the comparability of the individual tests

and reducing the scattering of the quality of concrete and composite properties could be ensured.

During the pull-out test, only one individual yarn (warp yarn) of the specimens was tested. Each specimen might be divided into three parts: the upper part and the lowest part used for clamping, whereas the middle one was the tested area where the pull-out failure of yarn carried out (see Figure 3.3). These parts of the specimen were separated by two holes with a diameter of 10 mm. At the position of the holes, the tested yarn also was cut, which ensure the pressure from clamp devices not affect the result of the test. In the tested area, there were two different types of the embedded length of warp yarn: the short and long anchorage length that was split up by the saw cuts on both sides of the specimen. These saw cuts with a width of 24 mm were created and controlled by wet saw cutter. They not only played the role of isolating tested yarn but also created the pre-determined breaking point of the specimen. The short anchorage length l_{E1} limited by the upper hole and the pre-determined breaking point. Besides, the length l_{E1} should not be smaller than 14 mm to ensure the safe handling of the specimen. If the distance of the adjacent transverse yarn is less than 14 mm, l_{E1} should be chosen as a multiple of this distance [Lorenz (2012)]. In this research, four different values of embedment length were chosen, the detail of the dimension of each type shown in Table 3.4. In contrast, the long anchorage length, l_{E2}, was defined by saw cuts and the second hole. This length must be sufficiently long to prevent the slippage at the free unloaded endpoint.

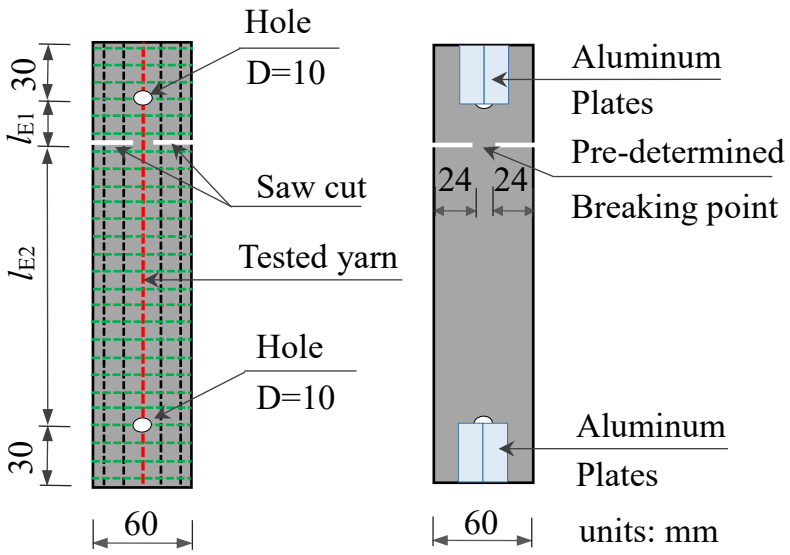

Figure 3.3 – Sketch of specimen used for pull-out test

Table 3.4 – Dimension of specimens

Series	l_{E1} (mm)	l_{E2} (mm)	Width (mm)	Length (mm)
Series 1	25	220	60	310
Series 2	50	220	60	330
Series 3	100	340	60	500
Series 4	200	740	60	1000

3.2.3. Test Setup

The test setup is shown in Figure 3.4. Before testing, aluminum plates were attached to both sides of the ends of the specimens by glue. These plates prevented the damage of concrete under the consequence of the direct lateral pressure of grips. The tensile load was applied via clamping devices on the upper and lower ends of the specimen. The type of used clamping device was a flat chuck tensile grip that had a flexible connection to the testing machine. The contact pressure was set in such a way that the slippage between clamp and specimen prevented, and the compressive strength of mortar was not exceeded. On top of the upper grip, a load cell with proper capacity was placed in order to measure the value of tensile force. The total deformation of the specimen measured by using two Displacement transducers (DT) placed on either side of the specimen. At the position of pre-determined breaking point, two Clip-on Displacement Transducers (CoDT) were arranged to determine crack-opening displacement.

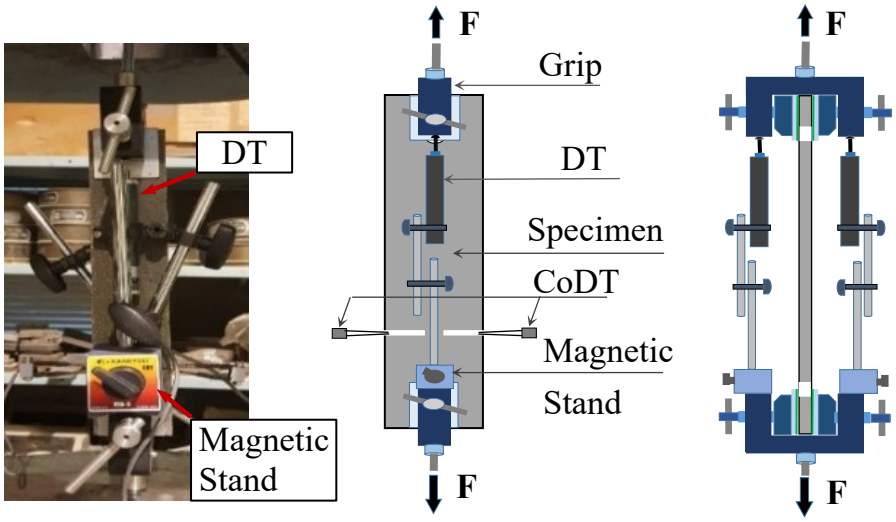

Figure 3.4 – Setup of pull-out test

3.3. Results and Discussion

3.3.1. Bond Behavior between Textile and High Strength Ordinary Mortar

The result of the pull-out test was a force–crack opening and force – total displacement relationship, which shown in Figures 3.5 and 3.6, respectively. The increase of the pull-out force combined with larger displacement was observed when the embedded length increased. Besides, the dominant failure mode was pull-out of multifilament yarns in surrounding mortar (Figure 3.9) when 19 out of a total of 20 specimens occurred in this failure mode.

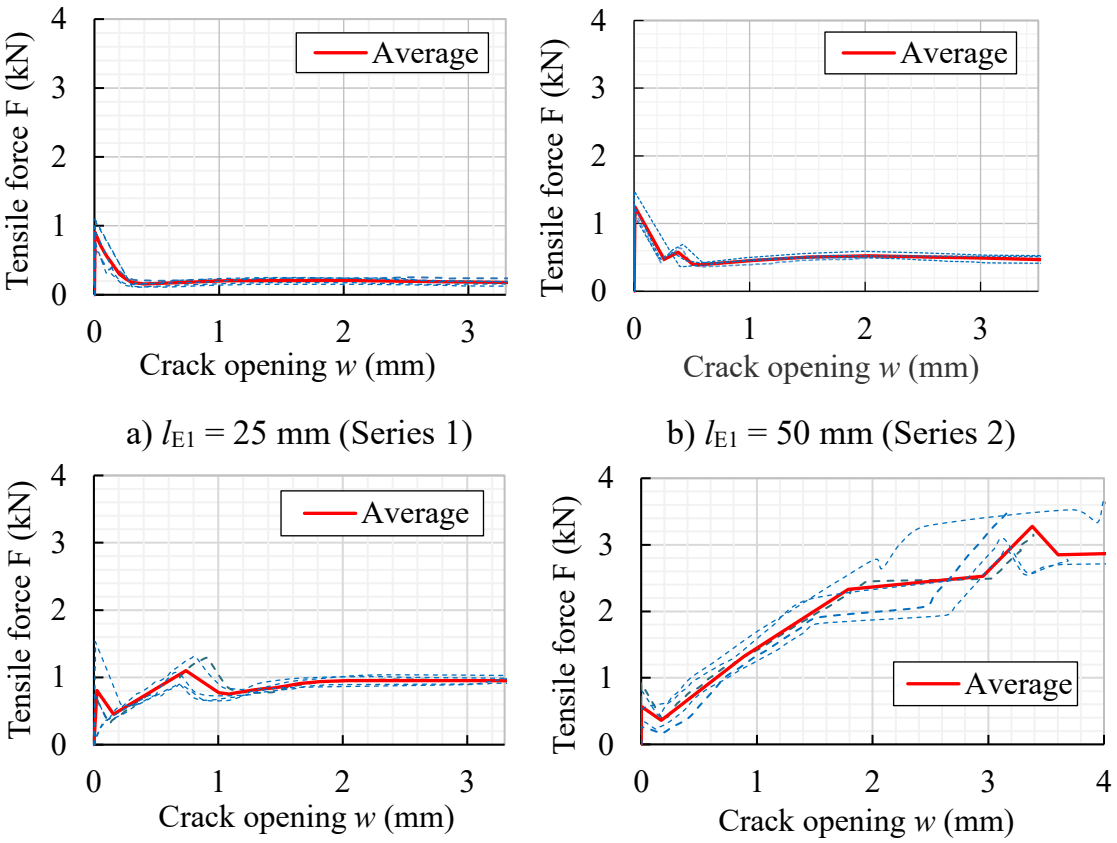

a) l_{E1} = 25 mm (Series 1) b) l_{E1} = 50 mm (Series 2)

c) l_{E1} = 100 mm (Series 3) d) l_{E1} = 200 mm (Series 4)

Figure 3.5 – Tensile force-crack opening relationship

Table 3.5 showed the dispersion of maximum loads and correlative crack opening that obtained from the pull-out test of four series. The range of scattering was not too wide. The standard deviations (SD.) were only about 10-23% of mean value, demonstrating the reasonableness and suitability of the test method.

Table 3.5 – Standard deviation of maximum pull-out load and corresponding displacement

Series	Series 1	Series 2	Series 3	Series 4
Average peak force corresponds to bond strength (N)	160	537	1103	3277
SD. of peak force (N)	38	148	201.6	281.4
Avg. of crack opening (mm)	0.368	0.452	0.740	3.378
SD. of crack opening (mm)	0.029	0.087	0.102	0.274

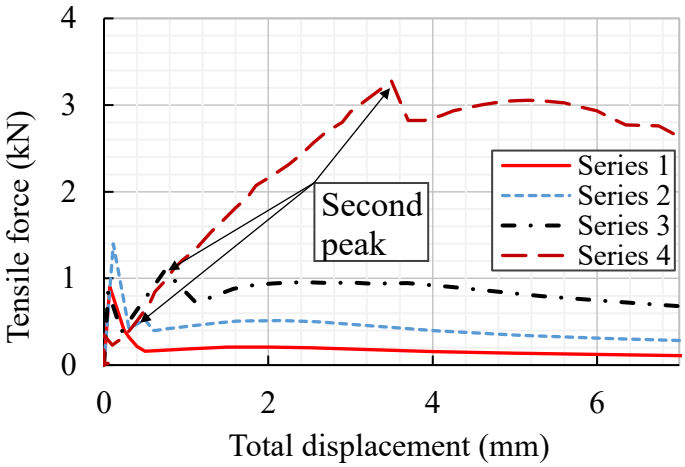

Figure 3.6 – Average tensile force-total displacement

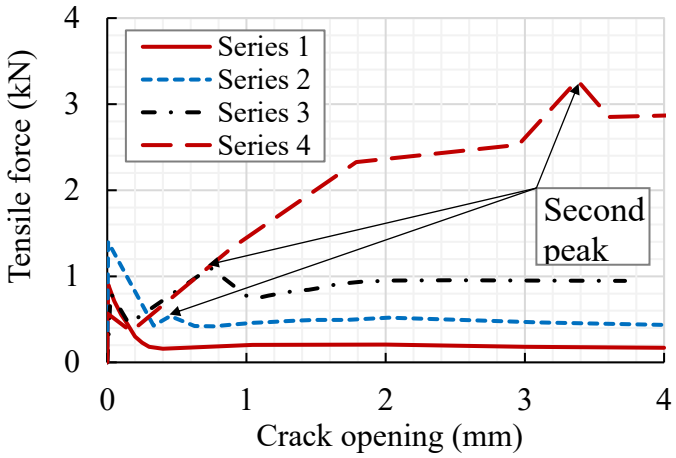

Figure 3.7 – Average tensile force-crack width

As shown in Figures 3.6 and 3.7, the characteristic of bond behavior in four series was slightly different. For the specimens with embedded length greater than 25 mm (Series 2, 3, and 4), the force-crack opening curve showed a double peak. The first peak might be attributed to the crack of mortar at the pre-determined

breaking point. As the matrix lost the load-bearing capacity, the adhesive bond between reinforcement and matrix was activated, which was depicted by an ascending branch of the curve. The inclination of this branch correlates closely to the stiffness of the bond layer. After reaching the bond strength, the destruction of the adhesive bond occurred due to the debonding of the yarn from the matrix. As a result, the force transmission fell dramatically. Simultaneously, there was a significant increase in the relative displacement between textile reinforcement and mortar. Lastly, the remaining pull-out force was based on friction, which was identified by a considerable plateau. When the relative displacement increased, the frictional force reduced regularly due to the decrease of embedded length. Besides, it was shown that the average value of friction bonding approximately equals bond strength. This feature might be one of the reasons suggesting the explanation for the characteristic of Series 1, which had a unique peak. As for a short embedment length of 25 mm, due to the insignificant effect of the mechanical adhesion, bond strength identified by friction, and there was not the existence of the second peak, which represented the effect of the adhesive bond (see Figure 3.5a).

For long embedment length (200 mm), as the result of the increasing tensile force, the load was gradually transferred from reinforcing yarn to the matrix. There was a buildup of stress in the matrix until the tensile strength of the matrix was exceeded. Therefore, in some specimens, additional cracks were formed (Figure 3.5d). In particular, the 5th specimen of Series 4 occurred fracture of tested yarn at a load of 3450 N and a crack width of 3.2 mm. It might provide a useful suggestion on determining the anchorage length of textile reinforcement in subsequent experiments.

The significant difference between the crack opening and total displacement, measured by CoDT and DT, respectively, might be observed in Series 1 and 2 (see Figure 3.8). Before the crack of mortar occurred, with the same tensile force level, the total displacement of the specimen was always higher than the value of crack opening. This deviation was due to the elastic elongation of the specimen under the impact of the tensile force. This deviation tended to steadily decrease together with the increase of crack opening and the transmission of tensile forces to roving. In the activated state of the adhesive bond and friction bond, both CoDT and DT gave the approximately equal value.

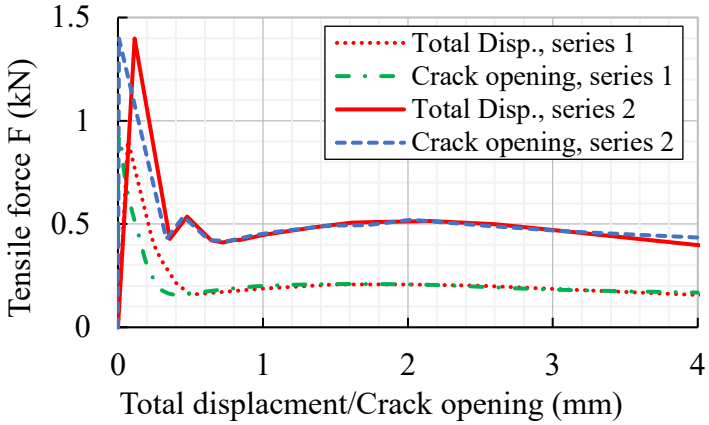

Figure 3.8 – Correlation between total displacement and crack opening of Series 1 and Series 2

In order to evaluate the influence of embedment length on bond strength, the results of the textile pull-out tests were described as bond flow – crack opening relationships. The bond flow T in N/mm was calculated by relating the pull-out force F to the anchorage length l_{E1} of yarn (equation (3.1)) [Schütze et al. (2015)].

$$T=F_G/l_{E1} \quad (3.1)$$

where,

T : bond flow (N/mm)

l_{E1} : embedded length of tested yarn (mm)

$F_G = F - F_W$

F : pull-out force obtained from test (N)

F_W : dead weight of the test setup's upper section

The values of T corresponding to pull-out resistance of series from 1 to 4 were 6.2, 10.6, 10.9, and 16.3 N/mm respectively. Obviously, T varied in a wide range, and T increased along with the rise of embedded length. The reason for the variability in the results was presumed to be the uneven and irregular geometry of multifilament yarn that induced potential mechanical bonding along anchorage length [Portal et al. (2014)].

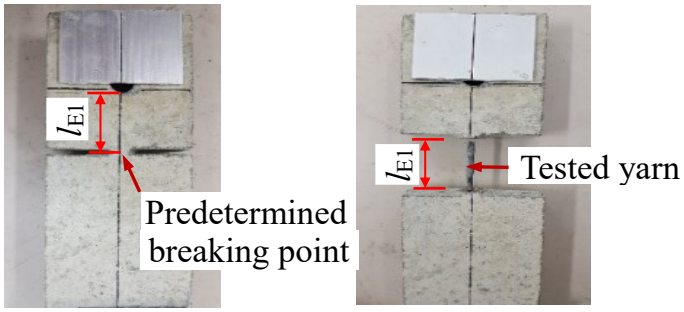

Figure 3.9 – Pull-out failure of warp yarn

3.3.2. Bond Behavior between Textile and Low Strength Ordinary Mortar

Figure 3.10 shows the tensile force-crack width relationship between the low strength ordinary mortar and textile of four different embedment lengths, including 25, 50, 100, and 200 mm. For Series 1 and Series 2, it can see that the peak loads are almost equal, and pull-out failure occurred simultaneously with the formation of the crack, which leads to the inability to determine the bond strengths. Besides, in the post-crack stage, the frictional forces of Series 1 and Series 2 are 0.1 and 0.2 MPa, respectively. The frictional forces increased linearly when then the embedment length increase from 25 mm to 50 mm. For Series 3 and Series 4, it is possible to determine the peak loads corresponding to the bond strength between textile and mortar. However, as shown in Figure 3.11 c and d, the peak loads are not much higher than the associated frictional forces. It suggests that the bond strength mainly based on friction between textile and mortar, whereas the contribution of mechanical and chemical adhesion is insignificant.

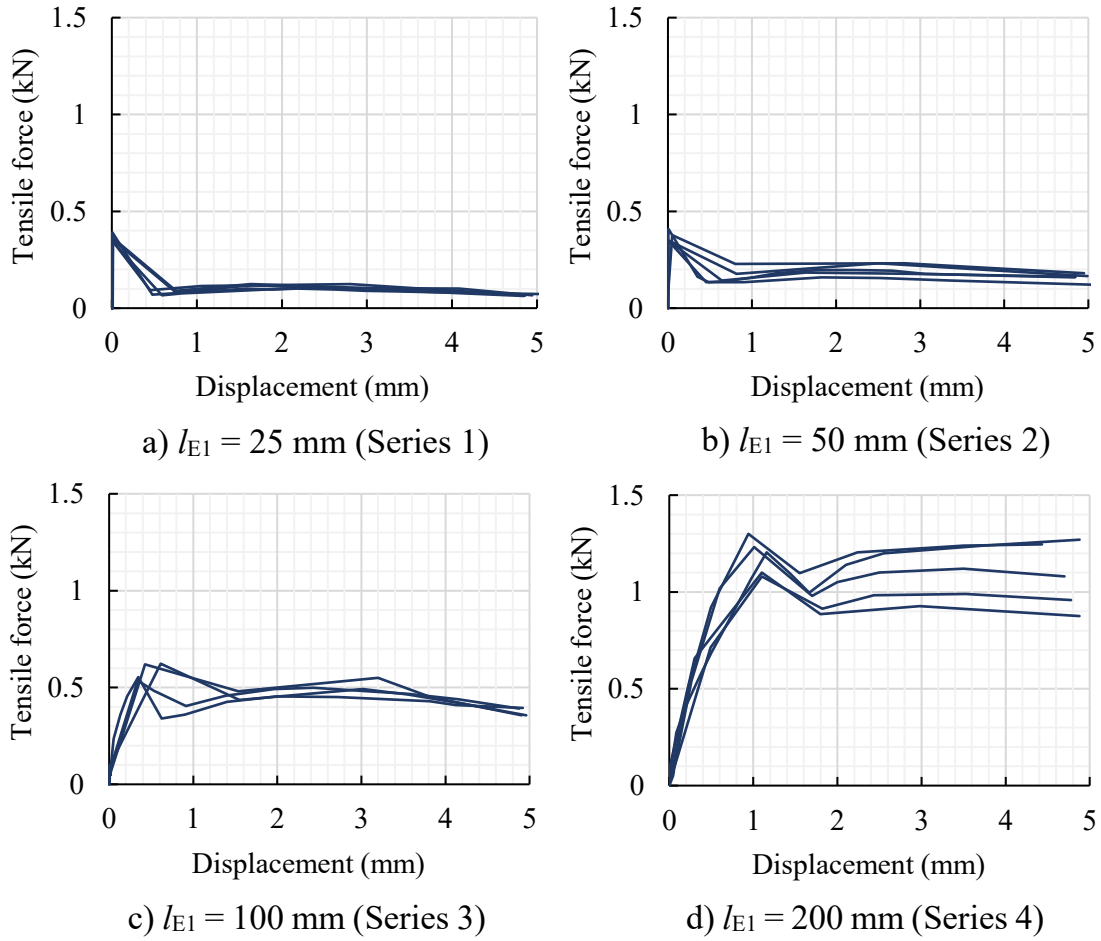

a) l_{E1} = 25 mm (Series 1)

b) l_{E1} = 50 mm (Series 2)

c) l_{E1} = 100 mm (Series 3)

d) l_{E1} = 200 mm (Series 4)

Figure 3.10 – Tensile force-Crack width relationship between textile and low strength ordinary mortar

Compared with high strength ordinary mortar, specimens made of low strength ordinary mortar feature much less bond strength (see Figure 3.11). For example, in the case of Series L100, the peak load and the frictional force of TRC specimens are two times greater than those of TRC-LS specimens (Figure 3.11a). Even, this superiority of TRC specimens increases significantly in Series 4 with larger embedment lengths (Figure 3.11b). Besides, due to the weak bond strength between the textile and low strength ordinary mortar, the TRC-LS specimen failed with a relatively small slip of the textile. In terms of bond mechanism, TRC and TRC-LS specimens exhibit similar mechanisms, whereas the bond strength is major based on friction.

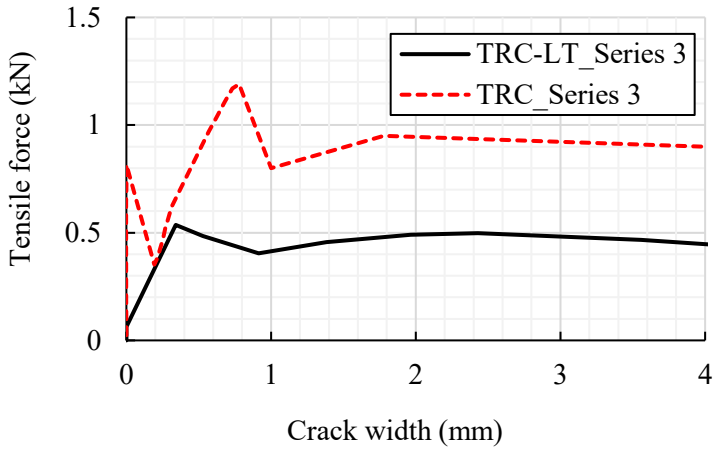

a) Series 3

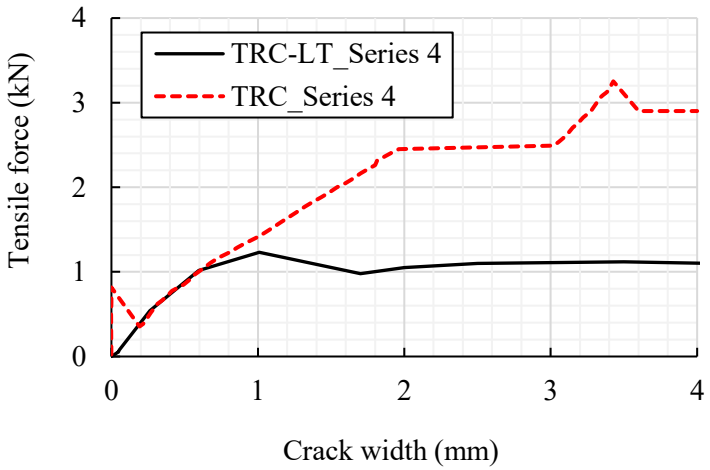

b) Series 4

Figure 3.11 – Comparision of Tensile force-Crack width relationship between TRC and TRC-LS specimens

3.3.3. Bond Behavior between Textile and SHCC

Similar pull-out tests were also conducted on specimens made of textile and SHCC (TR-SHCC). It can be observed from Figure 3.12 that dual peak response was not observed in Series 1, 2, and 3. For these series, the peak represented the crack of SHCC at the position of pre-determined breaking point as the strain of SHCC reached the ultimate value. The pull-out failure occurred immediately after the formation of crack, which depicted by a considerable plateau. Bond strength could not be determined for embedment lengths of 25, 50, and 100 mm. In the case of Series 3, although the embedment length of 100 mm was relatively large, the pre-peak response was not different from the series with much smaller embedment length. These indicated a weak bonding interaction between textile and SHCC, and the contribution of SHCC to pre-peak response was primary. The contribution of bonding, particularly fiction bonding, could be observed more remarkably during the post-peak stage. It can be seen that when pull-out failure occurring, the tensile force increased linearly with the increase of embedment length (see Figure 3.12).

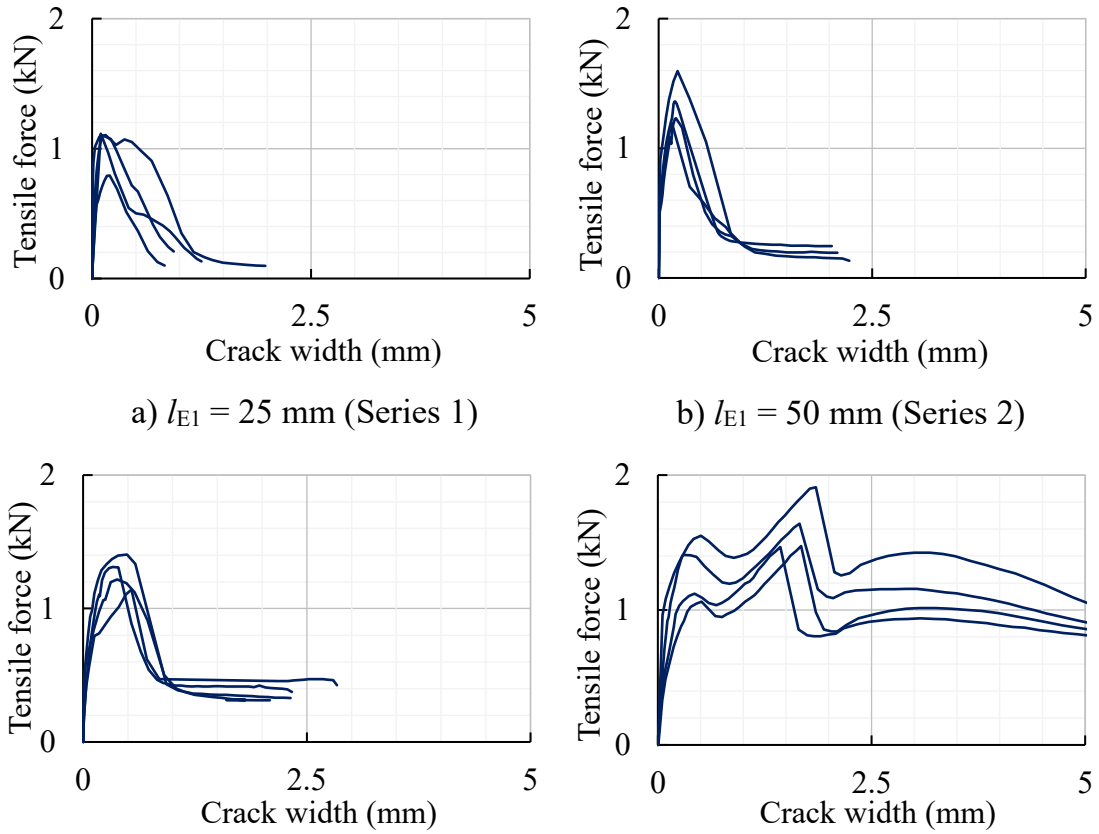

a) l_{E1} = 25 mm (Series 1)

b) l_{E1} = 50 mm (Series 2)

c) l_{E1} = 100 mm (Series 3)

d) l_{E1} = 200 mm (Series 4)

Figure 3.12 – Tensile force-crack width relationship of TR-SHCC

In the case of Series 4, this series showed up dual peak response. However, the average peak load corresponds to the bond strength of this series was 1.7 kN, relatively smaller that of high strength ordinary mortar. It indicated that the bond strength between textile and SHCC was significantly weaker than the bonding between textile and high strength ordinary mortar.

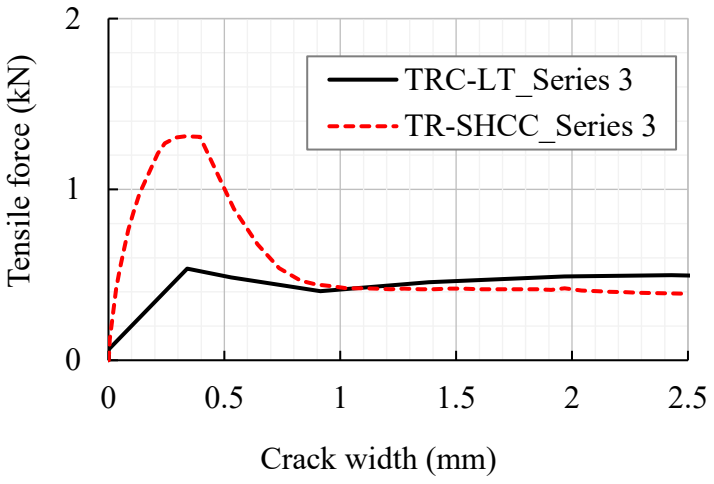

a) Series 3

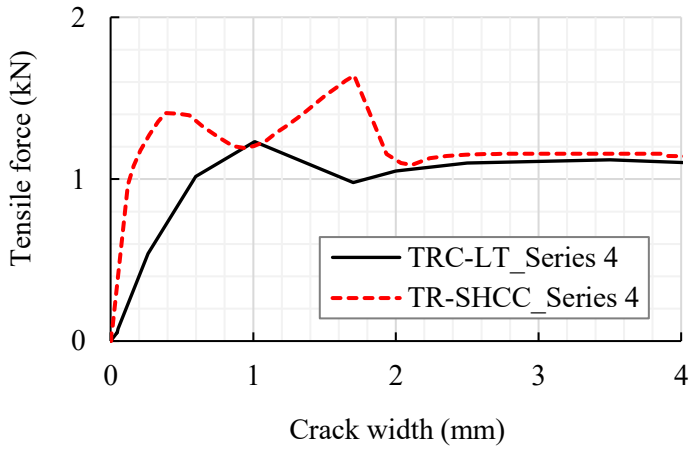

b) Series 4

Figure 3.13 – Comparision of Tensile force-Crack width relationship between TR-SHCC and TRC-LS specimens

For both TR-SHCC and TRC-LS specimens, it can be seen that the specification of the bond strength of the series with embedment lengths smaller or equal to 100 mm is difficult. For TR-SHCC specimens, the peak load of the Series 1, 2, and 3 is almost equivalent, around 1.2 kN. Whereas, the corresponding peak load in the case TRC-LS specimens is 0.5 kN. As a result, to verify the bond strength of TR-SHCC and TRC-LS specimens, the embedment lengths should be greater than 100 mm.

Figure 3.13 compares the tensile force-crack width relationship of TR-SHCC and TRC-LS specimens. The results show that the bond strength of TR-SHCC specimens is quite higher than that of TRC-LS specimens (Figure 3.13 b), while the frictional forces are approximately equal.

In summary, among the three examined matrixes, the combination of textile and high strength ordinary mortar exhibits the greatest bond strength. On the contrary, the textile-low strength ordinary mortar combination shows the lowest bond strength. In terms of friction bonding, the friction between textile and SHCC versus textile and low strength ordinary mortar is almost equal, and much smaller compared to the combination of textile and high strength ordinary mortar.

3.4. Determination of Bond Stress-Slip Relationship

3.4.1. Solution Approach

The determination of the bond stress - slip relationship (BSR) is based on the analytical modeling of the force-crack width relationships, which was determined in the pull-out tests based upon the multilinear, segmentally closed solutions of the bond differential equations described by Richter (2004). Figure 3.14 shows a mechanical model for pull-out, in which the shear stress at a location x in the interface within the representative pull-out specimen is always dependent on the slip at this location: $\tau(x) = \tau[s(x)]$. Equation 3.2 describes the relationship between the slip s at location x and the tangential stress $\tau(s)$.

$$\frac{d^2 s(x)}{dx^2} = \frac{u_Y}{A_Y E_Y} \tau[s(x)] \tag{3.2}$$

where u_Y , A_Y , E_Y are the circumference, the cross-sectional area and the Young's modulus of the yarns respectively. The energy balance of the applied load and the shear stresses results in a relation between the normal force $N_Y[s(x)]$ in the yarn and the slip.

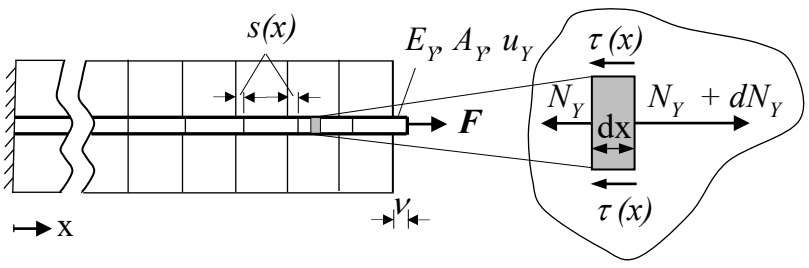

Figure 3.14 – Mechanical model for pull-out

$$N_Y[s(x)] = \sqrt{2u_Y A_Y E_Y \int_0^{s(x)} \tau[s(x)]ds} \tag{3.3}$$

According to Richter (2004), at least a triple linear approach for the shear stress-slip relationship is meaningful for the description of the bond behavior between yarns and the surrounding mortar. The constitutive law can be described as follows. The transferable shear stress is increasing with increasing slip up to the maximum value τ_m. If the slip exceeds the associated value of s_m, the damage of the interface initiates, and the transferable shear stress is decreasing. At the slip s_R bond turns from adhesion to friction. The described shear stress-slip relationship is shown in Figure 3.15. For the following expressions the gradients in the intervals 1 and 2 - Z_1 and Z_2 - and the abbreviations k_1 and k_2 are introduced:

$$Z_1 = \frac{\tau_m}{s_m},\ Z_2 = \frac{\tau_R - \tau_m}{s_R - s_m},\ k_1 = \sqrt{\frac{u_Y}{E_Y A_Y} Z_1}\ , \text{and}\ \ k_2 = \sqrt{-\frac{u_Y}{E_Y A_Y} Z_2} \tag{3.4}$$

The starting value of the normal force at each interval beginning is denoted with $N_{Y,i}$ (i=1-3). Equation 3.2 leads to the shear stress distribution along the interface for the three linear sections of the shear stress-slip relation:

$$\tau_1(x_1) = N_{Y,1} \frac{k_1}{2u_Y} (e^{k_1 x_1} - e^{-k_1 x_1}) \tag{3.5}$$

$$\tau_2(x_2) = \tau_m cos\ (k_2 x_2) - N_{Y,2} \frac{k_2}{u_f} sin\ (k_2 x_2) \tag{3.6}$$

and

$$\tau_3(x_3) = \tau_R \tag{3.7}$$

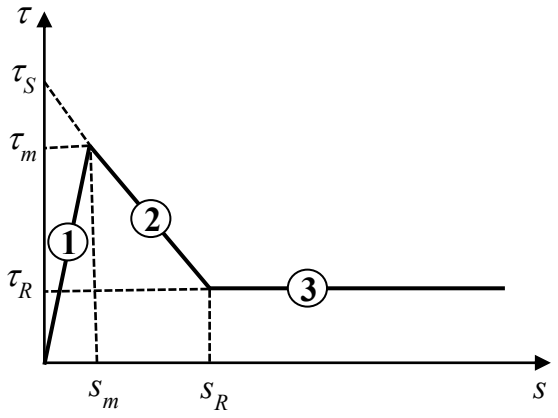

Figure 3.15 – Triple linear section of shear stress-slip relationship

As described in Figure 3.16, the crack opening $w(F)$ in the zone of the predetermined breaking point is the sum of the relative displacements $S_{A2}(F)$ and $S_{B2}(F)$ of the loaded yarn ends from both upper part and lower part of specimen, and the elongation of yarn $\Delta l(F)$ can be calculated in the crack according to equation 3.8.

$$w(F) = S_{A2}(F) + S_{B2}(F) + \Delta l(F) \tag{3.8}$$

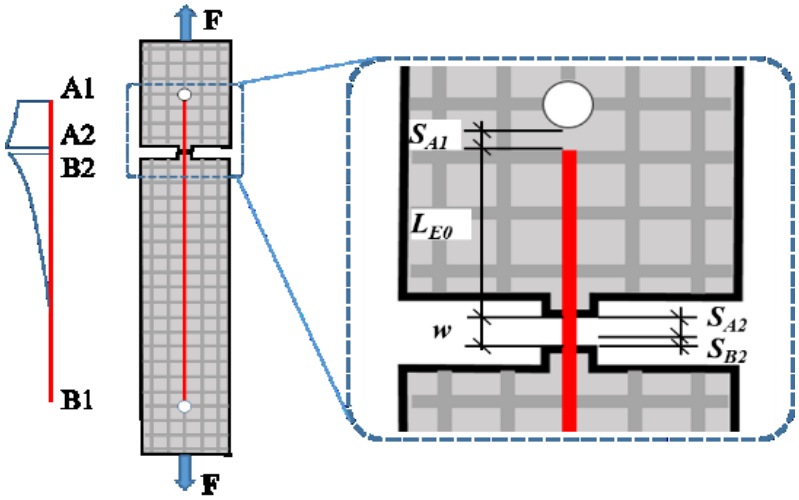

Figure 3.16 – Pull-out failure of warp yarn

In the upper area of the specimen, due to the short anchoring length L_E, a pull-out of the filament yarn from the fine-grained concrete occurs. A calculation of the pull-out force F independence on the slip of the free yarn end S_{A1} is possible. In this, the distribution of the bond stresses via the anchoring length L_{E0} results in the respective relative slip S_{A1} during yarn pull-out. Using the integral of the bond stress via the anchorage length (equations 3.5, 3.6, and 3.7), the yarn pull-out force F can then be calculated for every phase of the yarn pull-out. Due to the two functions $F(S_{A1})$ and $S_{A2}(S_{A1})$, a respective area-wise closed solution with a formulation of the function $S_{B1}(F)$ becomes possible. Due to the short anchoring lengths chosen as well as to the coated carbon-yarns, simultaneous activation of several sections of the BSR can, as a rule, be avoided. Only in the transition areas between two linear sections does it come to the activation of two sections of the BSR. The calculation shows here a local discontinuity. However, due to their insignificance, the resultant discontinuity can usually be smeared in a simplified fashion. In contrast to the yarn pull-out with partial activation of the BSR in the upper section of the test specimen, a yarn pull-out can be avoided in the lower part of the specimen due to the long

anchoring length chosen. The displacement of the free yarn end S_{B1} results in zero. For anchoring the yarn pull-out forces into the fine-grained concrete determined by the pull-out resistance of the short upper specimen part, only the activation of the adhesive stress is necessary. Therefore, the elastic behavior of the yarn can be assumed in the lower part of the specimen used. The corresponding displacement in the crack S_{B2} can be calculated in dependence on the yarn pull-out force F. For the consideration of the yarn strain in the area of the crack, this load-dependent additional strain $\Delta l(F)$ is simplifying determined in the crack by means of the strain of the yarn and the sum of the relative slips S_{A2} and S_{B2}.

3.4.2. General Assumption

The mortar (E_M, A_M) of the TRC components is clearly more rigid than the yarn (E_Y, A_Y). Therefore, by assuming linearly elastic material behavior and neglecting the matrix, the constant substitute strain rigidity $(E \times A)^*$ becomes simplifying assumed according to equation (3.9) [Richter (2004)].

$$(E \times A)^* = E_Y \times A_Y \tag{3.9}$$

The gradient of the BSR within the respective tested segment is called Z_x (Figure 3.17). For this, the increasing and decreasing areas must be differentiated. According to equation (3.10) [Richter (2004)] for the determination of the constant k_x within the respective linear area then applies:

$$k_x = \sqrt{\frac{u_G}{(E.A)^*}|Z_x|} \tag{3.10}$$

where,

u_G : perimeter of single yarn (mm).

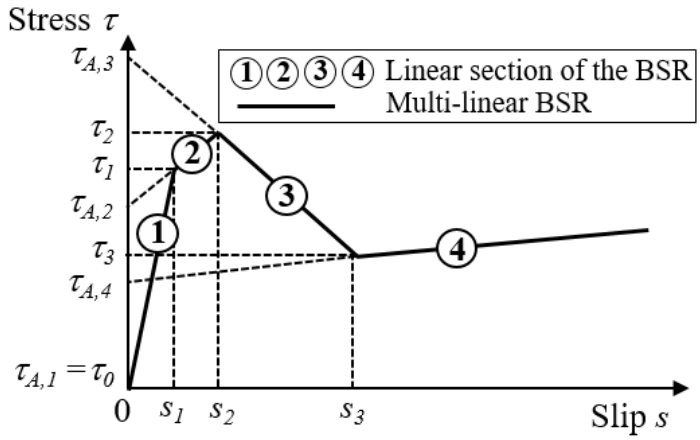

Figure 3.17 – A typical BSR [Lorenz and Ortlepp (2012)]

3.4.3. Analytical Solution

As mentioned in equation 3.8, the crack width is the sum of the relative displacements $S_{A2}(F)$, $S_{B2}(F)$, and the elongation of yarn $\Delta l(F)$. In the following, the solutions for the determination of $S_{A2}(F)$, $S_{B2}(F)$, and $\Delta l(F)$ based on approachs proposed by Richter (2004), Lorenz and Ortlepp (2012).

For the analytical consideration of the yarn pull-out in the upper specimen part, the reduction of the existing anchoring length L_E due to displacement of the free yarn end S_{A1} must be considered during the yarn pull-out according to equation (3.11). The reduced anchoring length is then called L_{E0}. In addition, once slip has occurred at the unloaded end a closed form analytical expression $F(S_{A2})$ cannot be found but the two functions $F(S_{A1})$ and $S_{A2}(S_{A1})$ can be formulated. It allows an implicit formulation of the pull-out force-displacement curve.

$$L_{E0} = L_E - S_{A1} \tag{3.11}$$

In the increasing section of the BSR, the displacement S_{A2} at the loaded yarn end in the upper part and tensile force F can be defined by equations (3.12) and (3.13).

$$S_{A2}\left(S_{A1}\right) = \frac{\tau_{A,x} + Z_x \times S_{A1}}{Z_x} \times \cosh\left(k_x \times L_{E0}\right) - \frac{\tau_{A,x}}{Z_x} \tag{3.12}$$

$$F\left(S_{A1}\right) = \frac{u_G}{k_x} \times \left(\tau_{A,x} + Z_x \times S_{A1}\right) \times \sinh\left(k_x \times L_{E0}\right) \tag{3.13}$$

In the decreasing section of the BSR, the displacement S_{A2} at the loaded yarn end in the upper specimen part and tensile force F can be defined by equations (3.14) and (3.15).

$$S_{A2}\left(S_{A1}\right) = \frac{\tau_{A,x} + Z_x \times S_{A1}}{Z_x} \times \cos\left(k_x \times L_{E0}\right) - \frac{\tau_{A,x}}{Z_x} \tag{3.14}$$

$$F\left(S_{A1}\right) = \frac{u_G}{k_x} \times \left(\tau_{A,x} + Z_x \times S_{A1}\right) \times \sin\left(k_x \times L_{E0}\right) \tag{3.15}$$

The elongation strain $\Delta l(F)$ of the yarn within the crack width is simplified calculated by means of the sum of the relative displacements S_{A2} and S_{B2} in the crack.

$$\Delta l\left(F\right) = \frac{F}{A_G} \times \frac{1}{E_G} \times \left(S_{A2}\left(F\right) + S_{B2}\left(F\right)\right) \tag{3.16}$$

3.4.4. To Determine Bond Stress-Slip Relationship of TRC specimens

In this section, the bond stress-slip relationship is determined using the solution mentioned above. The determination of the bond stress-slip relationship should be based on a series with short embedment length. For TRC specimens made of high strength ordinary mortar, Series 2 with an embedment length of 50 mm is the most suitable. At first, the modified force-crack width relationship of Series 2 is defined by removing lines represent crack formation at the predetermined breaking point of the experimental tensile force-crack width relationship (Figure 3.18). Assume in advance a BSR, then using Equations 3.8-3.16 to calculate values F, S_{A2}, S_{B2}, Δl, and w (Table 3.6). The measured and calculated force-crack width curves show a good agreement, which indicates the assumed BSR is appropriate (Figures 3.19 and 3.20).

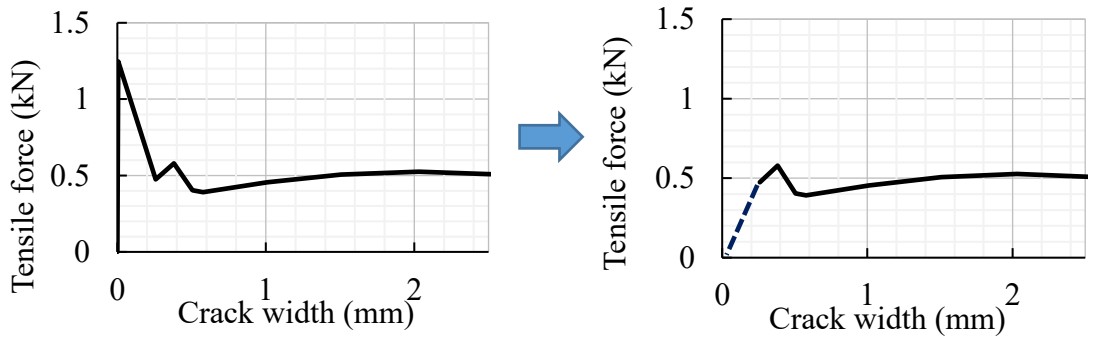

a) Tensile force-crack width relationship of Series 2 achieved from the pull-out test

b) Modified tensile force-crack width relationship of Series 2

Figure 3.18 – Tensile force-Crack width relationship used to determine BSR

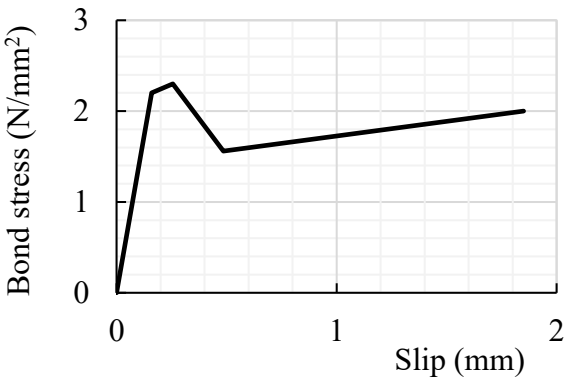

Figure 3.19 – Assumed BSR of high strength ordinary mortar

Table 3.6 – Calculated values for Series 2 of high strength ordinary mortar

F (N)	S_{A2} (mm)	S_{B2} (mm)	Δl (mm)	w (mm)
0	0	0	0	0
452	0.159	0.098	0.0004	0.258
567	0.255	0.123	0.0007	0.379
384	0.485	0.083	0.0007	0.569
552	1.837	0.120	0.004	1.961

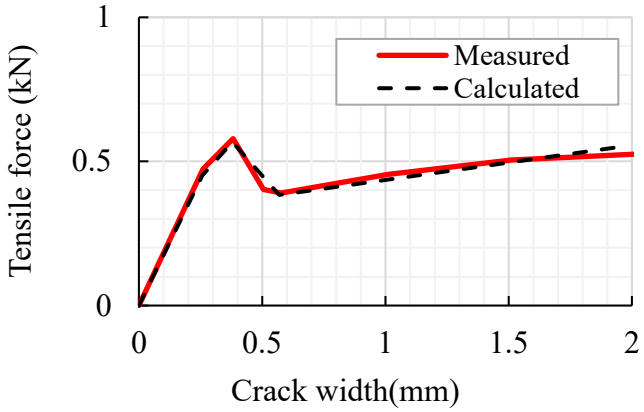

Figure 3.20 – Comparison between measured and calculated force-crack width relationship of Series 2

Using the BSR defined in the case of Series 2 to calculate the tensile force-crack relationship of Series 3 with an embedment length of 100 mm. Detailed results are described in Table 3.7 and Figure 3.21. A good agreement between the measured and calculated force-crack width curves confirms the BSR is suitable.

Table 3.7 – Calculated values for Series 3 of high strength ordinary mortar

F (N)	S_{A2} (mm)	S_{B2} (mm)	Δl (mm)	w (mm)
0	0	0	0	0
661	0.15	0.144	0.0006	0.30
1140	0.25	0.248	0.002	0.50
933	0.49	0.202	0.002	0.69
962	2.00	0.21	0.007	2.22

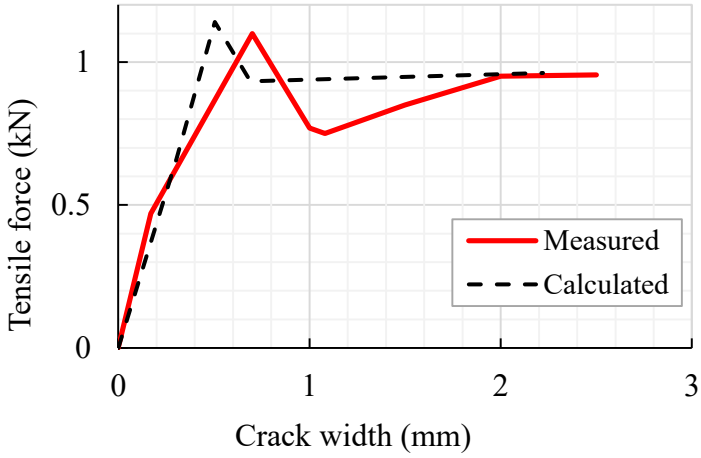

Figure 3.21 – Comparison between measured and calculated force-crack width relationship of Series 3

Similarly, the determination of BSR for low strength ordinary mortar described in Table 3.8 and Figure 3.22.

Table 3.8 – Calculated values for Series 3 made of low strength ordinary mortar

F (N)	S_{A2} (mm)	S_{B2} (mm)	Δl (mm)	w (mm)
0	0	0	0	0
551	0.27	0.20	0.0008	0.47
394	0.85	0.14	0.0013	0.99
505	2.03	0.18	0.0036	2.21

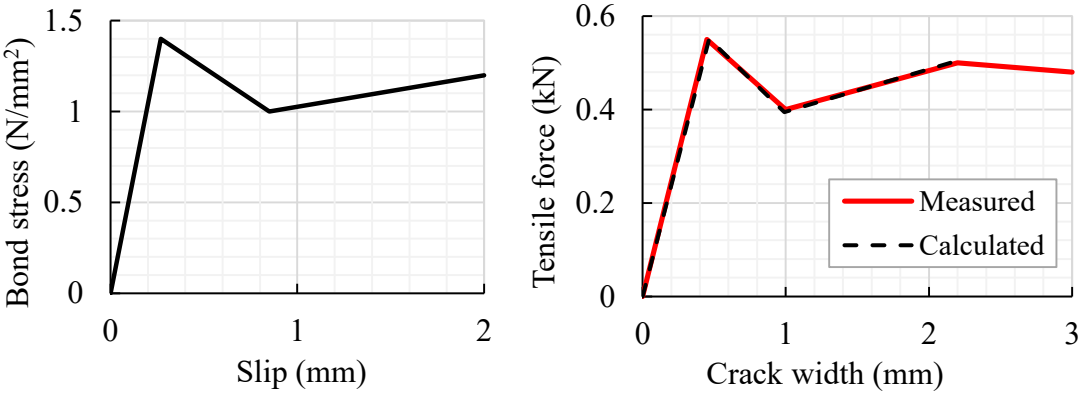

a) Determined BSR of low strength ordinary mortar

b) Measured and calculated force-crack width relationship of Series 3

Figure 3.22 – Determination of BSR of TRC-LS specimens

3.5. Summary

The increasing application of TRC in the construction field claims the formalization of the experimental method and design standards. This investigation provided an overview of pull-out tests to determine bond law between textile reinforcement and mortar. The strengths and the weaknesses of each experiment were analyzed and evaluated, therefore the most suitable and reliable pull-out test was proposed. The real tests were conducted that give an insightful understanding of the bond behavior of examined mortars and textile fabric. The investigation to determine the bond behavior of textile and three different matrixes, including low and high strength ordinary mortar and SHCC, were conducted and examined. The results indicated the specimens made of textile and high strength ordinary mortar exhibited the highest bond strength and friction bonding. On the contrary, the low strength ordinary mortar showed the least effective in terms of bond strength with the textile. This research introduced procedures to determine the bond stress-slip relationship based on the results of the doubled-side pull-out test. For determination of the bond stress-slip relationship, the embedment length should be in a range of 50 to 100 mm for specimens made of ordinary mortar, whereas, for TR-SHCC specimens, the embedment length must be greater than 100 mm. Additionally, results from experiments gave hints on choosing the anchorage length of TRC.

CHAPTER 4

LAP SPLICE LENGTH OF TEXTILE REINFOCED CONCRETE

4.1. Introduction and Background

In terms of the promising application of TRC, the practical use of this new material needs structural detailing provisions, especially overlap length. In many cases, the length of tension textile reinforcement is not sufficient to continue through the entire members such as beams, slabs, and walls. At the location of discontinuity, the tension force must be transferred effectively from one fabric to the other. Accordingly, providing the second textile fabric that overlapped the discontinued one is the most common method. The zone of overlapping between two textile reinforcements forms a lap splice. Typically, the mechanism of force transfer in a lap splices is as follows: the force is transferred from one fabric to the other through bond stresses. Force is firstly transferred to the concrete through bonding from one textile fabric and then is transferred to the other one, forming the splice through the bond between it and concrete. Thus, concrete at the point of splicing subjected to high shear stresses. Numerous potential failure modes might occur due to the effects of lap splices, including splitting failure, delamination failure, pull-out failure, and yarn rupture [Azzam and Richter (2011)]. The behavior and required overlap length depend on many factors, particularly the tensile strength of the mortar and the bond strength between adjacent layers of fabric

reinforcements. The lap splices are supposed to provide sufficient overlap length if they promote the failure of textile reinforcement before debonding of the overlapped textile fabrics [Donnini et al. (2019)]. Two types of members were examined: member under subjected to uniaxial tensile force and member under bending moment (see Figure 4.1).

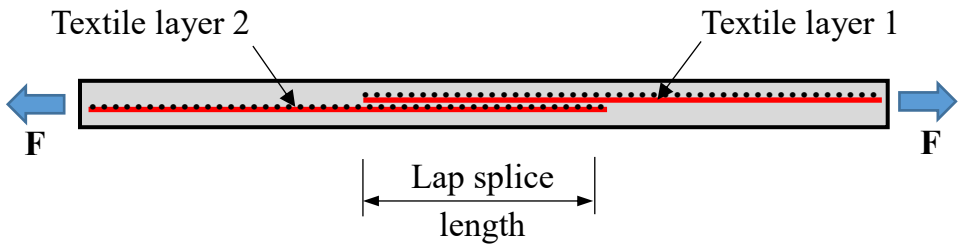

a) Member under uniaxial tensile force

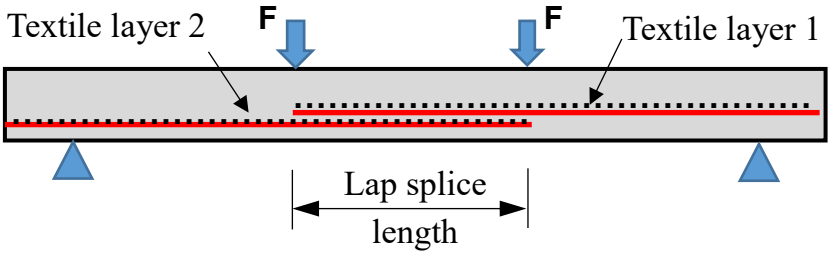

b) Member under bending moment

Figure 4.1 – Types of tests

4.2. Lap Splice Length of Members Subjected to Uniaxial Tensile Force

In the literature, some researches on investigating structural behavior and determining the overlap length of TRC members were conducted. However, most investigations carried out with specimens subjected to uniaxial tensile load. Lorenz and Ortlepp (2011) performed tensile tests by using specimens with symmetrical and asymmetrical reinforcement arrangements. A wide range of lap splice lengths from 30 mm to 150 mm was examined for determining the required overlap length. Two different failure mechanisms could be observed. While a pull-out failure occurred with overlap lengths of less than or equal 125 mm, yarn rupture was dominant for overlap lengths of 150 mm. The test results also showed that the required values for overlap length and anchorage length are equal. Donnini et al. (2019) investigated the tensile behavior of glass fabric reinforced cementitious matrix with fabrics' overlap. Three series with lap splice length of 100, 150 and, 200 mm were examined. The tensile load was transferred from a testing machine to

the mortar by shear adhesion, using metal tabs directly bonded to the mortar surface (see Figure 4.2). The test showed different failure modes depending on the configuration of fabric reinforcement. In the case of short overlap length (100 mm), the formation of longitudinal cracks led to a slippage of fabrics along with the overlay interface. For longer overlap lengths (150 and 200 mm), the breakage of the yarns was observed. Azzam and Richter (2011) studied textile reinforcement splice lengths using Finite-Element simulations and fracture mechanics approaches. The research pointed out two types of failure modes: the yarn pull-out or the yarn rupture and showed good agreement with experimental results by Lorenz and Ortlepp.

In this work, thin and narrow plates made of TRC constitute the core subject of the experimental program. Four cases of different lap splice lengths were examined, including 300, 200, 100, and 50 mm. Based on tensile tests, this research aimed to interpret the structural behavior, failure modes of members with lap splice under tensile force. The results of the tests also suggested the determination of the required lap splice length of TRC members.

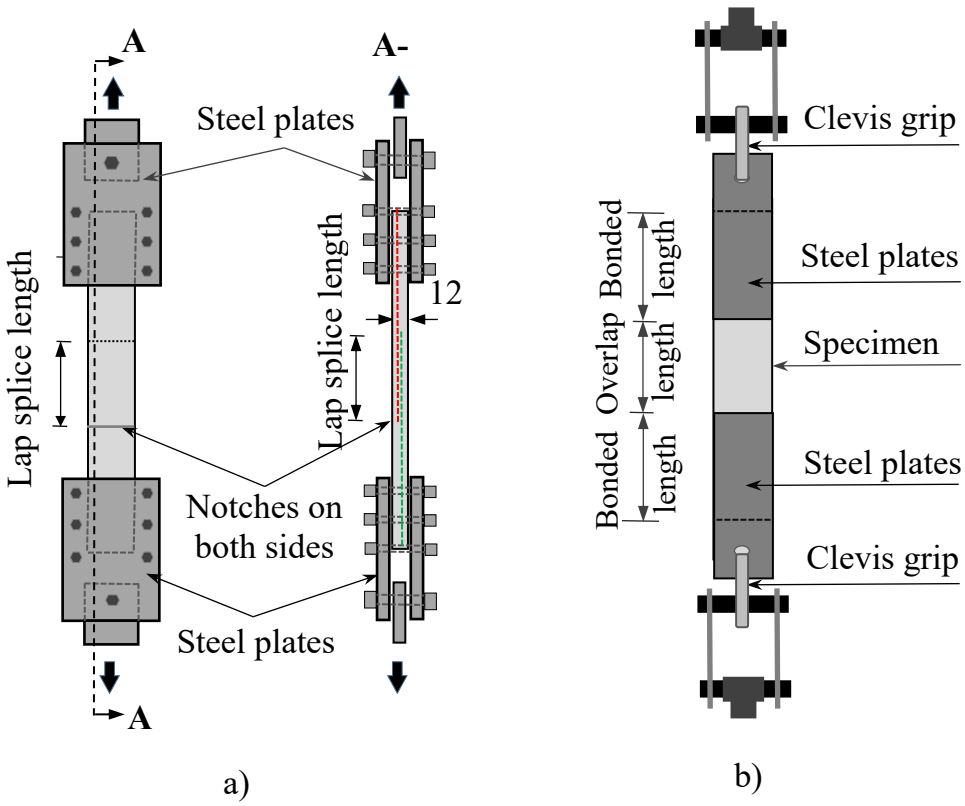

Figure 4.2 – Test setup of tensile test by Lorenz and Ortlepp (a) and by Donnini et al.

4.2.1. Materials

Refer to section 2.2 and 3.2.1 for the properties of textile reinforcement as well as the composition of ordinary mortar and SHCC. Tables 4.1, 4.2, and 4.3 described the mechanical properties of high and low strength ordinary mortars, and SHCC.

Table 4.1 – Mechanical properties of high strength ordinary mortar

Characteristics	Value
Compressive strength (N/mm^2)	70
Splitting strength (N/mm^2)	4.9

Table 4.2 – Mechanical properties of low strength ordinary mortar

Characteristics	Value
Compressive strength (N/mm^2)	36.5
Tensile strength (N/mm^2)	3.6

Table 4.3 – Mechanical properties of SHCC

Characteristics	Value
Compressive strength (N/mm^2)	40.5
Tensile strength (N/mm^2)	4.2

4.2.2. Specimen Preparation

The TRC specimens were produced by a hand lamination process in steel formworks resulting in large-format textile-reinforced concrete slabs with a dimension of 1000×1000×20mm. The textile layer and mortar layers were placed in the formwork alternately with a mortar layer in its bottom and top. At first, a layer of mortar of 10 mm cast into the formwork. Then, the first textile fabric was placed on the top of the matrix and spliced by the other textile fabric. Afterward, the remaining mortar layer with a thickness of 10 mm cast into the formwork. All specimens cured in a constant temperature room for 14 days. After the curing period, the slabs were cut into small rectangular shapes with proper dimensions (Figure 4.3). With this configuration, all investigated specimens in the test came from the same batch of mortar. As a result, the comparability of the individual tests and reducing the scattering of the quality of concrete and composite properties could be ensured. Five series of specimens were fabricated and examined. The test specimen properties, including dimensions, the number of specimens, and the

values of lap splice length have been listed in Table 4.4. In particular, Series L0 was fabricated with continuous textile reinforcements so that this series defined as reference series. For each specimen, two pre-determined breaking points used to specify the lap spliced zone. Each pre-determined breaking point was defined by two opposite notches that were sawn on both specimen surfaces. The position of these notches coincided with the discontinuous ending point of spliced textile fabric. It means that the distance between the two pre-determined breaking points equals the lap splice length of the considered specimen. For the controlled series (Series L0), the distance between two pre-determined breaking points was 300 mm (see Figure 4.4). Before conducting the test, steel plates glued to the expected areas of specimens that were clamped by grips.

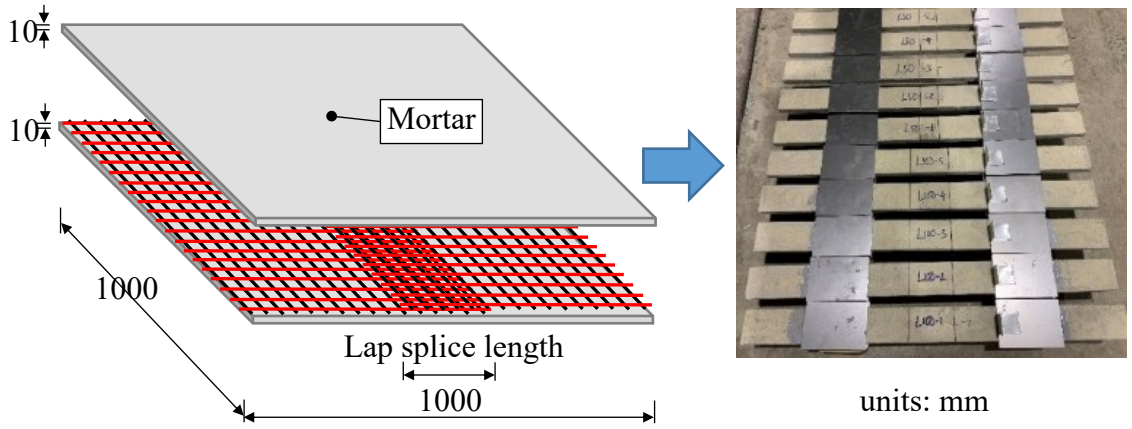

Figure 4.3 – Specimens used for the tests

Table 4.4 – Dimension and quantity of specimens

Series	Lap splice length L_l (mm)	Width x Length x Thickness (mm)	Number of specimens
L0	-	80 x 900 x 20	5
L50	50	80 x 900 x 20	5
L100	100	80 x 900 x 20	5
L200	200	80 x 900 x 20	5
L300	300	80 x 900 x 20	5

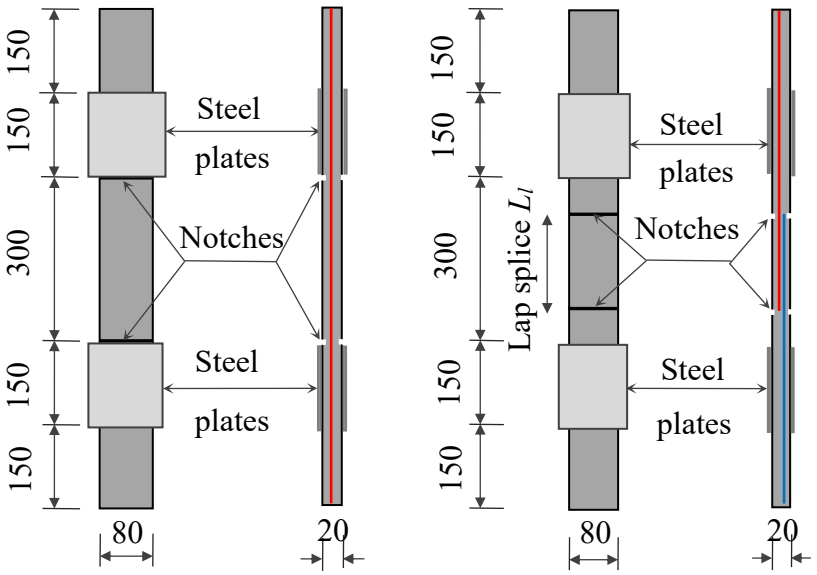

a) Controlled specimen b) Specimens with lap splice

Figure 4.4 – Detail geometry of the specimens

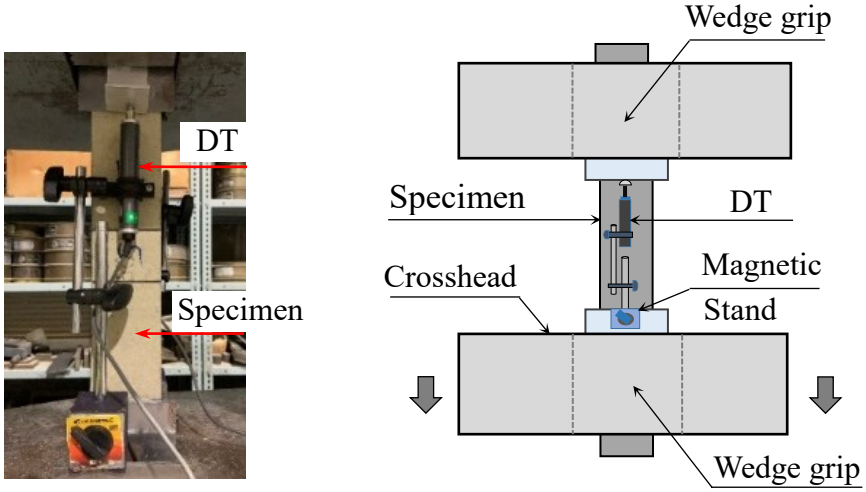

Figure 4.5 – Test setup

4.2.3. Test Setup

As illustrated in Figure 4.5, specimens were mounted into the testing device and clamped by wedge grips. The load was transferred from the testing machine to the mortar through the compressive stress normal to steel plates, which were directly bonded to the mortar surface. With such configuration, the load applied to mortar more evenly, therefore an excess of compressive strength of the specimens can be

avoided. The tests were conducted under displacement control by using a tensile machine with a load-bearing capacity of 50 kN. Two Displacement Transducers (DT) were employed on both specimen surfaces to record global displacement.

4.2.4. Results and Discussion of Specimens Made of Textile and High Strength Ordianry Mortar

The results of the tensile test in terms of failure mode, failure load, and corresponding displacement were reported in Table 4.5. It is recognized that the load-bearing capacity of specimens increased steadily together with the increase of lap splice length. The specimens with lap splice length of 300 mm (Series L300) provided the highest tensile capacity, whereas the specimens of Series L50 possessed the lowest efficiency. Besides, different failure modes were observed, including pull-out and delamination failures, but the breakage of textiles did not occur in all series.

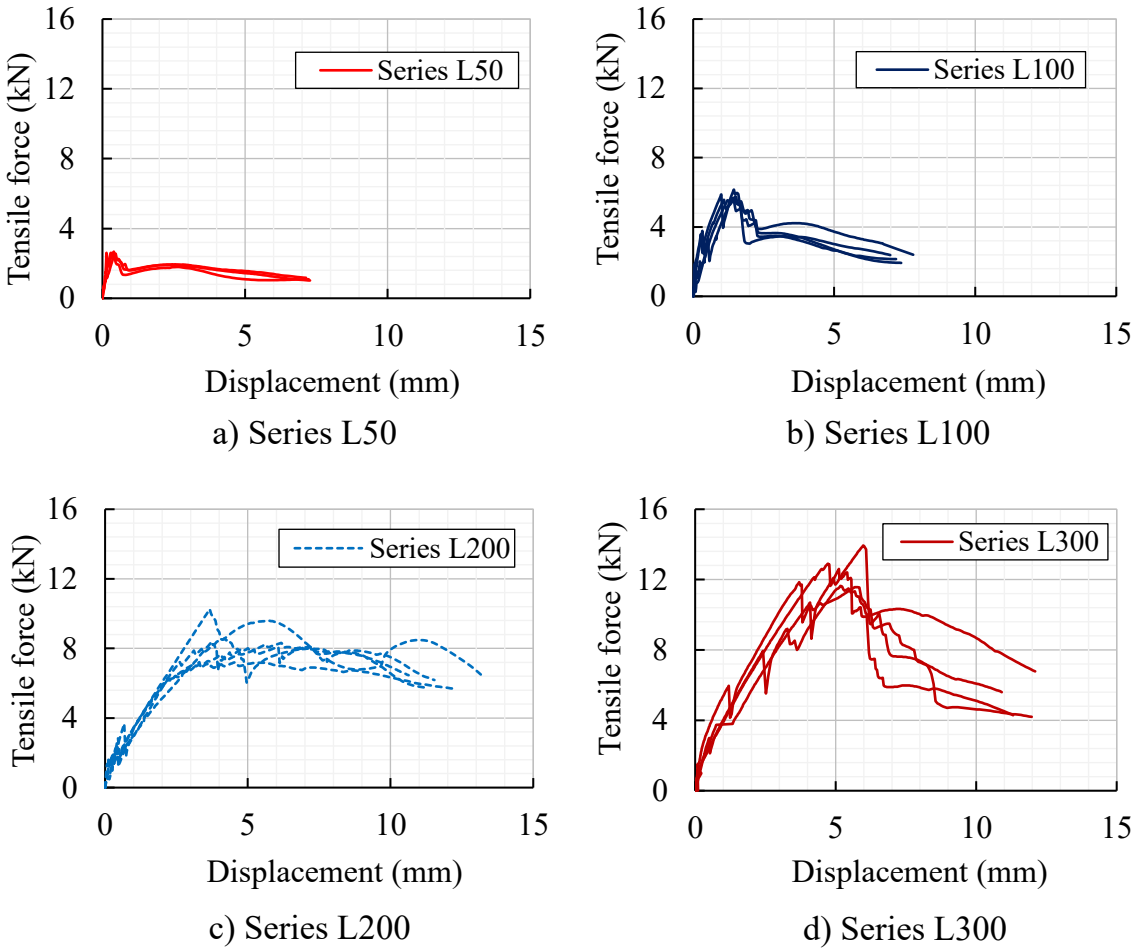

Figure 4.6 – Tensile force-displacement relationship of series with lap splice

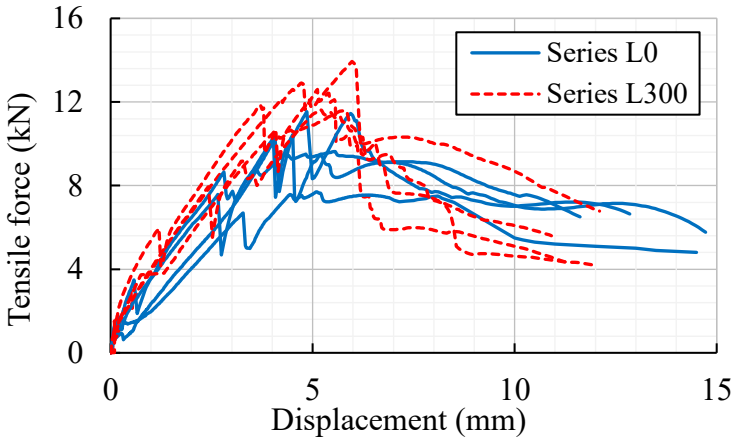

Figure 4.7 – Tensile force-displacement relationship of Series L0 and L300

The experimental tensile force-displacement relationship of all series was described in Figure 4.6. These curves could be divided into three phases. The first segment of the curves represents the uncracked state, in which the composite properties depend on the matrix characteristics. This phase ends as the formation of the first two cracks at the position of pre-determined breaking points associated with the drop of the load. After this phase, one the transfer of stress from the matrix to the fabric occurred, the applied loads start to increase again, with an evident hardening phase. This phase is mainly controlled by the fabric properties and bond behavior between fabric and mortar. After reaching the peak load, the failure of specimens occurs. Failure mode and Failure mechanism are determined according to the value of lap splice length.

For the Series L100 and L50, the result showed that the lap splice lengths were not enough to guarantee the complete transfer of tensile stress from one fabric to another. Fabrics slip on each other, and pull-out failure was the dominant failure mode in all specimens (see Figure 4.8). Consequently, the tensile capacity of the specimens significantly small. The average load-bearing capacity of Series L100 and L50 were 5.5 kN and 2.6 kN, respectively, much less than that of controlled Series L0 (10.1 kN). The tensile force-displacement curves of the two series in Figure 4.9 showed that the shape of these curves was quite similar, with a considerable plateau in the failure phase. These plateaus represented the friction between fabric and mortar as the pull-out failure occurring.

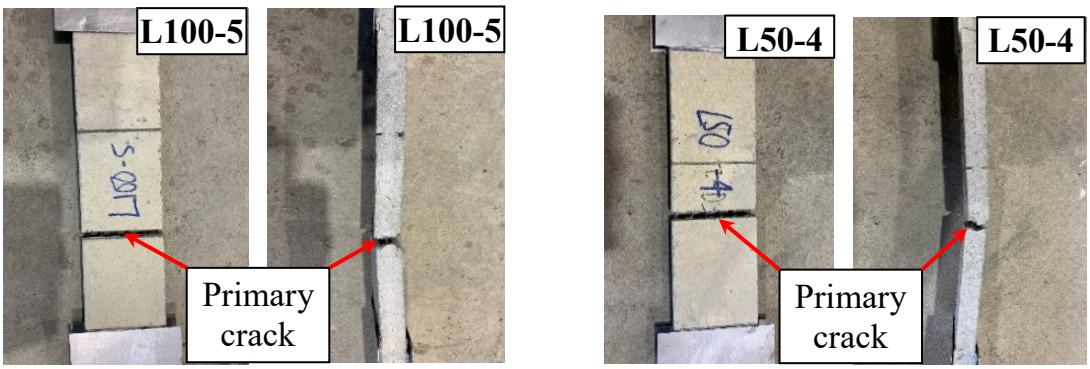

a) Series L100 b) Series L50

Figure 4.8 – Pull-out failure of Series L100 and L50

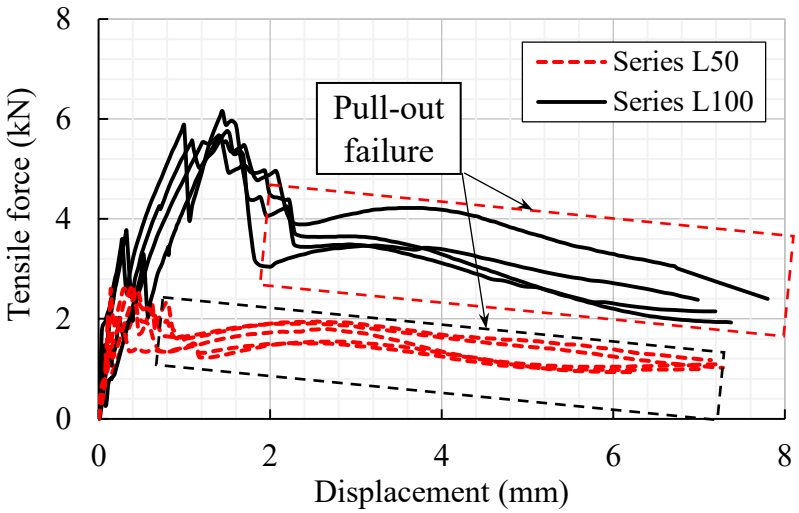

Figure 4.9 – Tensile force – displacement relationship of Series L100 and L50

Increasing the lap splice length up to 300 mm allowed to achieve the specimen integrity and to reach ultimate load-bearing capacity approximately equal to that of the Series L0 with continuous textile reinforcement. Figure 4.7 showed that the tensile behavior of Series L300 was not so different compared to the behavior of controlled series. In addition, the delamination failure occurred in all specimens of both Series L300 and L0 (Figure 4.10). These indicate that the lap splice length of 300 mm secures to transfer effectively the tensile stress one fabric to the other.

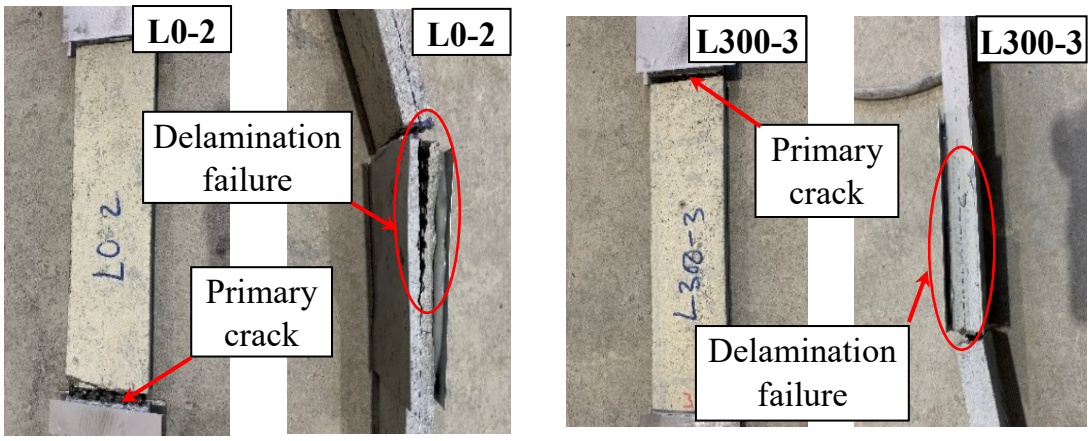

a) Series L0 b) Series L300

Figure 4.10 – Failure modes of Series L0 and L300

For the Series L200, the results showed a variety of failure modes. The delamination failure occurred in specimens L200-1 and L200-5, whereas the dominant failure mode of specimen L200-2, L200-3, L200-4 was the pull-out failure (see Figure 4.11). Besides, the average failure load of Series L200 was 8.6 kN, fairly smaller than the tensile capacity of reference series (10.1 kN). Therefore, it is reasonable to assume that the lap splice length of 200 mm is insufficient to achieve satisfactory performance.

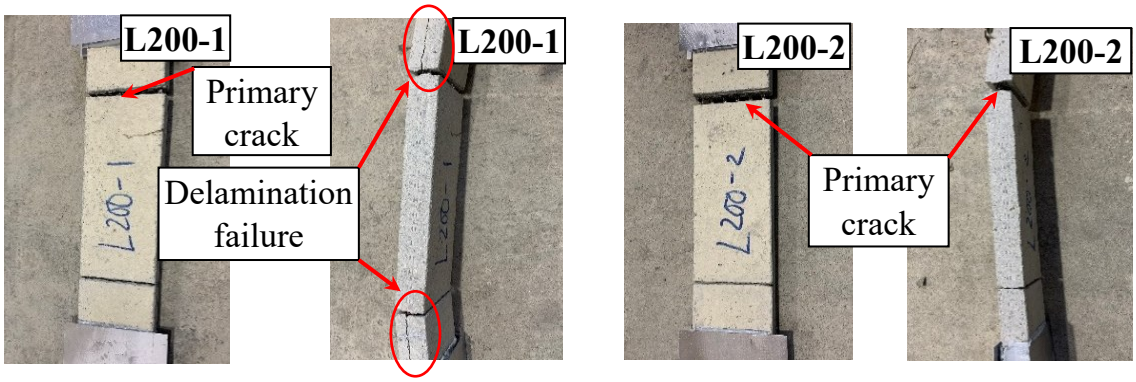

a) Specimen L200-1 b) Specimen L200-2

Figure 4.11 – Different failure modes of Series L200

Table 4.5 – Test result of TRC specimens

Series	Specimen	Failure load (kN)	Average failure load (kN)	Disp.* (mm)	Failure mode
L0	L0-1	9.4	10133	6.5	D
	L0-2	10.4		4.5	D
	L0-3	9.7		5.1	D
	L0-4	9.6		5.6	D
	L0-5	11.5		5.8	D
L300	L300-1	14.7	13002	7.4	D
	L300-2	12.9		4.7	D
	L300-3	13.9		5.3	D
	L300-4	11.6		5.6	D
	L300-5	11.9		5.1	D
L200	L200-1	8.4	8548	3.9	D
	L200-2	10.3		3.7	P
	L200-3	8.3		4.1	P
	L200-4	7.2		4.8	P
	L200-5	8.6		4.2	D
L100	L100-1	4.4	5530	1.4	P
	L100-2	5.7		1.4	P
	L100-3	5.7		1.4	P
	L100-4	5.8		1.5	P
	L100-5	6.2		1.5	P
L50	L50-1	2.5	2562	0.8	P
	L50-2	2.6		0.5	P
	L50-3	2.5		0.2	P
	L50-4	2.7		0.5	P
	L50-5	2.6		0.5	P

Disp. * – Displacement corresponding to failure load; D – Delamination failure; P – Pull-out failure

4.2.5. Results and Discussion of Specimens Made of Textile and Low Strength Ordinary Mortar

Figure 4.12 shows the tensile force-displacement relationship of four series, including control series L0 and series with lap splice length of 100, 200, and 300 mm. For series L100 and L200, the short lap splice lengths lead to pull-out failure, which was accompanied by low applied loads and corresponding displacements (Figures 4.12 a, b and 4.13). The respective average peak loads of series L100 and L200 are 2.6 kN and 5.4 kN, much smaller compared to the control series. It indicates that for all examined matrixes, the lap splice lengths of 100 mm and 200

mm are inadequate. For Series L300, the average peak load is 9.5 kN, significantly higher than that of Series L100 and Series L200. However, compared to the control series, the peak loads and corresponding displacement of Series L300 are still rather smaller than those of the control series. Besides, the dominant failure of Series L300 is pull-out (see Figure 4.14), which is different from the delamination failure of Series L300 made of SHCC or high strength ordinary mortar. Therefore, the combination of textile and low strength ordinary mortar requires an adequate lap splice length greater than 300 mm.

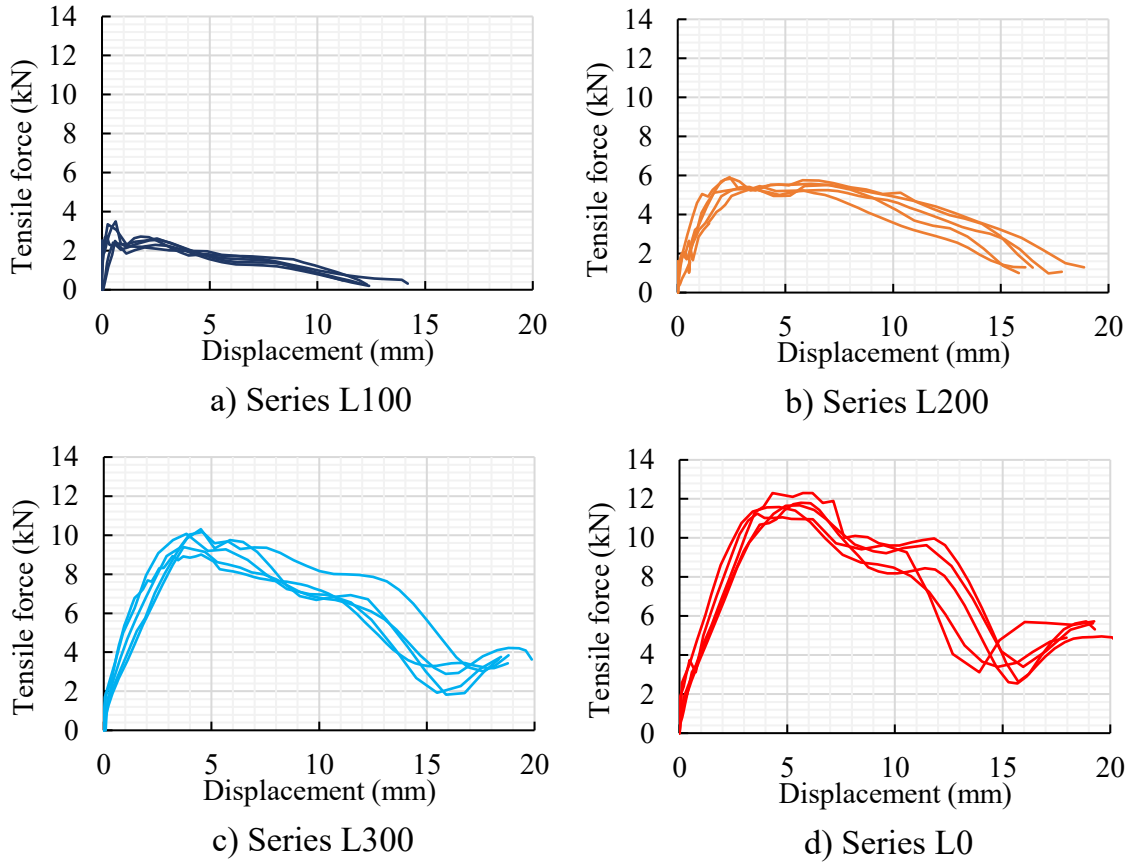

Figure 4.12 – Tensile Force-Displacement relationship of TRC specimens made of low strength ordinary mortar

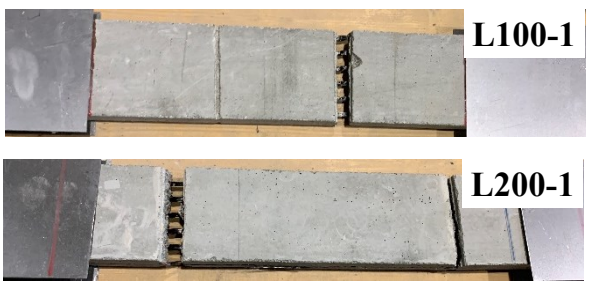

Figure 4.13 – Pull-out failure of Series L100 and L200

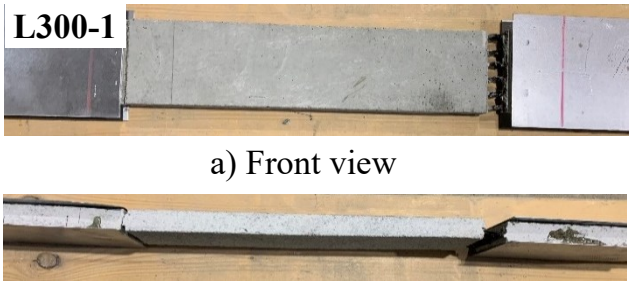

a) Front view

b) Side view

Figure 4.14 – Pull-out failure of Series L300

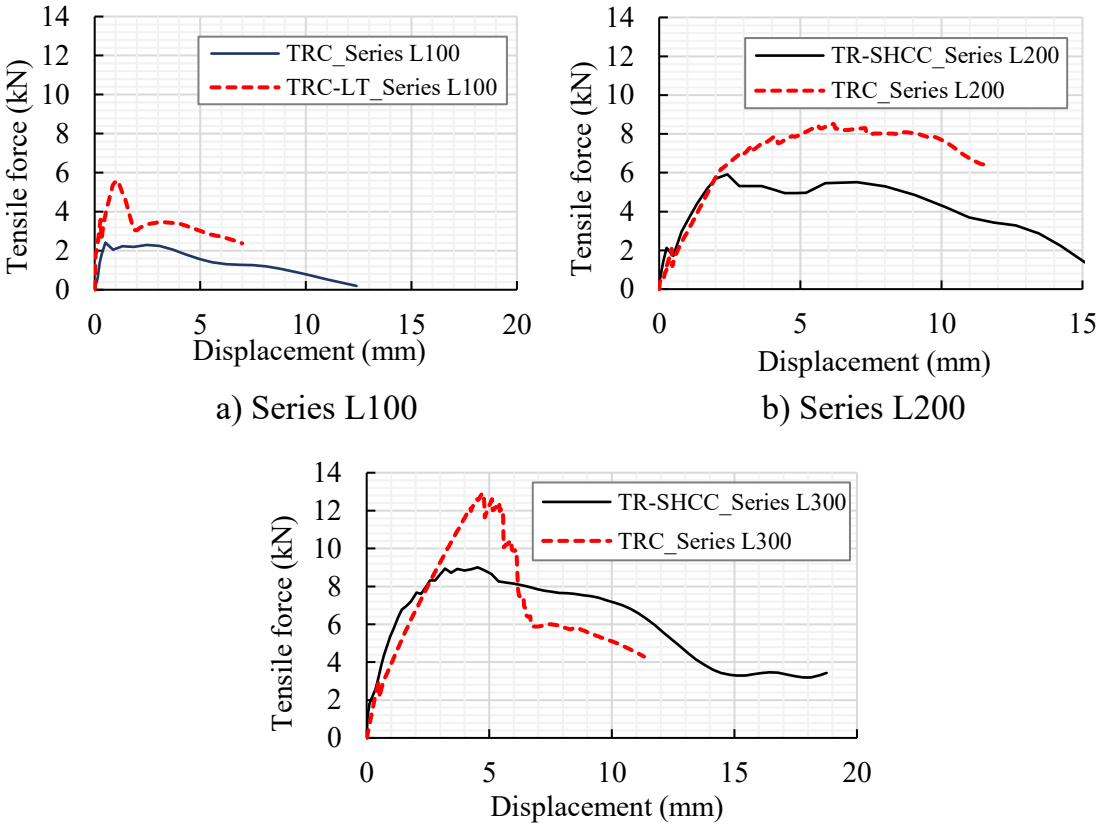

a) Series L100

b) Series L200

c) Series L300

Figure 4.15 – Comparision of Tensile force-Displacement relationship between TRC and TRC-LS specimens

Figure 4.15 compares the typical tensile force-displacement relationship between TRC and TRC-LS specimens. The results show that spliced TRC specimens exhibit significantly higher loading-bearing capacity than that of corresponding TRC-LS specimens. Besides, for lap splice lengths of 100 and 200 mm, the dominant failure mode of both TRC and TRC-LS is pull-out. However, in the cases of Series L300, TRC and TRC-LS specimens display different failure

modes. Due to low bond strength, TRC-LS specimens exhibit pull-out failure, and the load-bearing capacity gradually decreases after reaching peak load. Whereas, the delamination failure induces a drop of applied load in the pre-peak stage.

4.2.6. Results and Discussion of Specimens Made of Textile and SHCC

The results of the uniaxial tensile test on TR-SHCC specimens in terms of failure mode, failure load, and corresponding displacement were reported in Table 4.6. Besides, the load-displacement relationship of five series was described in Figure 4.16. Clearly, the results show that the load-bearing capacity of specimens increased steadily with the increase of lap splice length. However, Figure 4.16 also suggested that the failure load of Series L300 was still much smaller than the corresponding value of specimens with continuous textile fabric. It indicated that the examined lap splice lengths could not effectively transmit the tensile force between spliced textile meshes. Besides, different failure modes were observed, including pull-out and delamination failures, but the breakage of textiles did not occur.

For controlled series L0, the tensile behavior of specimens with continuous textile reinforcement was described in Figure 4.16e and Figure 4.17. The cracks firstly appeared at positions of two notches when the ultimate tensile strength of the SHCC was achieved. Increasing tensile force, delamination failure occurred at the interface between SHCC layers and textiles. The splitting initially formed within the area between two notches, then extended to the end anchorage area. However, due to the effect of compression force from clamping devices which provided confinement action, the splitting did not spread to the ends of specimens. The delamination within the end anchorage area led to the shortening of anchorage length. As a result, the final failure mode was the mix of delamination and pull-out failure of textiles within the end anchorage area. Secondary cracks were also observed before the specimens reached the failure load. It showed the good bond conditions which ensure the stress transmission from textile reinforcement to the SHCC. Besides, the average failure load of controlled series and the corresponding stress of roving are 11.1 kN and 969 MPa, respectively. It indicates that the tensile stresses of the yarns are much smaller than the tensile strength of textile (1700 MPa), and the combination of textile and SHCC cannot exploit the capacity of textile reinforcement to its full extent.

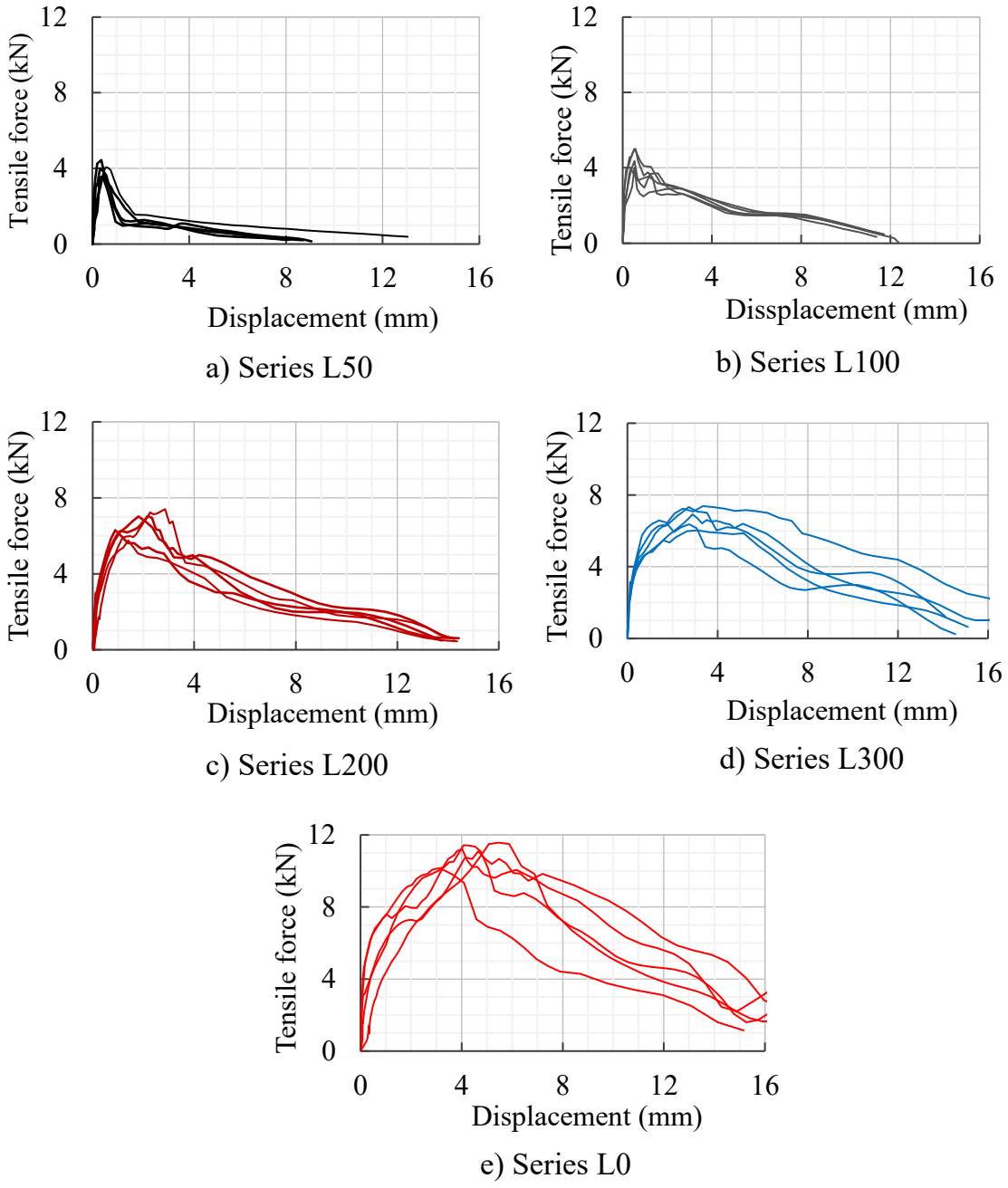

Figure 4.16 – Tensile Force-Displacement relationship of TR-SHCC

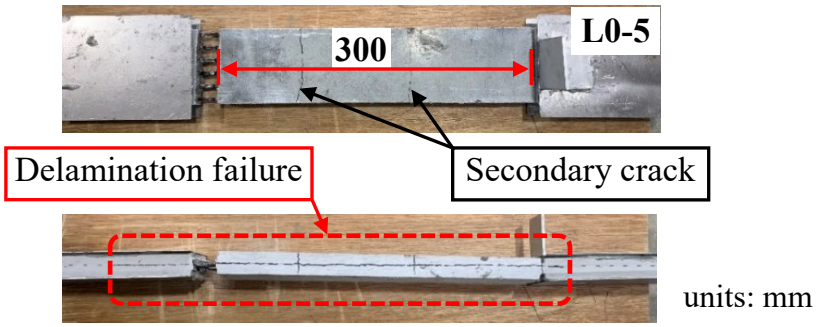

Figure 4.17 – Failure mode of Series L0

Results showed that the lap splice lengths of 50 and 100 mm (Series L50 and L100) are inadequate to establish satisfactory performance. Because of short lap splice length, only one crack could appear at one of the two notches, and pull-out failure had initiated before the second crack formed (see Figure 4.18). For series L50, the failure occurred simultaneously with the formation of crack. As a result, failure loads, as well as bond strength, were not defined. The bond between textiles and the mortar was only determined when textile reinforcements extracted from the mortar. In this stage, this bond based on the friction, which depicted by a considerable plateau. Compared to Series L50, Series L100 exhibited slightly different on behavior. As the crack had formed, the mechanical bond between matrix and reinforcement was activated that was depicted by an ascending branch of the load-displacement relation curve. After reaching the bond strength, the destruction of the mechanical bond occurred due to debonding of the yarn from the matrix. As a result, the pull-out failure occurs. Simultaneously, there is a significant increase in the relative displacement between textile reinforcement and mortar. Lastly, the remaining pull-out force was based on friction, which was identified by a considerable plateau. These characteristics of the pull-out failure in lap splice of members subjected to tensile forces are similar to the pull-out failure of lap splice that addressed in several pieces of research.

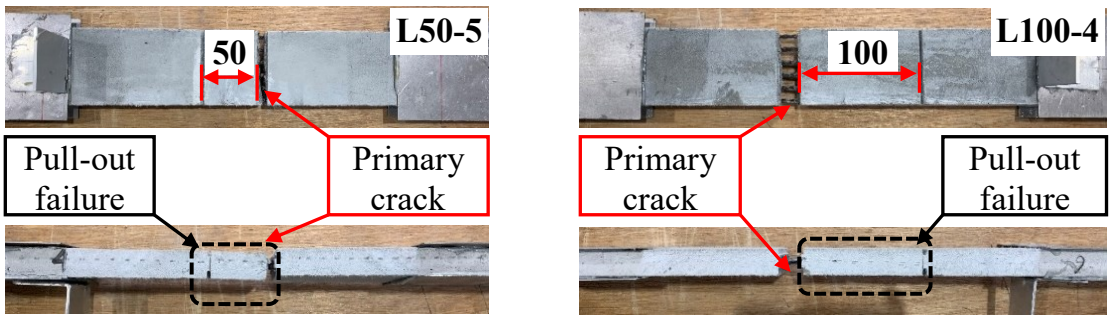

a) Series L50 b) Series L100 units: mm

Figure 4.18 – Pull-out failure of Series L50 and L100

For the lap splice length of 200 mm (Series L200), the load-bearing increased significantly, compared to Series L50 and L100. However, the average failure load of this series was still much smaller than this of the control series. A mixed failure, including delamination and pull-out failure, was observed (see Figure 4.19). The failure mechanism was carried out in the following order. Firstly, the cracks formed at the positions of two notches. Then, the delamination at the interface between textile fabric and concrete initiated at the location of one notch towards the other.

The expansion of the splitting area results in a shortening of the anchorage length. When the anchorage length was small enough (about 7-8 cm), a mixed failure including splitting and slipping occurred, which resulted in a sudden decrease in load-bearing capacity (see Figure 4.16c).

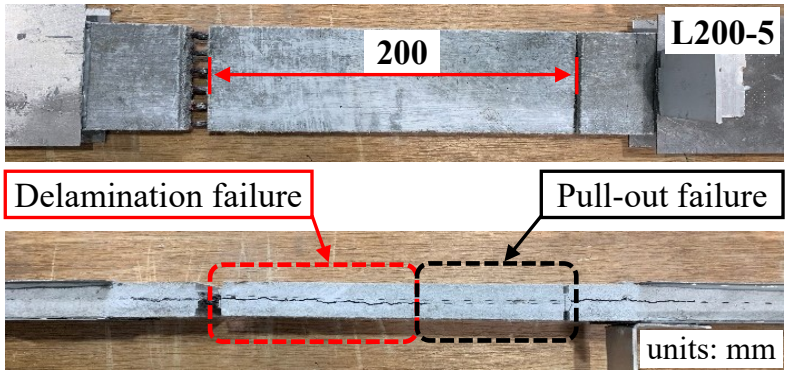

Figure 4.19 – Failure mode of Series L200

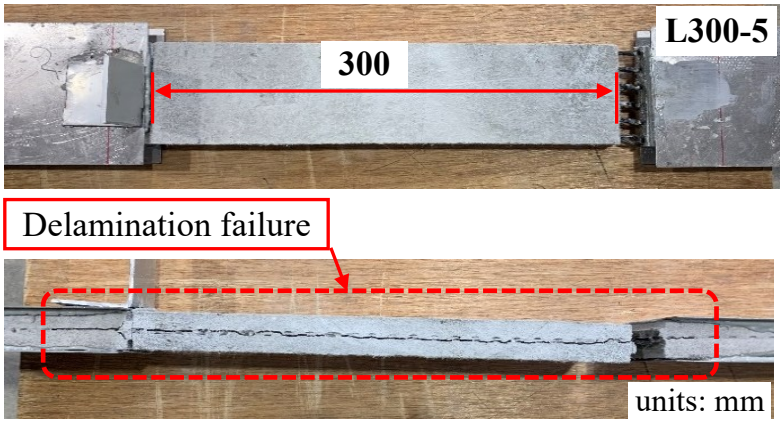

Figure 4.20 – Failure mode of Series L300

Increasing lap splice length to 300 mm, the dominant failure mode of specimens was delamination. The splitting along the entire lap splice length was observed (see Figure 4.20). Besides, for Series L300, although the lap splice length was much larger than Series L200, the load-bearing capacity of both series were almost equal, with the average failure loads of 6.9 kN and 6.7 kN, respectively. It is obvious, the required lap splice length must be greater than 300mm. In addition, previous research by Bui and Kunieda showed that the specimens with lap splice length of 300 mm exhibited similar behavior to the controlled series. The reason for this difference may be due to the tensile strength of examined mortar. Ortlepp (2009) indicated an approximately linear relationship between the delamination resistance

and the tensile strength of mortar. SHCC has a lower tensile strength, therefore being more vulnerable to delamination failure than the mortar in previous investigations. The controlled cracking behavior of SHCC did not contribute to enhancing the bonding and the composite between textile and mortar within the lap splice zone.

Table 4.6 – Test results of TR-SHCC specimens

Series	Specimen	Failure load (kN)	Average failure load (kN)	Disp.* (mm)	Failure mode
L0	L0-1	11.6	11.1	5.5	D+P*
	L0-2	10.1		3.2	D+P*
	L0-3	11.4		4.1	D+P*
	L0-4	11.1		4.7	D+P*
	L0-5	11.2		4.0	D+P*
L300	L300-1	6.6	6.9	1.4	D
	L300-2	7.4		3.4	D
	L300-3	6.3		3.1	D
	L300-4	7.3		2.7	D
	L300-5	6.9		2.9	D
L200	L200-1	5.8	6.7	1.4	D+P
	L200-2	6.3		0.9	D+P
	L200-3	7.0		1.8	D+P
	L200-4	7.4		2.9	D+P
	L200-5	7.0		2.2	D+P
L100	L100-1	3.7	3.4	1.6	P
	L100-2	3.8		1.3	P
	L100-3	3.0		2.2	P
	L100-4	3.0		2.3	P
	L100-5	3.5		1.3	P
L50	-	-	-	-	P
	-	-		-	P
	-	-		-	P
	-	-		-	P
	-	-		-	P

Disp.* – Displacement corresponding to failure load; P – Pull-out failure; D – Delamination failure; P* – Pull-out failure at end anchorage area.

Figure 4.21 compares the peak loads of lap spliced specimens made of SHCC, low and high strength ordinary mortar. For the examined matrixes, TRC specimens made of high strength ordinary mortar exhibits the highest load-bearing capacity. Besides, the lap splice length of 300 mm is adequate for the combination of this

mortar and the textile. On the contrary, for the specimens made up of SHCC or low strength ordinary mortar, the peak loads are much smaller, and the required lap splice length must be greater than 300 mm. Concerning the failure mode, different failure modes were observed among specimens with lap slice length of 300 mm. Low strength ordinary mortar has the weakest bond strength with textile (see section 3.3.3), and pull-out is the dominant failure of the specimens made of the textile and this mortar. Whereas, high strength ordinary mortar exhibits the greatest tensile strength, and has the highest bond strength with textile. Delamination is the primary failure mode of TRC specimens made of high strength ordinary mortar. For the TR-SHCC specimens, the bond strength and the tensile strength of SHCC is higher than those of low strength ordinary mortar. However, with lap splice length of 300 mm, the TR-SHCC specimens show a quite lower peak load than the specimens made of low strength ordinary mortar. The result for this might be the intense delamination failure, which leads to the decreasing of composite action between textile and SHCC. It verifies that the performance of textile reinforced concrete, particularly within the lap splice zone, is vulnerable to delamination.

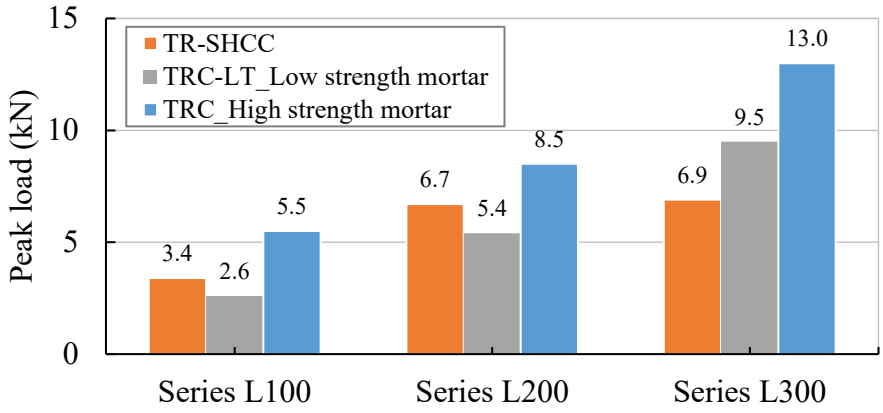

Figure 4.21 – Comparision the peak loads of specimens made of SHCC, low and high strength ordinary mortar

4.3. Lap Splice Length of Members Subjected to Bending Moment

Most researches on lap splice length of TRC members were carried out under pure tension loading. However, in many cases, textile reinforcement is spliced within flexural members. Thus, lap splices undergo moment or even both moment and shear. As a result, the behavior of splices within flexural members is more complicated as compared to lap splices within members subjected to uniaxial tensile load. One of the many reasons is that the presence of randomly primary or secondary

cracks in the concrete results in additional bond stresses due to the tension carried by the concrete between the cracks. Therefore, this section aimed to interpret the flexural failure behavior of lap splices in flexural beams through a four-point bending test.

4.3.1. Materials

Refer to section 2.2 for the properties of textile reinforcement as well as the composition of high strength ordinary mortar and SHCC. Tables 4.7 and 4.8 described the mechanical properties of ordinary mortar and SHCC.

Table 4.7 – Mechanical properties of high strength ordinary mortar

Characteristics	Value
Compressive strength (N/mm^2)	69
Splitting strength (N/mm^2)	3.9

Table 4.8 – Mechanical properties of SHCC

Characteristics	Value
Compressive strength (N/mm^2)	40.5
Tensile strength (N/mm^2)	4.2

4.3.2. Specimen Preparation

The TRC specimens with a dimension of 200×1200×50 mm were manufactured within steel formworks. The thickness of specimens determined by considering the application for repairing existing structures. The textile layer and mortar layers were placed into the formwork alternately with a mortar layer in its bottom and top. At first, a thin layer of mortar of about 10 mm cast into the formwork. Then, the textile fabric was placed on the top of the mortar and spliced by the other textile fabric. Special attention is the longitudinal yarns set along the length of formworks, and the lap splices are arranged in the middle of specimens. Afterward, the remaining mortar layer with a thickness of 4 cm cast into the formwork. All specimens cured in a constant temperature room (20^{o}C) for seven days.

Four series of test specimens were fabricated. The test specimen properties, including geometrical details, the number of specimens, and the values of lap splice length, have been listed in Table 4.9. In particular, Series L0 was fabricated without any splices as reference series. All investigated specimens came from the same

batch of mortar. Hence the comparable properties of examined mortars could be ensured.

Before the test, textile fabrics were stuck to specimens by glue. These textile layers partly covered specimens to prevent the delamination failure that might form outside the overlap area. The dimension and location of these covered textile layers were described in Figures 4.22 and 4.23. Besides, two notches were sawn using a diamond saw with a depth of 5 mm at the bottom surface of each specimen. The position of each notch coincided with the ending point of each spliced textile fabric. It means that the distance between the two notches equals the overlap length of the considered specimen. Pre-determined cracks initiated at the position of the notches. If the notches were not created, the primary cracks would form randomly in the pure moment area resulting in the variation of lapped splice length. For specimens containing the continuous textile reinforcement (Series L0), the distance between two notches was 300 mm.

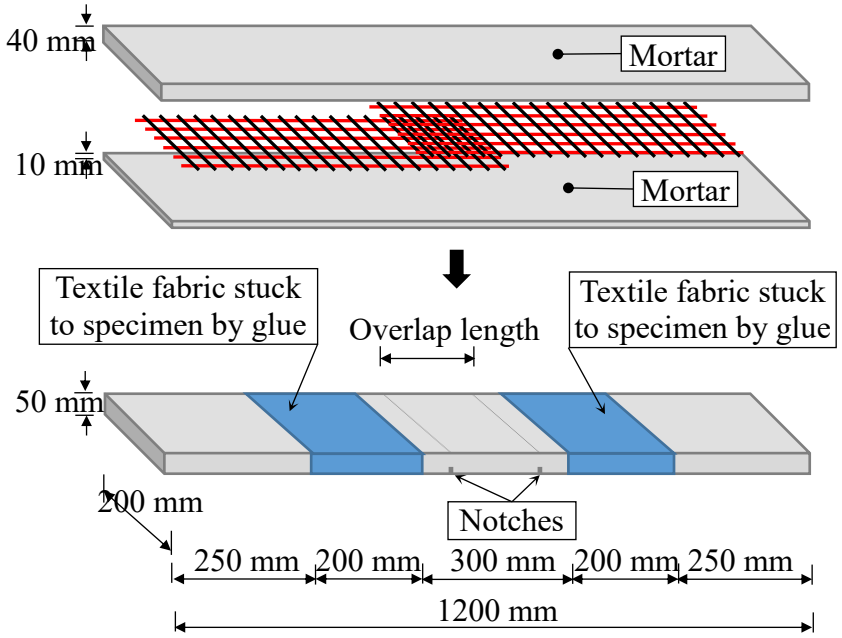

Figure 4.22 – Detail geometry of the specimens

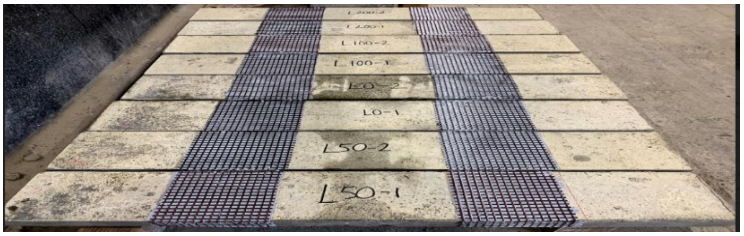

Figure 4.23 – Specimens used for the tests

Table 4.9 – Dimension and quantity of specimens

Series	Overlap length L_l (mm)	Width x Length x Height (mm)	Number of specimens
L0	-	200 x 1200 x 50	2
L50	50	200 x 1200 x 50	2
L100	100	200 x 1200 x 50	2
L200	200	200 x 1200 x 50	2
L300	300	200 x 1200 x 50	2

4.3.3. Test Setup

As illustrated in Figure 4.24, four-point bending tests were conducted on test specimens where the middle part of the beams was subjected to pure bending. The lap splices were located in the middle zone to eliminate the effects of shear actions on the results. The test setup was designed to provide simple supports at both ends of the beams. Two-point loads were applied to the top face of the specimens through a spreader beam by means of an actuator. The distance between two point loads was 300 mm. On the top of the spreader beam, a load cell with a capacity of 100 kN was utilized to measure applied loads. Two Displacement Transducers (DT) were employed at the bottom surface to record the deflection at the sections that load applied. Two other DTs were placed on the top surface to measure the displacements at the section of supports.

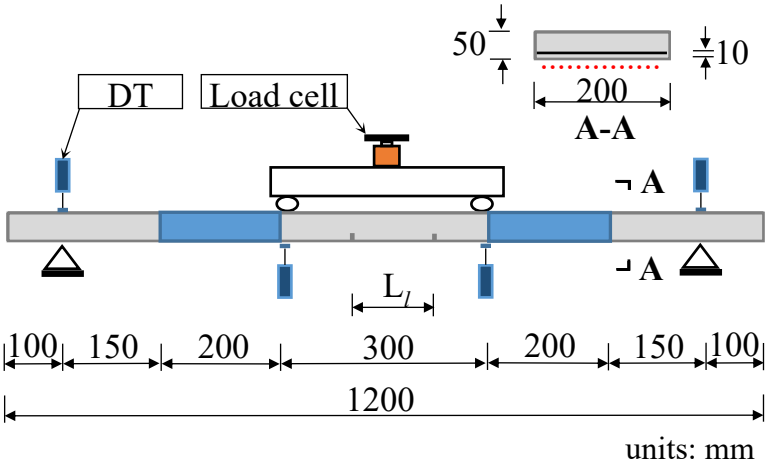

Figure 4.24 – Schematic of test setup of four-point bending test

4.3.4. Results and Discussion of High Strength Ordinary Mortar Case

The results of the four-point bending test on TRC members in terms of failure mode, failure load, and corresponding displacement are reported in Table 4.10. In addition, the load-displacement relationship of five series is described in Figure 4.25. Clearly, the results show that the load-bearing capacity of flexural specimens increased steadily with the increase of lap splice length. The average failure load of Series L200 is 3.3 kN, which is approximately 2 and 4 times higher than the average failure loads of Series L100 and L50, respectively. Besides, different failure modes were observed including pull-out and delamination failures, but the breakage of the textile did not occur.

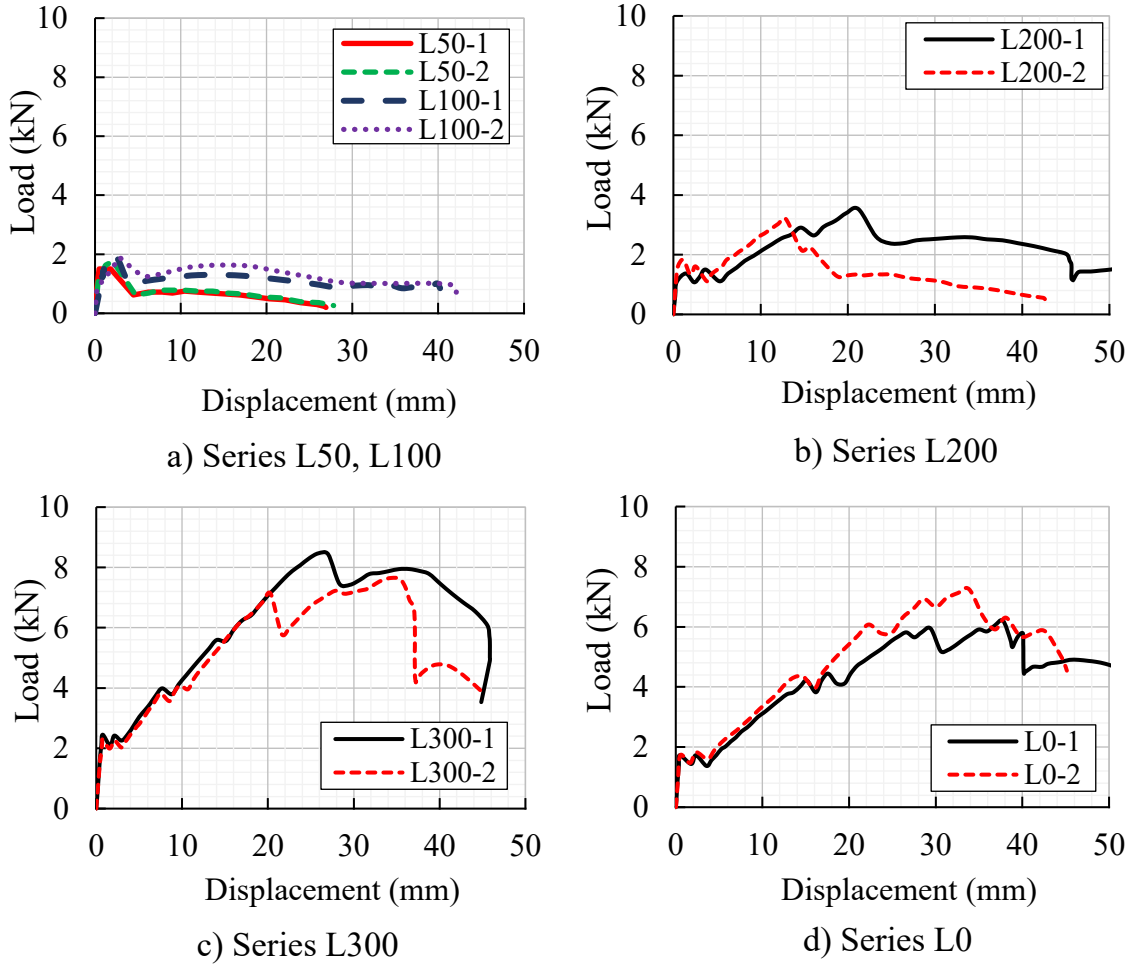

a) Series L50, L100

b) Series L200

c) Series L300

d) Series L0

Figure 4.25 – Load - Displacement relationship

Table 4.10 – Report of result of four-point bending test

Series	Specimen	Failure load (kN)	Disp.* (mm)	Failure mode
L0	L0-1	6.2	37.7	D
	L0-2	7.3	33.8	D
L50	L50-1	0.75	10.4	P
	L50-2	0.75	13.7	P
L100	L100-1	1.89	7.68	P
	L100-2	1.63	17.9	P
L200	L200-1	3.4	19.8	P
	L200-2	3.2	12.9	D
L300	L300-1	8.5	25.9	D
	L300-2	7.6	35.4	D

Disp. * – Displacement corresponding to failure load;
D – Delamination failure (the separation between textile layer and mortar together with the occurrence of horizontal cracks on both sides of specimens);
P – Pull-out failure.

For reference Series L0, the flexural behavior of specimens with continuous textile reinforcement is described in Figure 4.25d. The deflection increases linearly together with the increase of applied load in the elastic stage for the uncracked specimens. The cracks firstly appear at one of two notches in the pure flexural zone when the ultimate tensile strain of the matrix at the edge of the tension zone is achieved. Then the second crack forms at the position of the remaining notch. The load-displacement curves fluctuate during the development of cracks. Delamination failure mode that occurred inside and outside the pure flexural zone could be observed when the load exceeds the load-bearing capacity of the specimens (Figure 4.26).

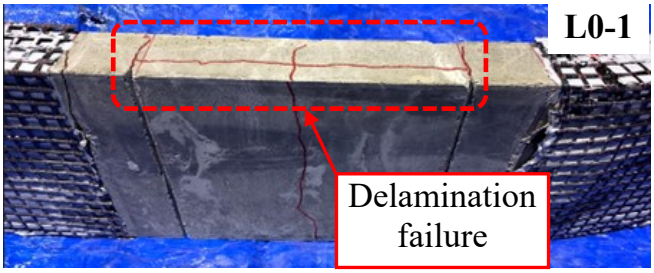

Figure 4.26 – Failure mode of Series L0

Results show that the overlap length of 50 and 100 mm (Series L50 and L100) is not enough to guarantee the complete transfer of tensile stresses from one fabric

to another, as shown in Figure 4.25. For a very short lap splice length of 50 mm, only one crack could appear at the location of the notch (see Figure 4.27a). Because of weak composite, failure had started before the second crack forming. In Figure 4.25a, the applied load suddenly drops when the crack forms in the pure flexural zone. As the matrix lost the load-bearing capacity, the mechanical bond between the matrix and reinforcement was activated, which was depicted by an ascending branch of the load-displacement relation curve. After reaching the bond strength, the destruction of the mechanical bond occurred due to debonding of the yarn from the matrix. As a result, the pull-out failure occurs. Simultaneously, there is a significant increase in the relative displacement between textile reinforcement and mortar. Lastly, the remaining pull-out force was based on friction, which was identified by a considerable plateau. These characteristics of the pull-out failure in lap splice of members subjected to bending are similar to the pull-out failure of lap splice under a uniaxial force that addressed in several pieces of research [Bui and Kunieda (2019, 2020)]. When the deflection increases, the embedded length of textile reinforcement within the lap splice zone reduces, which leads to a gradual decrease of applied force. The increase of the overlap length up to 100 mm allows more effective force transmission between textile fabrics. Compare to Series L50, the behavior of lap splice of Series L100 is slightly different. Longer overlap length leads to larger force transmission from one textile fabric to another. As a result, the second crack formed at the position of the remaining notch, and the load-bearing capacity of specimens increases significantly.

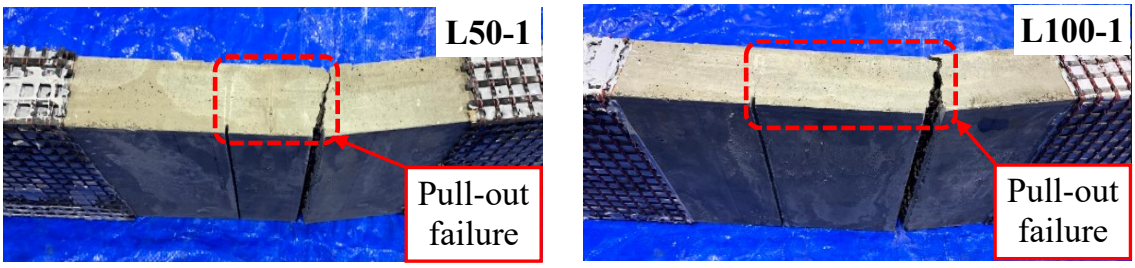

a) Series L50 b) Series L100

Figure 4.27 – Failure mode of series L50, L100

For the lap length of 200 mm (Series L200), before reaching the ultimate limit state, the flexural behavior of this series seems similar to Series L0 (Figure 4.25b). However, the flexural behavior became more complicated when specimens were under failure load. Two examined specimens provided different types of failure

modes. The first specimen L200-1 occurred pull-out failure associated with a crack at the middle of the lap splice length (Figure 4.28a). Meanwhile, delamination failure was dominant in specimen L200-2 (Figure 4.28b). The position of primary crack has a strong effect on the failure mode of the TRC beam with lap splice. For Series L200, the lap splice length is sufficiently long, so that in addition to cracks at the position of notches, the primary crack might form randomly in the lap splice area. If the primary crack forms at one of two notches, the delamination failure will dominate. If primary crack forms in the region between two notches, the pull-out failure might occur.

For Series L300, the failure load of this series is approximately equal to the control series (Table 4.9). Also, the load-deflection curves and the failure mode of both Series L300 and L0 are not too much different (Figure 4.29). These indicate that the lap splice length of 300 mm can provide sufficient composite performance between textile and concrete, hence the Series L300 is fully mechanically guaranteed compared to control beams with continuous textile fabrics.

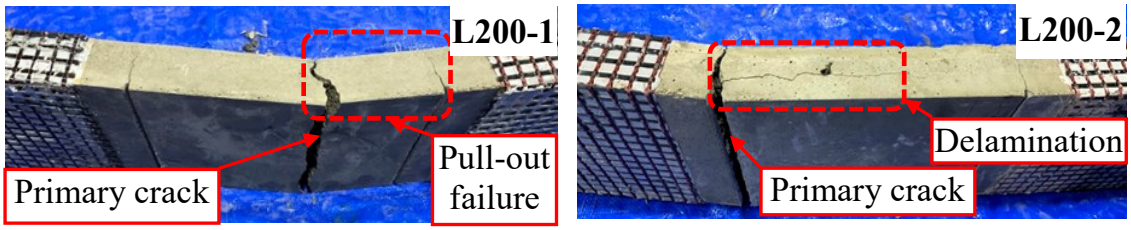

a) Specimen b) Specimen

Figure 4.28 – Different failure modes of series L200

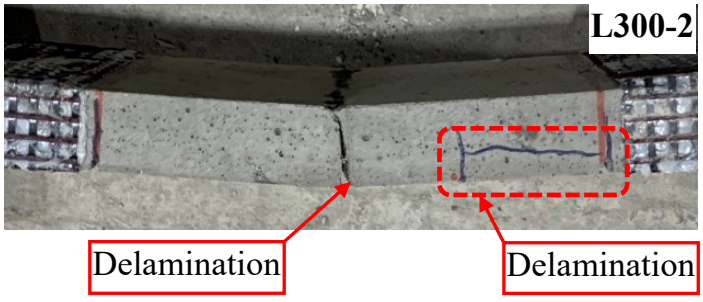

Figure 4.29 – Failure modes of series L300

4.3.5. Results and Discussion of TR-SHCC Specimens

Similar four-point bending tests were also conducted on TR-SHCC beams. Figure 4.30 and Table 4.10 showed the load-deflection relationship and other results of the four-point bending test. It can be observed that the peak load and the corresponding deflection of specimens increased with the increase of lap splice length. For all test specimens, the first crack, which was also the primary crack, formed at one of the two notches. Besides, before reaching the peak load, fine cracks within the pure moment area were observed (Figures 4.31 and 4.32). These fine cracks were a characteristic of SHCC, which exhibits high inelastic deformations and crack bridging ability in the strain-hardening phase. In the post-peak stage, different failure modes were observed. The controlled Series L0 showed delamination failure. The splitting at the interface of textile and SHCC initiated at the position of the primary crack, then extended to the entire of pure moment zone. For Series L300 and L200, a mixed failure, including delamination and pull-out was reported. The delamination originated at the position of the crack towards the discontinued endpoint of the textile fabric. The expansion of the splitting area results in a shortening of the anchorage length. When the anchorage length was inadequate, a mixed failure, including splitting and slipping occurs, which resulted in a sudden decrease in load-bearing capacity (Figure 4.30 b and c). For Series L100 and L50, due to short lap splice length and the weak bond between textile and SHCC, dominant failure was pull-out.

In terms of load-bearing capacity, Series L300 and L200 provided the average peak load of 5.75 and 6.15 kN respectively, almost equal to controlled series. However, the deflection corresponding to the peak load of these two series was much smaller than that of Series L0 (see Table 4.11). Obviously, Series L300 and L200 exhibited lower ductility, comparing to the control series. This indicated that the lap splice lengths of 200 and 300 mm were insufficient to ensure the performance of TR-SHCC members.

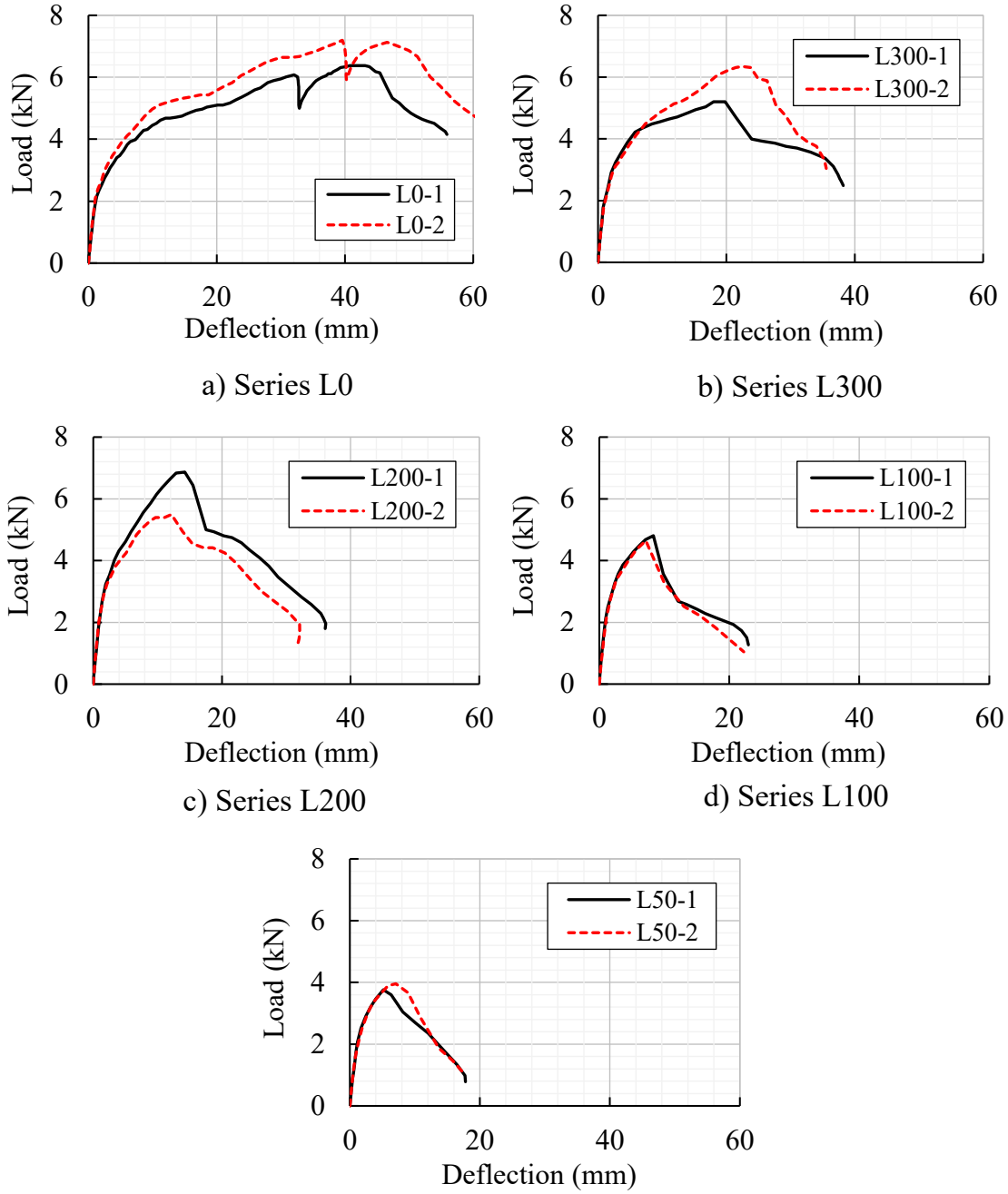

Figure 4.30 – Load-Deflection relationship of TR-SHCC beams

Table 4.11 - Test results of four-point bending test of TR-SHCC

Series	Specimen	Failure load (kN)	Disp.* (mm)	Failure mode
L0	L0-1	6.5	43.1	D
	L0-2	7.2	40.0	D
L30	L300-1	5.2	19.8	D+P
	L300-2	6.3	22.4	D+P
L200	L200-1	6.8	14.2	D+P
	L200-2	5.5	12.1	D+P
L100	L100-1	4.8	8.3	P
	L100-2	4.6	7.1	P
L50	L50-1	3.8	5.1	P
	L50-2	4.0	7.1	P

Disp. * – Displacement corresponding to failure load; D – Delamination failure (the separation between textile layer and mortar together with the occurrence of horizontal cracks on both sides of specimens); P – Pull-out failure.

a) Series L0

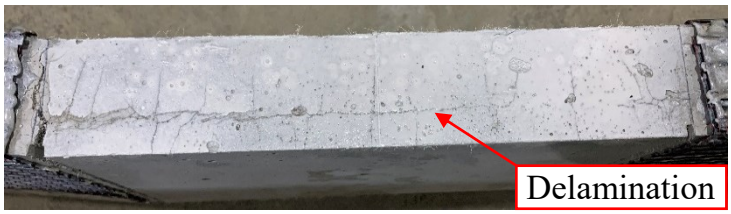

b) Series L300

Figure 4.31 – Crack patterns of Series L0 and L300

a) Series L200

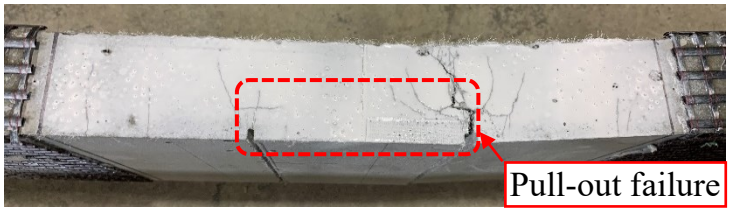

b) Series L100

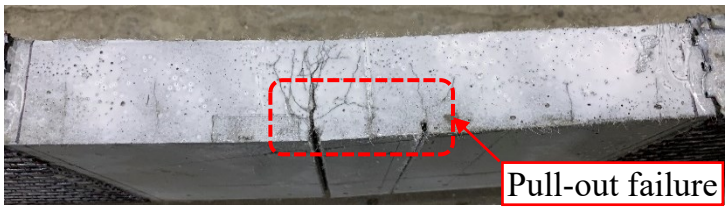

c) Series L50

Figure 4.32 – Crack patterns of Series L50, L100, and L200

Figures 4.33 and 4.34 compared the results of TRC and TR-SHCC specimens. For control series, it can be seen that the peak loads and associated deflections of TRC and TR-SHCC were almost equal. Meanwhile, for the lap splice length less than or equal to 200 mm, the load-bearing capacity of TR-SHCC specimens was much greater than that of TRC members. The reason may be the major contribution of SHCC in pre-peak response. In contrast, in the post-peak stage, due to the weak frictional bonding between textile and SHCC, TR-SHCC specimens exhibited low performance, particularly in Series L100 and L50.

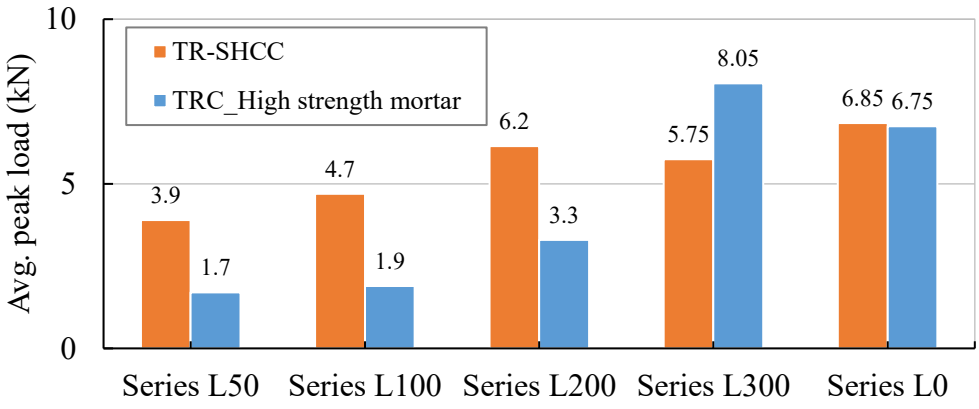

Figure 4.33 – Average peak load of TRC and TR-SHCC specimens

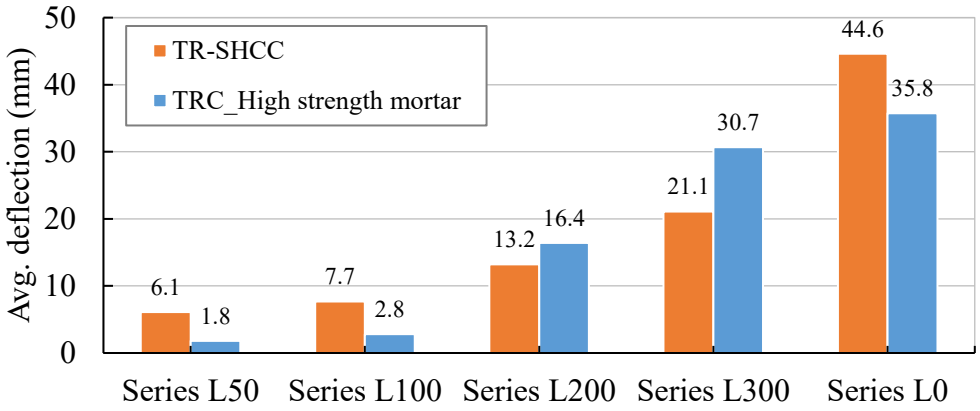

Figure 4.34 – Average deflection corresponding to peak load of TRC and TR-SHCC specimens

4.4. Summary

In this chapter, an experimental investigation on lap splice length of textile reinforced concrete members was conducted. Two types of the member were examined, including members subjected to tensile force and members under bending moment. This research also compared the results of members made of ordinary mortar versus SHCC. The following conclusions are given:

(1) The load-bearing of the specimens increased with the increase of lap splice length.

(2) The dominant failure of all specimens with a short overlap length of 50 and 100 mm was pull-out.

(3) Different failure modes were observed, including pull-out and delamination failures, but the breakage of textiles did not occur. The combination of textile and examined mortars could not exploit the capacity of textile reinforcement to its full extent.

(4) For the specimens made of high strength ordinary mortar, the lap splice length of 300 mm is adequate for both type of members

(5) For specimens made of SHCC, in the case of specimens subjected to tensile force, the load-bearing capacity of test specimens with lap splice was much smaller than the corresponding value of controlled specimens. In the case of specimens subjected to bending moment, although the peak loads of control series and Series L300 were almost equal, their ductility was markedly different. For TR-SHCC specimens, the required lap splice length must be greater than 300 mm.

(6) TR-SHCC exhibited weak frictional bonding that depicted by a sudden drop of applied load in the post-peak stage. The crack width control function of SHCC was not efficient to improve bond strength.

(7) For TRC-LS specimens made of low strength ordinary mortar, due to the weak bond strength between textile and mortar, the dominant failure mode is pull-out, and lap splice length of 300 mm is inadequate. Delamination failure occurred in specimens with better bond strength (specimens made of SHCC or high strength ordinary mortar). The extent of delamination seems to be more intense in the lap spliced specimens made of lower tensile strength matrix (TR-SHCC specimens). As a result, for Series L300, the load-bearing capacity of TR-SHCC specimens is much lower compared to TRC specimens made of high strength ordinary mortar.

(8) The research verifies the performance of textile reinforced concrete, particularly within the lap splice zone, is vulnerable to delamination failure.

CHAPTER 5

STRESS TRANSFER LENGTH BETWEEN TEXTILE AND REBARS

5.1. Introduction and Background

The main features of TRC are its high tensile strength and ductile behavior, as well as its high corrosion and temperature resistance. TRC, with its excellent mechanical properties, is expected to deliver protection, namely, isolate the structure from the environment by preventing the penetration of fluids and deleterious materials, and achieving all of these when used as a thin-sheet component. It is of particular importance when used as a repair material and combined in a reinforced concrete element where it is expected to act as an external skin to facilitate the protection of the reinforcing steel while keeping the cover quite small in depth. When repairing an old concrete structure, all deteriorated concrete is removed, and steel bars are exposed. The thin TRC layer is poured over the rebars to make the strengthening layer and provide cover protection (see Figure 5.1). The force transfer from the textile reinforcement to the aged concrete and rebars is the fundamental factor influence the effectiveness of the strengthening layer, therefore this issue should be considered and examined.

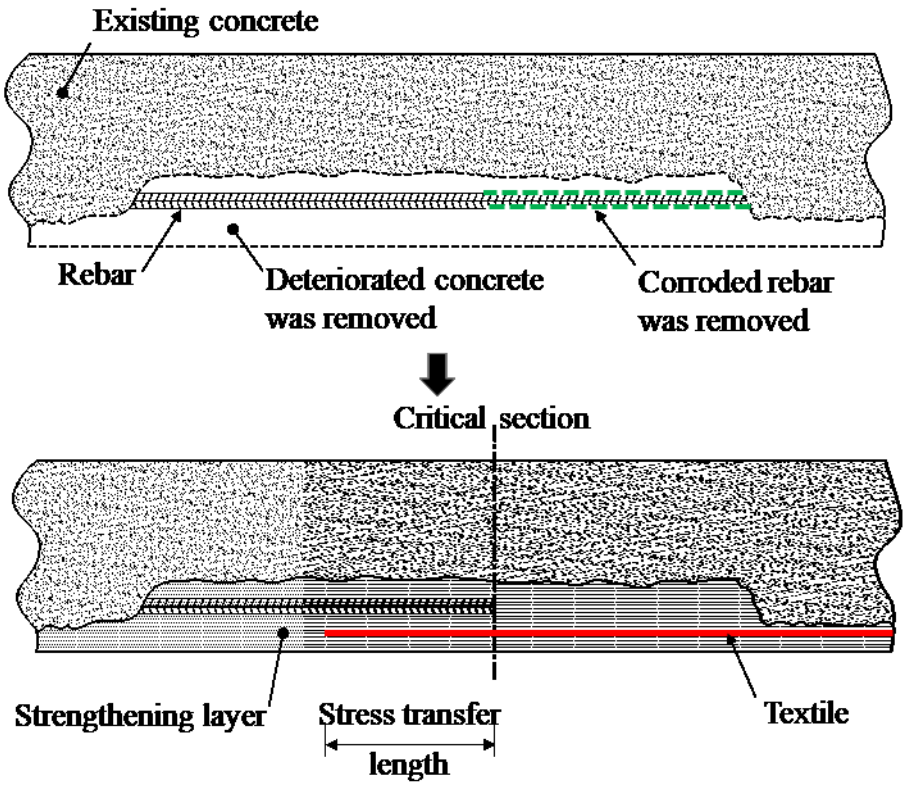

Figure 5.1 – Using TRC to repair existing flexural concrete structures

In terms of the promising application of TRC, the practical use of this new material needs structural detailing provisions, including stress transfer length between textile reinforcement and rebars. The fundamental requirements of strength and robustness of a TRC structure cannot be met unless the tensile reinforcing bars at each critical section are adequately embedded on both sides of the critical section. The anchorage on each side of a critical section (also referred to as "embedment length") must ensure that the bar force is fully transferred to surrounding concrete and rebars through bonding.

In the literature, most researches on stress transfer length of TRC members were carried out under uniaxial tensile loading. However, the conditions favorable for the development of bond stress in the tensile tests are very rarely present in practical TRC members, where the situation is more complicated due to the presence of one or more cracks crossing the embedment length. Also, factors such as splitting, diagonal tension, shear force, and the change of moment along the embedment length may lead to more complicated flexural behavior within the anchorage zone of flexural members. As a result, the determination or estimation of stress transfer length based on the result of the tensile test is not reasonable and reliable. Therefore,

this research aimed to interpret the flexural failure behavior of the embedment zone and determine the stress transfer length of TRC beams through a four-point bending test.

5.2. Test Program

5.2.1. Materials

Refer to section 2.2 for the properties of textile reinforcement as well as the composition of ordinary mortar and SHCC. Tables 5.1 and 5.2 described the mechanical properties of high strength ordinary mortar and SHCC.

Table 5.1 – Mechanical properties of high strength ordinary mortar

Characteristics	Value
Compressive strength (N/mm^2)	75.3
Splitting strength (N/mm^2)	7.8

Table 5.2 – Mechanical properties of SHCC

Characteristics	Value
Compressive strength (N/mm^2)	40.5
Tensile strength (N/mm^2)	4.2

5.2.2. Specimen Preparation

The TRC specimens with a dimension of 200mm×1200mm×100mm cast into metal formworks. The textile fabric, rebars, and mortar layers were placed into the formwork alternately with a mortar layer in its bottom and top. At first, a thin layer of mortar of 20 mm poured into the formwork. Then, the textile fabric was placed on the top of the mortar layer. Special attention was the longitudinal yarns were set along the length of formworks, and the embedment zone arranged in the middle of specimens. Afterward, three rebars with a diameter of 10 mm were used to reinforce the beams. Plastic spacers were adopted to keep the accuracy of a concrete cover thickness of 30 mm. Finally, the remaining mortar layer with a depth of 80 mm was poured into the formwork (Figure 5.2). All specimens cured in a constant temperature room (20oC) for 28 days. Five series of specimens were fabricated. The test specimen properties, including geometrical details, the number of specimens, and the values of embedment length have been listed in Table 5.3. In particular, Series L0 made from continuous textile fabric without any rebars.

Before the test, textile fabrics were stuck to specimens by glue. These textile layers partly covered the specimens to isolate the embedment zone and prevent the failure that might form outside the constant moment zone. The dimension and location of these textile layers described in Figure 5.2. Besides, a notch with a depth of 5 mm was sawn at the soffit of each specimen. The position of the notch coincided with the discontinued point of the rebars. It means that the distance between the notch and the halted point of textile fabric was the stress transfer length of the considered specimens. Pre-determined cracks initiated at the position of the notches. If the notches were not created, the primary cracks would form randomly in the pure moment area resulting in the variation of embedment length. For the control specimens (Series L0), the notch located at one of two bottom edges of the constant moment zone.

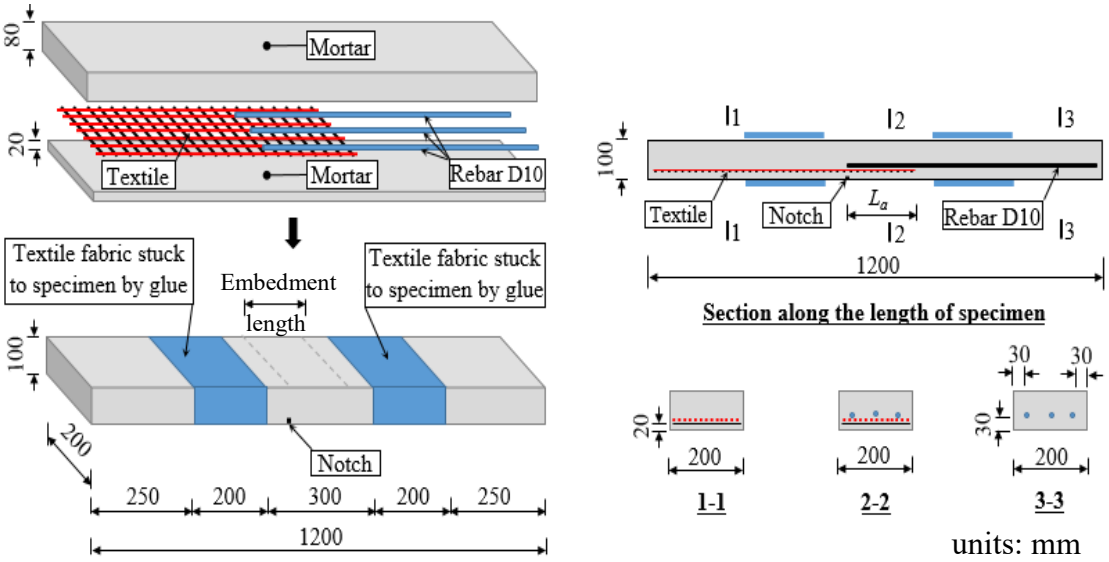

Figure 5.2 – Sketch of specimen used for flexural test

Table 5.3 – Dimensions and quantity of specimens

Series	Embeddment length L_a (mm)	Width x Length x Thickness (mm)	Number of specimens
L0	-	200 x 1200 x 100	2
L50	50	200 x 1200 x 100	2
L100	100	200 x 1200 x 100	2
L200	200	200 x 1200 x 100	2
L300	300	200 x 1200 x 100	2

5.2.3. Test Setup

As illustrated in Figure 5.3, four-point bending tests were conducted on test specimens where the middle part of the beams was subjected to pure bending. The embedment zone was located in the middle part to eliminate the effects of shear actions on the results. The test setup was designed to provide simple supports at both ends of the beams. Two-point loads were applied to the top face of the specimens through a spreader beam using an actuator. The distance between two point loads was 300 mm. On the top of the spreader beam, a load cell with a capacity of 100 kN utilized to measure applied loads. Two Displacement Transducers (DT) were employed at the bottom surface to record the deflection at the sections that load applied. Two other DTs were placed on the top surface to measure the displacements at the section of supports.

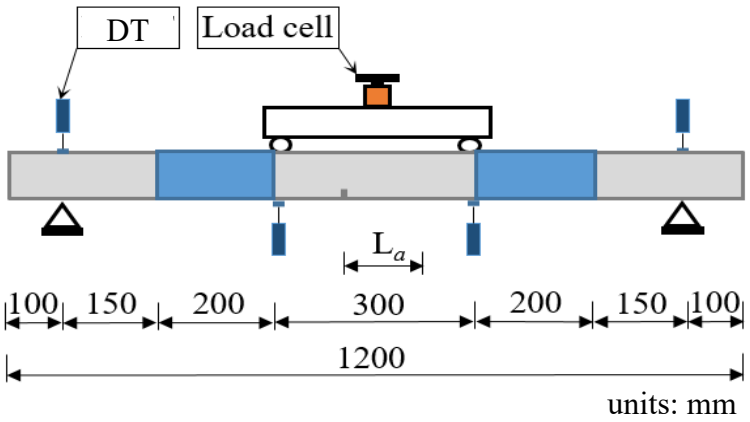

Figure 5.3 – Sketch of test setup

5.3. Results and Discussion

5.3.1. High Strength Ordinary Mortar Case

The results of the four-point bending test on TRC members in terms of failure mode, failure load, and corresponding displacement were reported in Table 5.3. Furthermore, the load-deflection relationship of five series was described in Figure 5.4. It is obvious, the load-bearing capacity of flexural specimens increased steadily with the increase of stress transfer length. Series L300 has an average bearing capacity of 17.2 kN, which is much greater than the average failure loads of Series L200, L100, and L500. Also, the results show that the failure loads of both Series L300 and L0 are approximately equal, and their flexural behavior is almost the

same. These indicate that the embedment length of 300 mm could effectively transmit the tensile force from textile reinforcement to surrounding concrete. Besides, different failure modes were observed, including pull-out, delamination, and mixed failures, but the fracture of the textile itself did not occur.

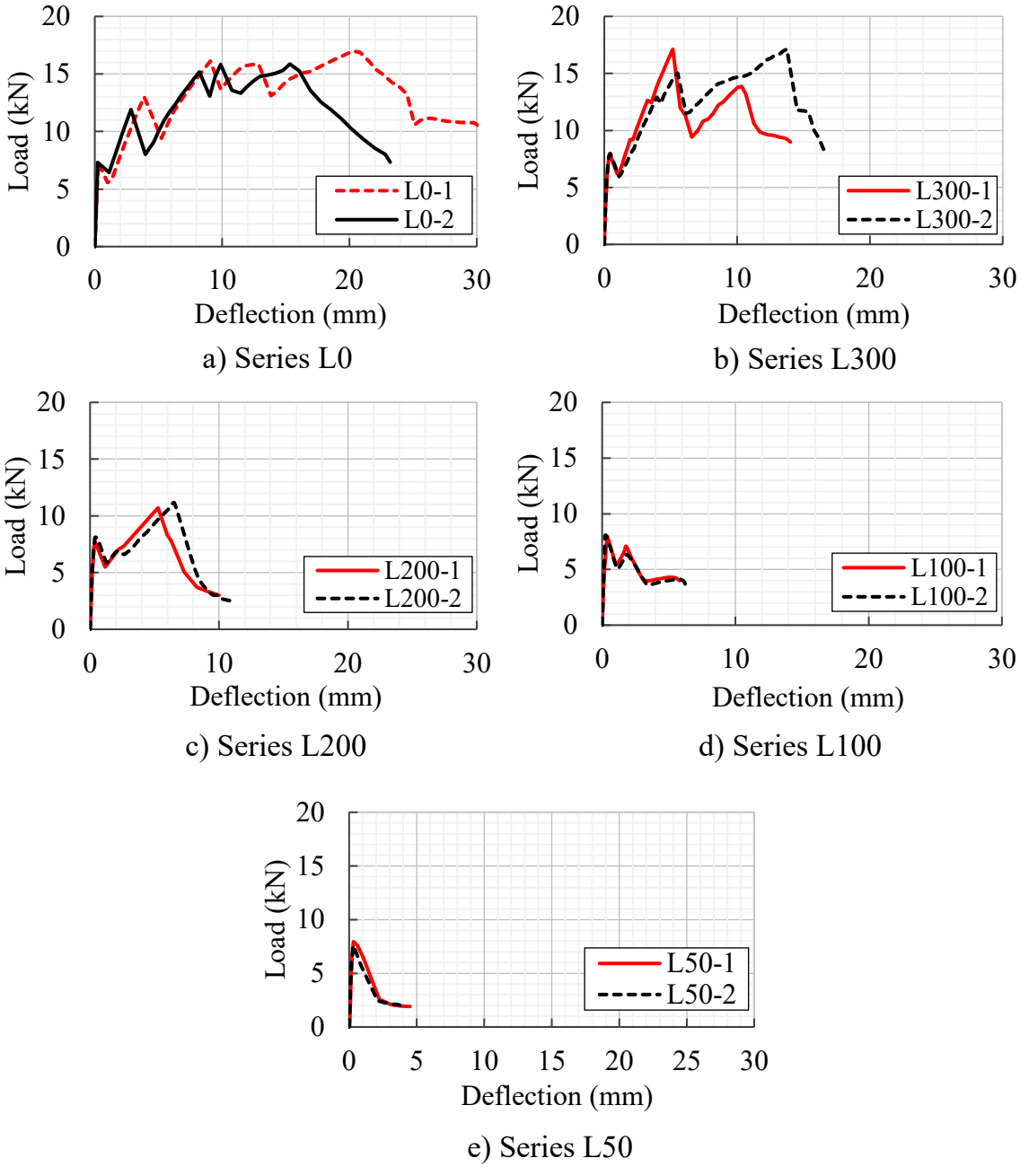

Figure 5.4 – Load-deflection relationship of all series

Table 5.4 – Test result of TRC specimens

Series	Specimen	Failure load (kN)	Disp.* (mm)	Failure mode
L0	L0-1	17.1	20.5	D
	L0-2	16.1	15.4	D
L50	L50-1	N/A	N/A	P
	L50-2	N/A	N/A	P
L100	L100-1	7.1	1.8	P
	L100-2	6.3	1.9	P
L200	L200-1	10.3	4	D + P
	L200-2	11.1	6.6	D + P
L300	L300-1	17.3	5.0	D
	L300-2	17.1	13.8	D

Disp. *– Displacement corresponding to failure load.
D – Delamination failure (the separation between the textile layer and mortar together with the occurrence of horizontal cracks on both sides of specimens).
P – Pull-out failure.
N/A – Not Available due to pull-out failure occurred as soon as the first crack had formed.

For the control Series L0, the flexural behavior of specimens with continuous textile reinforcement was described in Figure 5.4a. The deflection increased linearly combined with the increase of applied load in the elastic stage of the uncracked specimens. The first crack initiated at the position of the notch when the ultimate tensile strain of the concrete at the edge of the tension zone had achieved. The load-displacement curve fluctuated during the formation of secondary flexural cracks within a constant moment zone. The dominant failure of this series was delamination/longitudinal concrete splitting between textile and concrete. Furthermore, this delamination failure occurred outside the pure flexural zone, as shown in Figure 5.5.

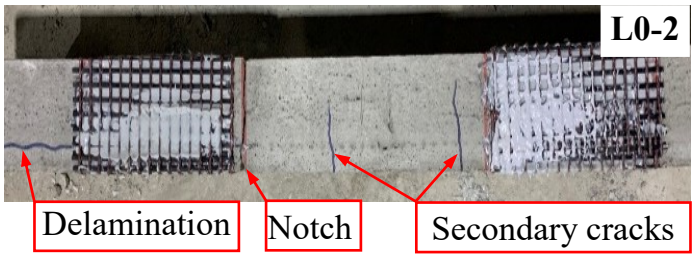

Figure 5.5 – Side view of specimen L0-2

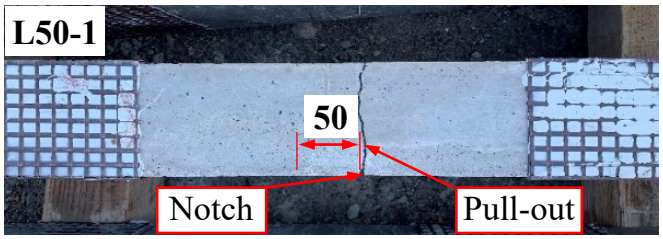

a) Side view of specimen L50-1

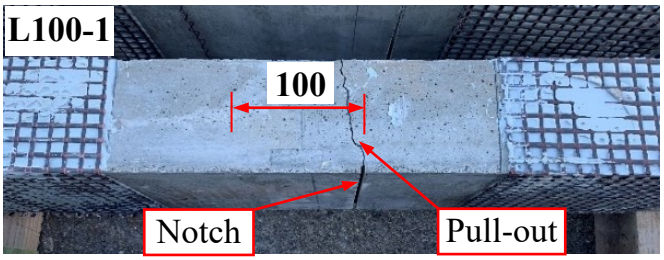

b) Side view of specimen L100-1 units: mm

Figure 5.6 – Pull-out failure of series L50 and L100

The results showed the embedment length of 50 and 100 mm (Series L50 and L100) was not enough to guarantee the complete transfer of tensile stresses from the textile fabric to surrounding concrete, and the dominant failure mode was pull-out. All specimens of these two series had unique crack formed at the position of the notch, and the extraction of the yarns was accompanied by the widening of this crack (see Figure 5.6). The load-deflection relationship of Series L100 in Figure 5.4d presents the typical characteristics of pull-out failure. Firstly, the deflection increased almost linearly with the increase of the applied load. When the concrete reached tensile strength, a crack initiated at the position of the notch, and the applied load suddenly dropped. As the concrete lost the load-bearing capacity, the mechanical bond between the concrete and reinforcement was activated that depicted by an ascending branch of the load-deflection curve. After reaching the bond strength, the destruction of the mechanical and chemical bond occurred due to debonding of the yarn from the matrix. As a result, the failure due to yarn extraction happened. Simultaneously, there is a significant increase in the relative displacement between textile reinforcement and mortar. Lastly, the friction mechanism between textile reinforcement and surrounding concrete was contributed to the bond strength resistance, which was identified by a considerable plateau. These pull-out characteristics are similar to those of members under a uniaxial force that addressed in section 4.2. Decreasing the embedment length to 50 mm resulted in a slight change in the flexural behavior of Series L50. Shorter embedment length led to smaller bond strength. Therefore, Series L50 was vulnerable to the damage under the impact of crack propagation. As shown in Figure

5.4e, the extraction of textile yarns from concrete occurred immediately after the cracking of concrete and the second peak was almost not observed. Besides, the results of the two series showed that the average applied load during the pull-out phase was proportional to the embedment length of the textile reinforcement. The applied load of Series L50 was 2 kN which is half that of Series L100.

For Series L200, increasing the embedment length to 200 mm led to the significant increase of load-bearing capacity compared to those of Series L100 and L50. Series L200 failed in flexure at an average load of 10.7 kN, greater than the failure loads of Series L100 and L50. Besides, as illustrated in Figure 5.4c, the load-deflection curve of the Series L200 is relatively similar to that of the Series L100 with a dual-peak response. However, Series L200 displayed a markedly different failure mode than Series L100 and L50. A mixed failure, including delamination and pull-out failure, was observed (see Figure 5.7). The failure mechanism was carried out in the following order. The delamination at the interface between textile fabric and concrete originated at the position of the crack towards the discontinued endpoint of the textile fabric. It means that the expansion of the splitting area results in a shortening of the embedment length. When the embedment length was small enough, a mixed failure including splitting and slipping occurs, which resulted in a sudden decrease in load-bearing capacity.

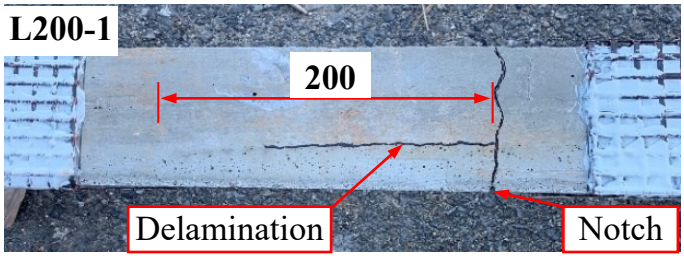

Figure 5.7 – Delamination failure of Series L200

In the series under consideration, the series L300 displays a flexural behavior broadly similar to the control series L0. This is evidenced by several characteristics: (i) It can be seen that the load-deflection curves of both series L300 and L0 are insignificantly different; (ii) These two series have the average failure load, respectively, 17.2 kN and 16.6 kN, which are approximately equal; (iii) Series L300 shows a crack pattern quite similar to control series with the formation of secondary cracks within pure moment zone (see Figure 5.8); (iv) Both series failed by the

delamination between textile fabric and concrete although the distribution of splitting zones among two series is slightly different. These indicate that the stress transfer length of 300 mm can provide satisfactory composite performance between textile and concrete, hence the series L300 is fully mechanically guaranteed compared to control beams with continuous textile fabrics. In previous tests on determining lap splice length of textile reinforcement, a minimum lap splice length of 300 mm was also required to provide for TRC members.

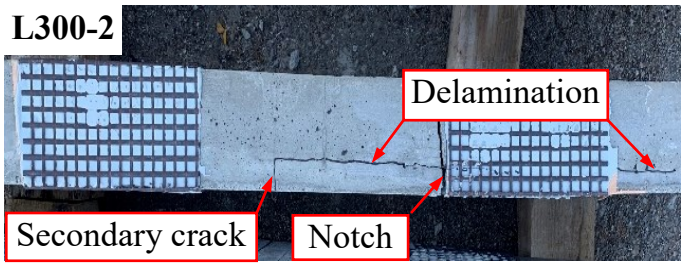

Figure 5.8 – Side view of specimen L300-2

5.3.2. TR-SHCC Case

Similar four-point bending tests were also conducted on TR-SHCC beams. Figure 5.9 and Table 5.5 showed the load-deflection relationship and other results of the four-point bending test. For all test specimens, the first crack, which was also the primary crack, formed at the position of the notch. In addition, before reaching the peak load, the development of fine cracks within the pure moment area was observed, which led to the decrease of the stiffness of TR-SHCC beams. For control series, two specimens exhibited different failure modes. Specimen L0-2 showed a breakage of textile rovings that represented a sudden drop of applied load in the post-peak stage. Meanwhile, the dominant failure of specimen L0-1 was delamination (Figure 5.11). The decrease in load-bearing behavior occurred gradually as illustrated in Figure 5.9 a.

For Series L300, L200, and L100, the average peak loads of these series were almost equal and were not significantly smaller compared to controlled Series L0. It is obvious that the embedment lengths of textile reinforcement affected slightly on the magnitude of the peak load. In the pre-peak stage, the behavior of TR-SHCC beams mainly influenced by the contribution of SHCC. Meanwhile, in the post-peak stage, the shorter embedment lengths led to a more sudden drop in the applied load.

Besides, the deflections at the peak load of Series L300, L200, and L100 was much smaller than that of the controlled series. These series exhibited lower ductility, comparing to the control series. This indicated the lap splice lengths of 200 and 300 mm were insufficient to ensure the performance of TR-SHCC members.

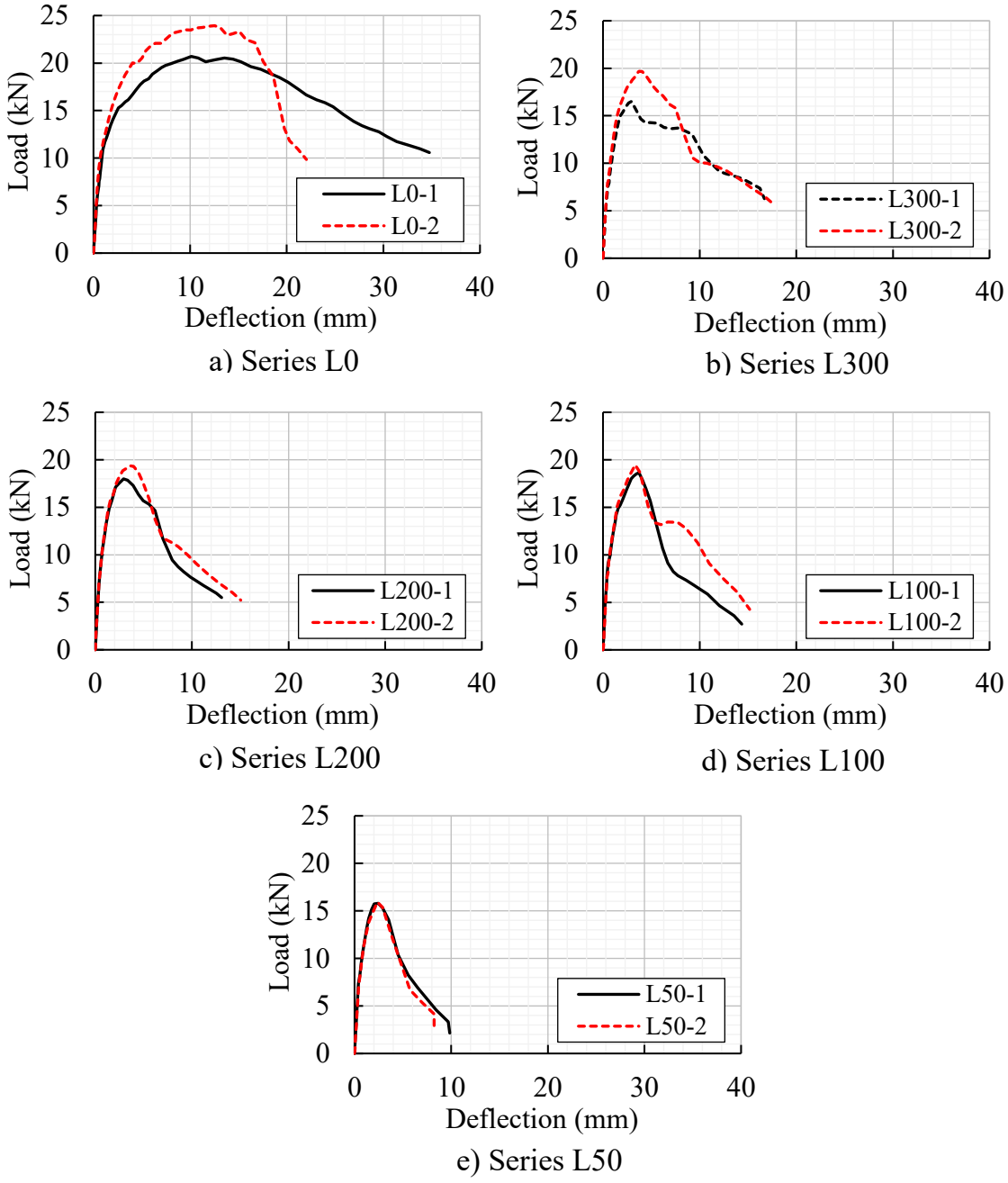

Figure 5.9 – Load-deflection relationship of TR-SHCC specimens

Figure 5.10 compared the results of TRC and TR-SHCC specimens. It can be seen that the peak loads TR-SHCC beams were remarkably higher than those of TRC beams, in particular Series L100 and L200. The reason may be the multiple

cracking behaviors and crack bridging characteristics of SHCC, which enhanced the contribution of SHCC in the pre-peak stage. In contrast, in the post-peak stage, due to the weak frictional bonding between textile and SHCC, TR-SHCC specimens exhibited low performance with a sudden drop in the applied load.

Table 5.5 – Test result of TR-SHCC specimens

Series	Specimen	Failure load (kN)	Disp.* (mm)	Failure mode
L0	L0-1	20.7	10.1	D
	L0-2	23.9	12.5	B
L300	L300-1	16.5	3.0	P
	L300-2	19.7	3.7	P
L200	L200-1	18.0	3.0	P
	L200-2	19.4	3.6	P
L100	L100-1	18.6	3.7	D + P
	L100-2	19.5	3.3	D + P
L50	L50-1	15.8	2.5	D
	L50-2	15.9	2.3	D

Disp. *– Displacement corresponding to failure load.
B – Breakage of textile reinforcement.
D – Delamination failure (the separation between the textile layer and mortar together with the occurrence of horizontal cracks on both sides of specimens).
P – Pull-out failure.

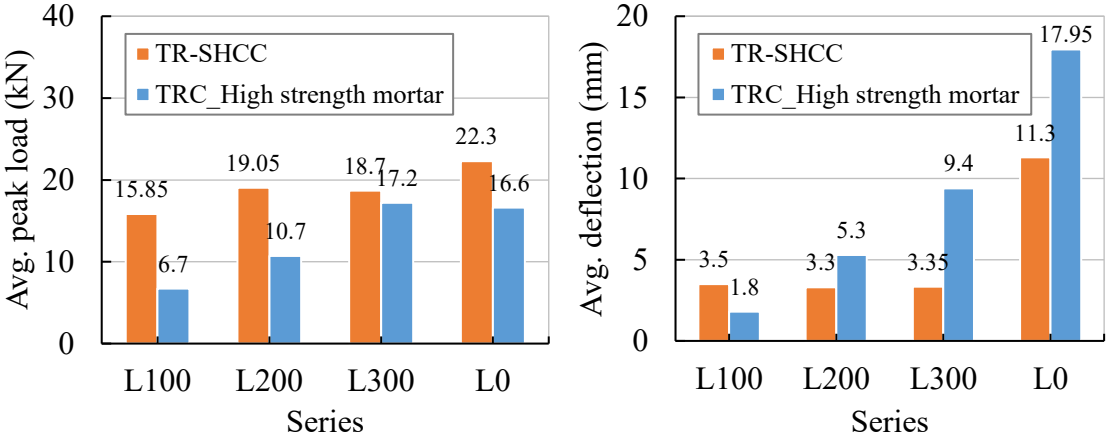

a) Average peak load of TRC and TR-SHCC specimens

b) Avg. deflection corresponding to peak load of TRC and TR-SHCC specimens

Figure 5.10 – Comparison peak load and corresponding deflection of TRC and TR-SHCC specimens

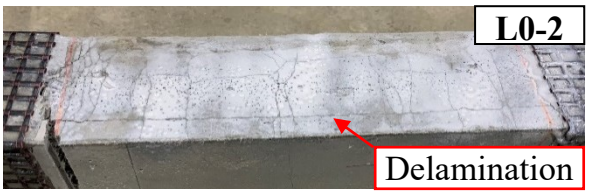

a) Series L0

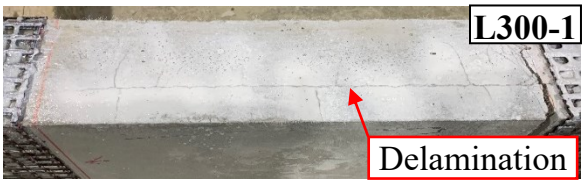

b) Series L300

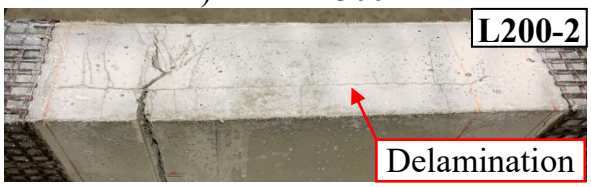

c) Series L200

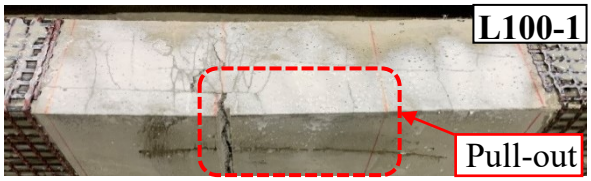

e) Series L100

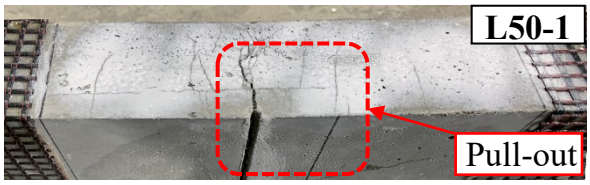

d) Series L50

Figure 5.11 – Crack patterns of TR-SHCC specimens

5.4. Summary

In this chapter, an experimental program on five series of TRC beams with different stress transfer lengths was carried out to investigate flexural failure behavior. The following conclusions are given:

(1) For the short embedment length of 50 and 100 mm, pull-out failure was dominant.

(2) A mix failure consisted of delamination and pull-out failure occurred in specimens of Series L200.

(3) To ensure the mechanical performance of TRC beams made of high strength ordinary mortar, the stress transfer length of textile reinforcement should be more than or equal to 300 mm.

(4) For TR-SHCC specimens, the average peak loads of series with lap splice were almost equal and were not significantly smaller compared to control series. However, these series exhibited lower ductility, compared to the control series. It indicated the lap splice lengths of 200 and 300 mm were insufficient to ensure the performance of TR-SHCC specimens.

(5) The fracture of yarn was not a dominant failure. The reason may be due to the splitting between textile and concrete. Hence, delamination was the most critical failure mode hindering the exploitation of the capacity of textile reinforcement to its full extent. Further experiments and discussions are needed to improve composite performance between textile fabric and concrete.

CHAPTER 6

EFFECT OF TEXTILE CONFIGURATION ON COMPOSITE BEHAVIOR BETWEEN TEXTILE AND MORTAR

6.1. Introduction and Background

Upgrading and structural strengthening of existing concrete structures has become an urgent need in recent years due to deterioration and/or the necessity to meet more strict design requirements. One of the traditional strengthening techniques for RC members involves the use of concrete/cement mortar overlays or external reinforcement such as steel plate, carbon sheet. Over the past decades, the technique of externally layers TRC reinforcement has become a highly attractive alternative to the traditional technique. TRC is a low cost, resistant at high temperature, compatible with masonry or concrete substrates and friendly for manual workers material, which can be applied at low temperatures or on wet surfaces. Therefore, the use of TRC is becoming attractive for the retrofitting of existing concrete or masonry structures. The comparison between textile and FRP strengthening systems in enhancing the flexural capacity of RC beams was conducted and reported. In addition, the experimental results also revealed the effect of mesh size on composite behavior between textile fabric and mortar.

6.2. Test Program

6.2.1. Material

FRP grids and textile fabrics were used for the external reinforcement, and SHCC served as the cementitious matrix to impregnate the reinforcements to form an external overlay for the flexural strengthening of RC beams. The FRP grids are characterized by square meshes with nominal dimensions of 100mm×100mm. They are made up of untwisted yarns consisting of continuous carbon fibers impregnated with epoxy resin. Before strengthening, the FRP grids were cut into appropriate sizes according to the bottom dimensions of the RC beams, as illustrated in Figure 6.1a.

Two types of textiles were used in this research. One textile (denoted T) was the original textile, which was mentioned in chapter 2. The second textile (denoted Tm) was created by modifying the textile T. The rovings of textile T were removed in an alternating manner, resulting in a mesh size of 21mmx22mm instead of 8.5mm x10mm. Details of the textiles, such as geometry, mesh size, and cross-sectional area, are presented in Figure 6.1. Table 6.1, 6.2 summarize the mechanical properties of used materials, including concrete, FRP grids, textiles, SHCC, and steel bars in this study.

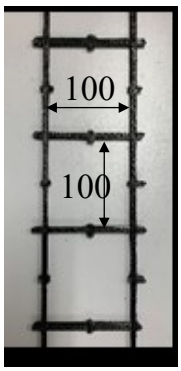

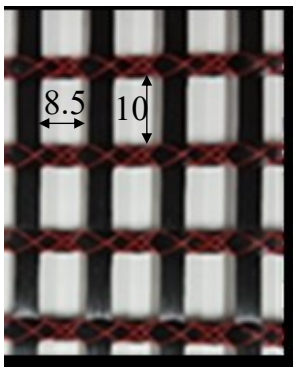

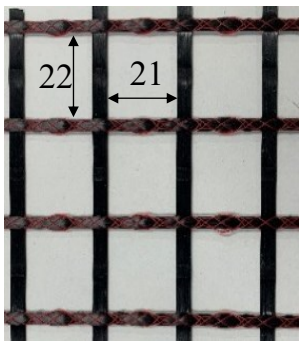

units: mm

a) FRP	b) Textile T	c) Textile Tm
- Cross-sectional area of individual bar: 17.5 mm^2 - Total Cross-sectional area of 2 bars: 35 mm^2	- Cross-sectional area of individual yarn: 1.91 mm^2 - Total Cross-sectional area of 16 warp yarns: 30.6 mm^2	- Cross-sectional area of individual yarn: 1.91 mm^2 - Total Cross-sectional area of 8 warp yarns: 15.8 mm^2

Figure 6.1 – FRP and textiles used in this study

Table 6.1 – Mechanical properties of rebar

Rebar	Yielding strength (N/mm^2)	Ultimate Strength (N/mm^2)	Elastic Modulus (N/mm^2)
SD295A-D10/D13	≥295	440-660	2.0×10^5

Table 6.2 – Mechanical properties of used materials

Material	Tensile strength (N/mm^2)	Elastic modulus (N/mm^2)	Compressive strength (N/mm^2)
Concrete	-	30×10^3	28
FRP	1400	100×10^3	-
Textile T/Tm	1700	$160\text{-}200 \times 10^3$	-
PCM	-	21.5×10^3	59
SHCC	-	17×10^3	40

6.2.2. Specimen Preparation

Eighteen RC beams with dimensions of 150 mm in depth, 200 mm in width, and 1800 mm in span length were prepared and tested under four-point bending loading, as illustrated in Figure 6.2. Two ϕ13 mm deformed steel bars were longitudinally placed as the tensile steel reinforcement. The concrete cover thickness was set as 25 mm for the longitudinal steel bars. Deformed steel bars with a diameter of 10 mm and spaced at 100 mm center-to-center were also used as the stirrups.

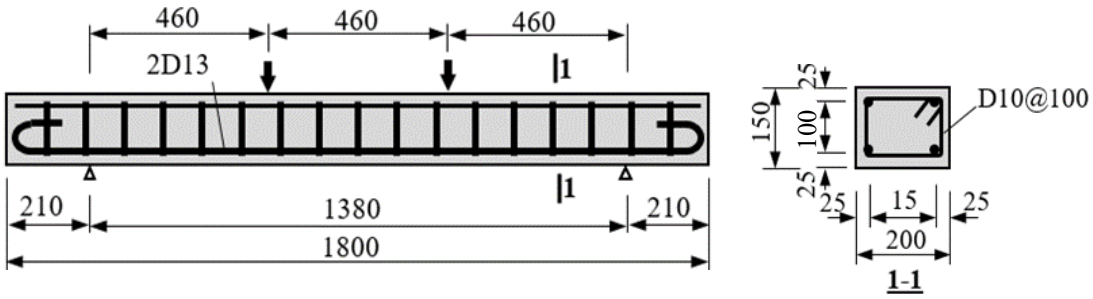

Figure 6.2 – Sketch of control beam units: mm

The eighteen beams were divided into nine series. The first series served as controlled specimens. For the next six series (denoted by Group A), a layer of the concrete cover with a thickness of approximately 50 mm was removed and replaced by strengthening layers (Figure 6.3). For the remaining two series (denoted as

Group B), as illustrated in Figure 6.4, the strengthening overlay has a thickness of 20 mm and a bond length of 1280 mm. That is the two ends of the overlay are 50 mm away from the supports.

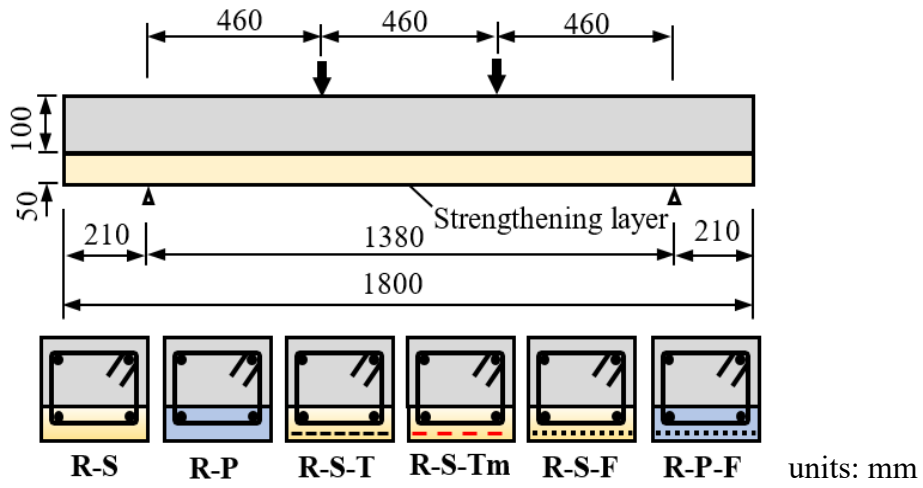

Figure 6.3 – Beams strengthened without section enlargement

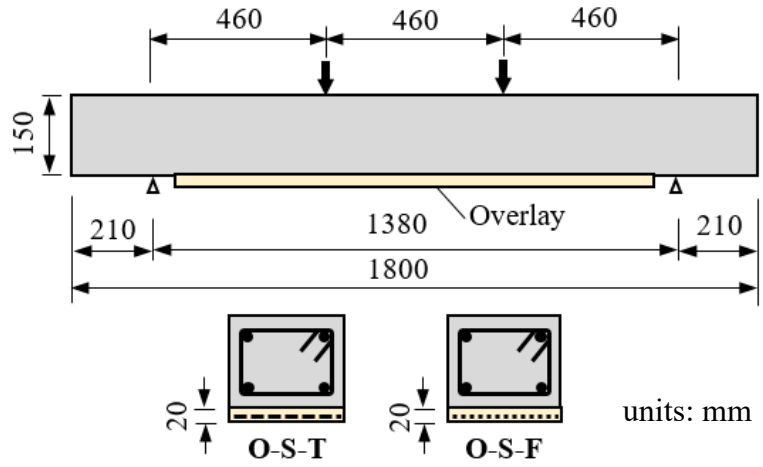

Figure 6.4 – Beams strengthened with overlay

The installation procedures of the overlay strengthening system consisted of the following steps. To improve the bond between the concrete substrate and repair layer, the bottom surface of each RC beam was roughened and exposed with coarse aggregates. Subsequently, wood formworks were fixed onto the two sides of each beam to prevent the flowing away of the cement matrix. The concrete surface was cleaned from dust with compressed air and then, dampened with water. Repair material with a thickness of 10 mm was applied to the primed surface using a shotcrete method. Afterward, the strengthening reinforcements were slightly

pressed into the first layer of the matrix to ensure good impregnation with repair material. After that, an additional repaired layer was placed.

After one day curing, the plate was demolded and cured for 7 days. During the curing, the strengthening layer was sprayed with water to avoid drying shrinkage of the mortar. As for group A, the construction procedure was almost similar to those of group B. The difference came from the position of the strengthening layer. In the first step, the soffit of the beam was removed by high-pressure water jetting to the required depth of 50 mm. In addition, in the second step, a 40 mm thickness of mortar, strengthening reinforcements, and the rest mortar layer were placed into formwork respectively to gain the original dimension of the beam.

The notation of the strengthened series is X-Y-Z. X represents the type of strengthening configuration (O for overlay strengthening technique, and R for strengthening solution without section enlargement), Y refers to the mortars (S for SHCC, P for PCM). Z denoted by strengthening reinforcement (F for FRP and T versus Tm for textile T and textile Tm, respectively). The description of the series is summarized in Table 6.3.

Table 6.3 – Summary of series

N°	Group	Series	Type of Mortar	Type of strengthening material	Number of specimen
1	-	CON	-	-	2
2	A	R-S	SHCC	-	2
3	A	R-S-T	SHCC	Textile T	2
4	A	R-S-Tm	SHCC	Textile Tm	2
5	A	R-S-F	SHCC	FRP	2
6	A	R-P	PCM	-	2
7	A	R-P-F	PCM	FRP	2
8	B	O-S-T	SHCC	Textile T	2
9	B	O-S-F	SHCC	FRP	2

6.2.3. Text Setup

All beams were subjected to four-point bending, as shown in Figure 6.5. The loading span was 1380 mm, and the 460 mm-long constant moment span and a 460 mm-long shear span were selected, respectively. Five Displacement Transducers

(DT) were employed to measure the vertical beam deflections. A strain gauge with the base length of 30 mm was used to measure the strain responses of concrete in the compression zone.

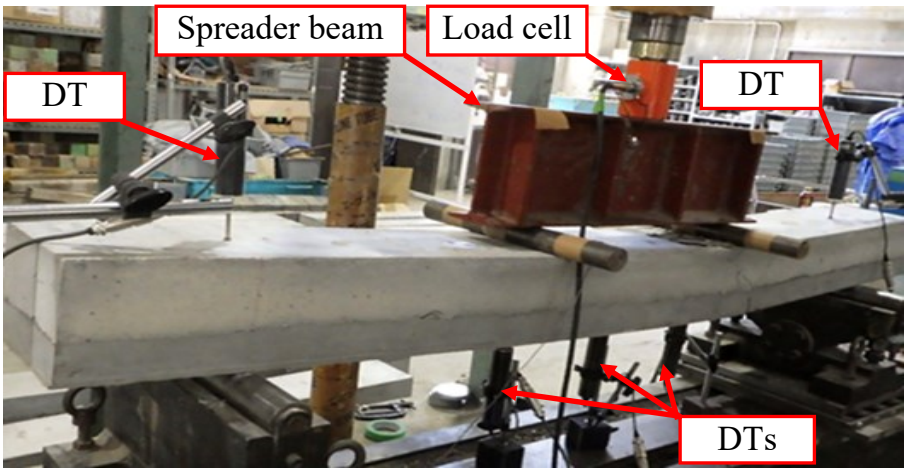

Figure 6.5 – Four-point bending test setup

6.3. Result and Discussion

The flexural performance of the all series in terms of the crack pattern, failure mode, and load-deflection curves were obtained and are herein discussed.

6.3.1. Crack Patterns and Failure Modes

a) Control beams (Series CON)

Figure 6.6a described the crack pattern of the control series. The control beams failed in a typical failure mode, which is concrete crushing at the compression zone after the yielding of the longitudinal steel reinforcement. The vertical flexural crack first initiated within the constant moment region at a load level of around 4 kN. As the load increased, new cracks developed, however, diagonal shear cracks were not observed in this series.

b) Beams strengthened without section enlargement using SHCC (Series R-S, R-S-T, R-S-Tm, and R-F)

For these series, the concrete at the tensile zone was replaced by SHCC, which was higher tensile strength than ordinary concrete. The first crack of specimens initiated at a load ranging from 18 kN to 22 kN. The principle cracks formed within the strengthening layer then propagated towards the substrate concrete. As the applied load increased, multiple fine cracks formed in the adjacent wide cracks

within the SHCC layer. Also, no debonding failure at the interface of the strengthening layer and substrate concrete was observed during the loading process, indicating that the composite action of the strengthening system achieved. In addition to the main characteristics mentioned above, there are still differences in crack behavior and failure mode among the series as follows.

Figure 6.6b illustrates the crack patterns of Series R-S (using SHCC). All major cracks occurred in the constant moment zone. The failure mode was characterized by the yielding of the tensile steel and the spalling of concrete in the compression zone. However, compared to control beams, more fine cracks and wider major cracks were observed within the specimens. As using the FRP grid-reinforced SHCC matrix to strengthen RC beams (Series R-S-F), the number of cracks significantly increased, particularly the fine cracks in the strengthening layer (see Figure 6.6e). At the ultimate state, failure occurred due to concrete crushing followed by the rupture of FRP grids without any debonding.

Series R-S-T showed a different failure mode compared to the preceding three series. The Debonding of TRC due to fracture at the surface of the textile-mortar interface initiated within the pure moment area then propagated to the ends of the beam (Figure 6.7a). This kind of failure, which can also be described as inter-laminar shearing, is attributed to the effect of coating and configuration of the textile. Coating material penetrates the spaces between individual filaments lead to an increase in the rigidity of the textile in both directions. Also, threads create stable joints in the junctions between the longitudinal and transversal yarns. As a result, the failure due to slippage of the fiber through the mortar was prevented, and the damage was shifted to the textile-mortar interface, which was the weakest among all interfaces. The effective area fraction plays a crucial role in preventing delamination failure. The investigation by Ortlepp (2009) showed an approximately linear relationship between the effective area and the adhesive tensile strength measured in the textile layer. The effective area fraction results from the ratio of the effective area (matrix area) to the total area (Figure 6.8, Equation (6.1)).

$$k_{A,eff} = \frac{\sum A_i}{A} \tag{6.1}$$

where $k_{A,eff}$ = effective area factor; A_i = effective area; and A = total area.

Therefore, increasing the effective area may prevent delamination failure. The experimental result achieved from Series R-S-Tm confirmed this assumption. As mentioned above, the textile Tm was created by removing half the number of

rovings from textile T. As a result, the effective area of Series R-S-Tm was greater than that of Series R-S-T. The result showed that the failure of the Series R-S-Tm was due to textile rupture instead of debonding failure (see Figure 6.7b).

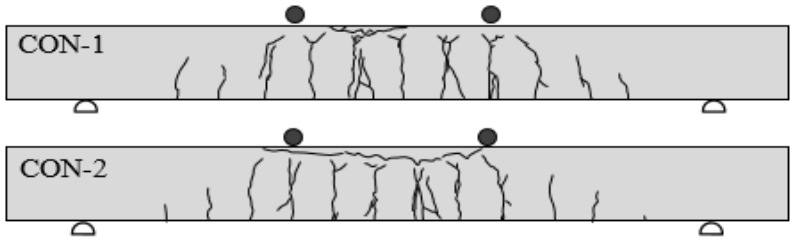

a) Control series

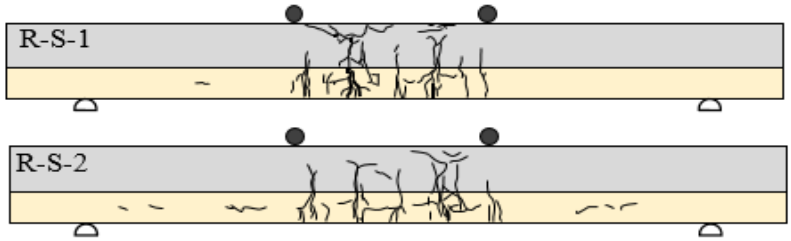

b) Series R-S (pure SHCC)

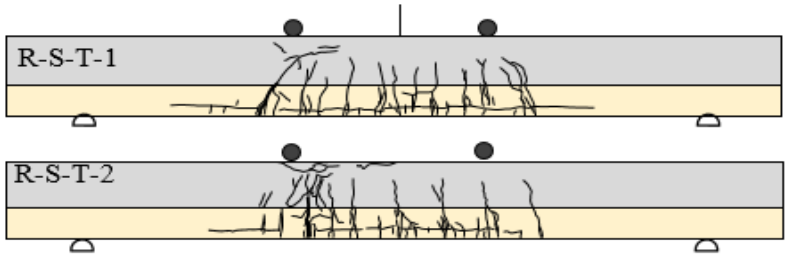

c) Series R-S-T (SHCC and textile T)

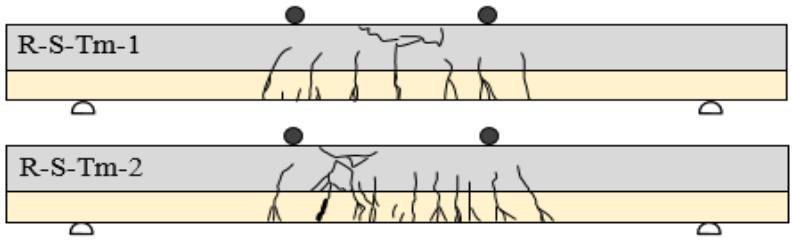

d) Series R-S-Tm (SHCC and textile Tm)

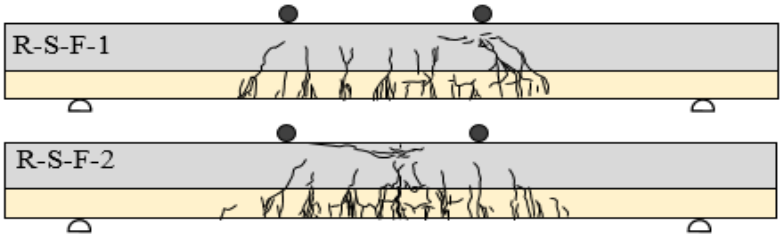

e) Series R-S-F (SHCC and FRP)

Figure 6.6 – Crack patterns of series strengthened with SHCC

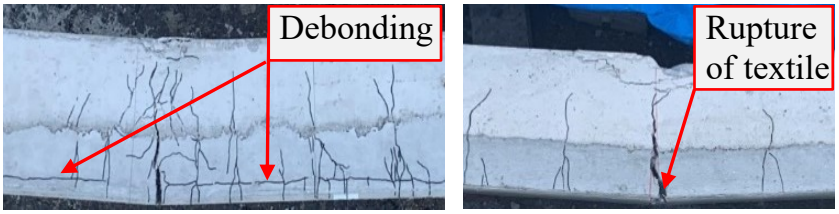

a) Series R-S-T b) Series R-S-Tm

Figure 6.7– Failure mode of series R-S-T and R-S-Tm

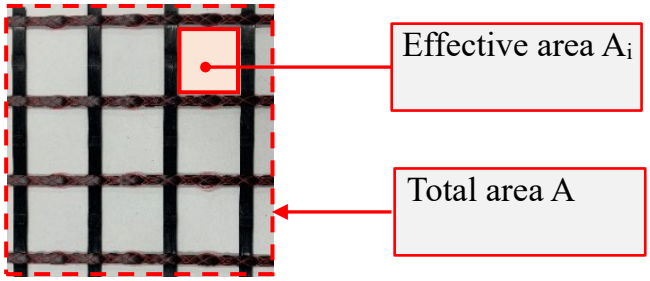

Figure 6.8 – Effective area of textile Tm

c) Beams strengthened without section enlargement using PCM mortar (Series R-P and R-P-F)

The crack patterns and failure modes are described in Figure 6.9. Initial cracks occurred in the PCM mortar at a load level of 12-16 kN. The cracking load was slightly smaller than those of the previous series fine cracks formed along with the interface between the strengthening layer and the substrate concrete. However, there was no sign of debonding and local slip occurring at the interface, demonstrating that satisfactory bond performance was maintained throughout the loading process. Two types of failure modes were observed: concrete crushing of Series R-P and FRP rupture of Series R-P-F.

d) Beams strengthened with overlay (Series O-S-T and O-S-F)

Figure 6.10 illustrates the crack pattern and failure mode of overlay strengthened RC beam with textile versus FRP. The cracking loads of these series beams ranged from 18-22 kN, similar to the previous series strengthened with SHCC. The wide cracks formed within the substrate concrete transformed into multiple diffused fine cracks in the cast-in-place SHCC layer. The crack numbers in this series of beams were more than those in the other series. Besides, both the overlay debonding and the intermediate crack-induced debonding (IC debonding) were not observed and recorded. Two different failure modes were noted in the retrofitted beams

depending on the type of strengthening material. The failure of strengthened beams with textiles was due to debonding at the interface of textile-mortar, followed by concrete crushing, whereas the rupture of FRP was the dominant failure of Series O-S-F.

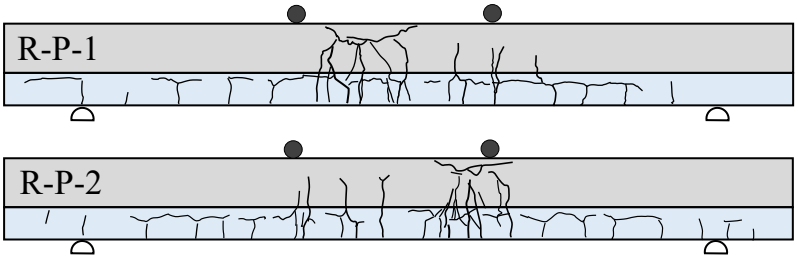

a) Crack pattern of Series R-P

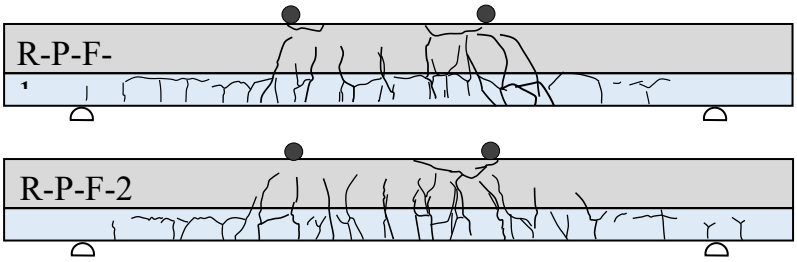

b) Crack pattern of Series R-P-F

Figure 6.9 – Crack patterns of Series R-P and R-P-F

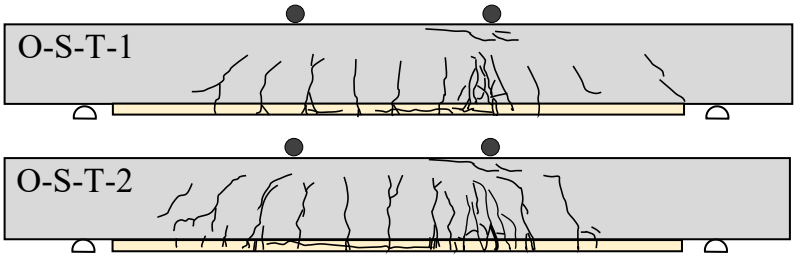

a) Crack pattern of series O-S-T

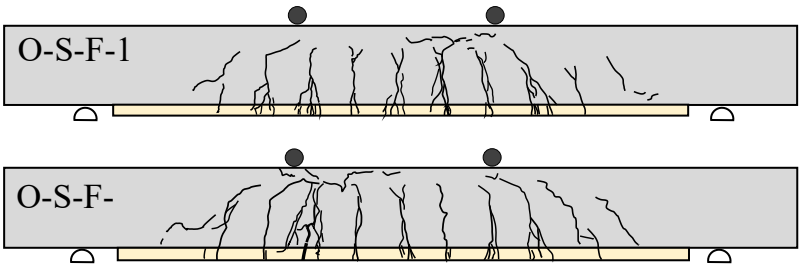

b) Crack pattern of series O-S-F

Figure 6.10 – Crack patterns of series O-S-T and O-S-F

6.3.2. Load-Deflection Behavior

Load versus mid-span deflection curves are presented as shown in Figure 6.11, 6.12, and 6.13 for all test beams. Tables 6.4 shows a summary of the flexural behavior of all test beams in terms of flexural loading capacity, ultimate mid-span deflection, and failure mode. As demonstrated in Figure 11, the control specimens displayed the standard nearly-bilinear response characteristics of under-reinforced beams. They failed in flexure through the formation of wide flexural crack at the mid-span with the final mode of failure being concrete crushing at the critical section. The average peak load and ultimate deflection of the two beams were 50.1 kN and 26.4 mm, respectively.

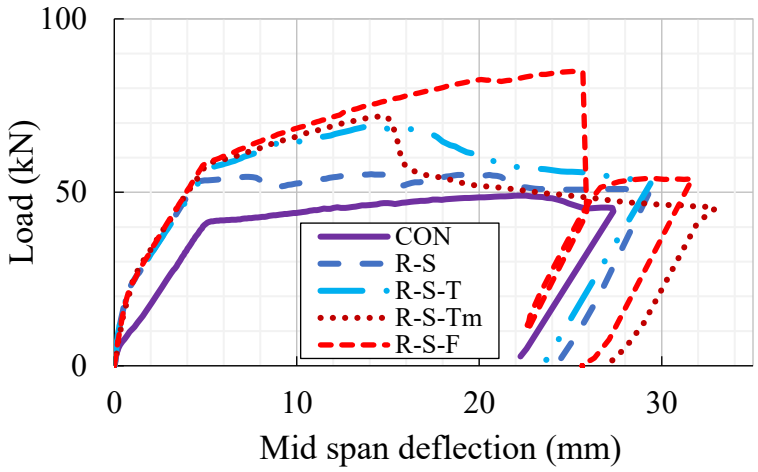

Figure 6.11 – Load-deflection of series strengthened by SHCC

As shown in Figure 6.11, the series strengthened with SHCC had a relative increase in cracking load and ultimate load. The characteristics of the load-deflection behavior of these series may be summarized as follows. Initially, the relationship is linear. As cracks forming within the beam's mid-span the curve begins to deviate from the linear path. After the strengthened beams reach their ultimate load, the load decrease from the peak to a significantly lower load level round the control beam capacity, and then the beam's behavior was controlled by the original steel reinforcement as before the application of the strengthening scheme. All beams strengthened with SHCC failed in flexure at loads substantially higher than the control beams (Table 4). The ultimate load recorded for Series R-S, R-S-T, R-S-Tm, and R-S-F was 55.5, 69.5, 71.4, and 84.9 kN, respectively. Thus, the contribution of various strengthening materials in increasing the flexural capacity was 10.8%, 38.7%, 42.5%, and 69.5%, respectively. Three post-peak

behaviors were identified. The failure due to rupture of FRP or textile in Series R-S-T and R-S-F characterized by a sudden drop in the flexural capacity. Meanwhile, the debonding failure of Series R-S-T was represented by a more gently decrease of load-bearing capacity. For the Series R-S, after reaching the peak, the ductile behavior of beams was depicted by the almost constant load and large deflection.

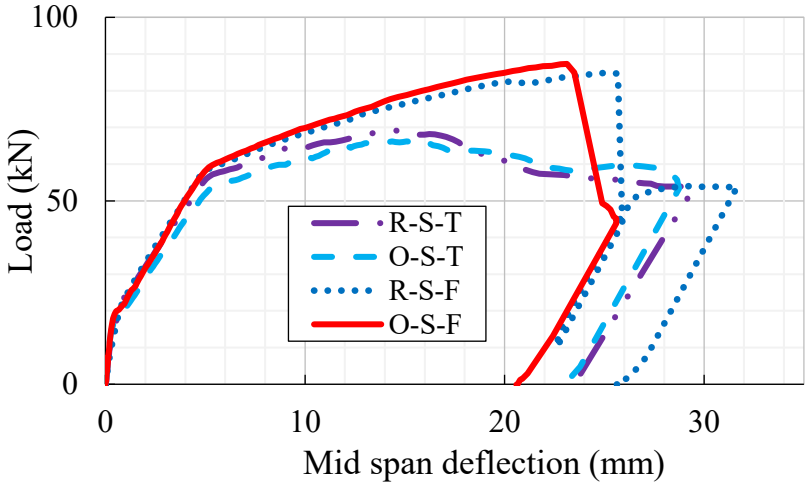

Figure 6.12 – Load-deflection of series strengthened without section enlargement versus overlay

In this research, two types of cement-based mortar were investigated, including SHCC and PCM. As indicated in Figure 13, each beam strengthened with the SHCC (Series R-S, R-S-F) had relatively higher load-bearing capacity when compared to its counterparts in Series R-P and R-P-F. However, it is shown that the load-deflection response and the failure mode of beams strengthened with two types of these mortar, were not significantly different.

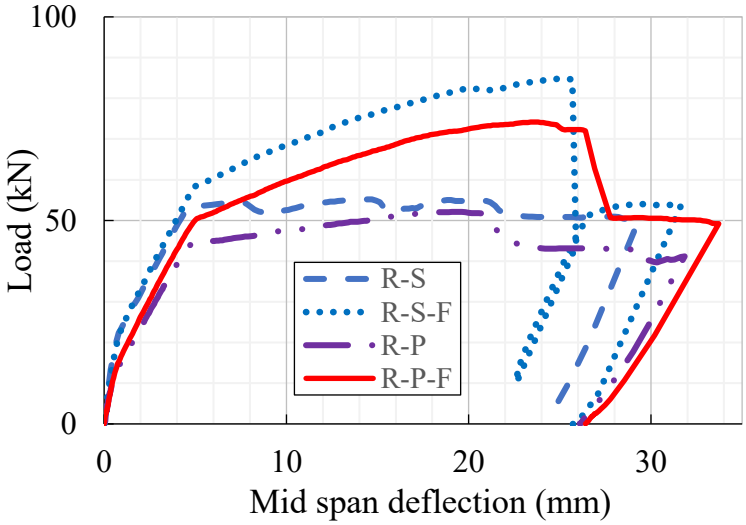

Figure 6.13 – Load-deflection of series strengthened by SHCC and PCM

Table 6.4 – Summary of test result

Series	Average peak load F_u (kN)	Increase in F_u * (%)	Average ultimate deflection e (mm)	Failure mode
CON	50.1	-	26.4	SY+CC
R-S	55.5	10.8	29.1	SY+CC
R-S-T	69.5	38.7	29.5	DB+SY+CC
R-S-Tm	71.4	42.5	32.9	RT+SY+CC
R-S-F	84.9	69.5	32.3	RT+SY+CC
R-P	51.4	2.6	32.1	SY+CC
R-P-F	74.6	48.9	34.1	RT+SY+CC
O-S-T	68.4	35.5	28.2	DB+SY+CC
O-S-F	86.7	73.1	25.7	RT+SY+CC

CC-concrete crushing, SY-steel yielding, DB-debonding, RT-rupture of textile or FRP

* Percentage increase in peak loads F_u of strengthened beams to controlled beam

6.3.3. TRC vs FRP Effectiveness

Table 6.5 summaries the values of the TRC versus FRP effectiveness factor (k), which is defined as the ratio of the strengthening materials to FRP in terms of flexural capacity enhancement. For TRC, this factor varied between 0.48 and 0.61 for the different parameters examined in this study. In terms of strengthening configuration, the Series R-S-T recorded an effectiveness factor of 0.56, which is greater than that of the Series O-S-T. Although the tensile capacity of this textile was similar to that of used FRP, the effectiveness factor was quite low. This low value of k factor was due to the debonding at the textile-mortar interface. This failure considerably reduced the TRC's effectiveness and prevented a full composite action. The textile configuration had a significant effect on the effectiveness factor. Although the tensile capacity of textile Tm was lowest, this textile exhibited the highest value of factor k, equal to 0.61. It might be due to the increase in the effective area.

The nominal flexural strengths of the beams strengthened by FRP/TRC were calculated based on the US code (ACI 440.2R-08). The following assumptions were adopted:

(1) There is a perfect bond between the FRP/TRC strengthening layers and the concrete substrate.

(2) At the ultimate state, FRP/TRC fractures and concrete fails by crushing.

(3) The ultimate compressive strain of concrete is 0.003.

Figure 6.14 illustrates the internal strain and stress distribution for a rectangular section under flexure at the ultimate limit state. The calculation procedure used to arrive at the ultimate strength should satisfy strain compatibility and force equilibrium and should consider the governing mode of failure.

The calculation involves selecting an assumed depth to the neutral axis *c,* calculating the strain level in each material using strain compatibility, calculating the associated stress level in each material, and checking internal force equilibrium. If the internal force resultants do not equilibrate, the depth to the neutral axis should be revised and the procedure repeated. For any assumed depth to the neutral axis *c*, the strain level in the strengthening reinforcements can be computed from equation 6.1.

$$\varepsilon_{fe} = \varepsilon_{cu}\left(\frac{d_f - c}{c}\right) - \varepsilon_{bi} \leq \varepsilon_{fd} \tag{6.1}$$

where,

ε_{cu} – the ultimate axial strain of unconfined concrete;

ε_{bi} – strain level in concrete substrate at time of strengthening layer installation;

ε_{fd} – debonding strain of externally bonded FRP reinforcement.

The effective stress level in the streingthening reinforcements can be found from the strain level in the FRP or textile, assuming perfectly elastic behavior.

$$f_{fe} = E_f \varepsilon_{fe} \tag{6.2}$$

Based on the strain level in the strengthening reinforcements, the strain level in the nonprestressed steel reinforcement can be found from equation 6.3 using strain compatibility.

$$\varepsilon_s = \left(\varepsilon_{fe} + \varepsilon_{bi}\right)\left(\frac{d - c}{d_f - c}\right) \tag{6.3}$$

The stress in the steel is determined from the strain level in the steel using its stress-strain curve.

$$f_s = E_s \varepsilon_s \leq f_y \tag{6.4}$$

The stress level in the SHCC layer can be found from the strain level in the bottom free surface of the SHCC layer. Because of the small thickness of the strengthening layer and the high tensile ductility of SHCC, the stress is assumed to be uniformly distributed throughout the section of the SHCC layer. At the ultimate

load-bearing capacity of strengthened beams, the tensile stress of the SHCC layer is 4 N/mm^2.

With the strain and stress level in the strengthening reinforcements and rebars determined for the assumed neutral axis depth, internal force equilibrium may be checked using equation 6.5.

$$c = \frac{A_s f_s + A_f f_{fe} + A_{sh} f_{sh}}{\alpha_1 f_c' \beta_1 b} \tag{6.5}$$

where,

α_1 and β_1 in are parameters defining a rectangular stress block in the concrete equivalent to the nonlinear distribution of stress (refer to ACI 318-05).

The nominal flexural strength of the section is computed from 6.6.

$$M_n = A_s f_s \left(d - \frac{\beta_1 c}{2}\right) + \psi_f A_f f_{fe} \left(d_f - \frac{\beta_1 c}{2}\right) + \psi_f A_{sh} f_{sh} \left(d_{sh} - \frac{\beta_1 c}{2}\right) \tag{6.6}$$

where,

A_s, f_s – area and stress of steel reinforcement, respectively;

A_f, f_{fe} – area and stress of strengthening reinforcement, respectively;

A_{sh}, f_{sh} – area and stress of SHCC layer, respectively;

ψ_f – an additional reduction factor, is applied to the flexural-strength contribution of the strengthening reinforcement. The recommended value of ψ_f is 0.85;

d – distance from extreme compression fiber to centroid of tension reinforcement;

d_f – effective depth of FRP flexural reinforcement;

d_{sh} – distance from extreme compression fiber to centroid of tension SHCC layer.

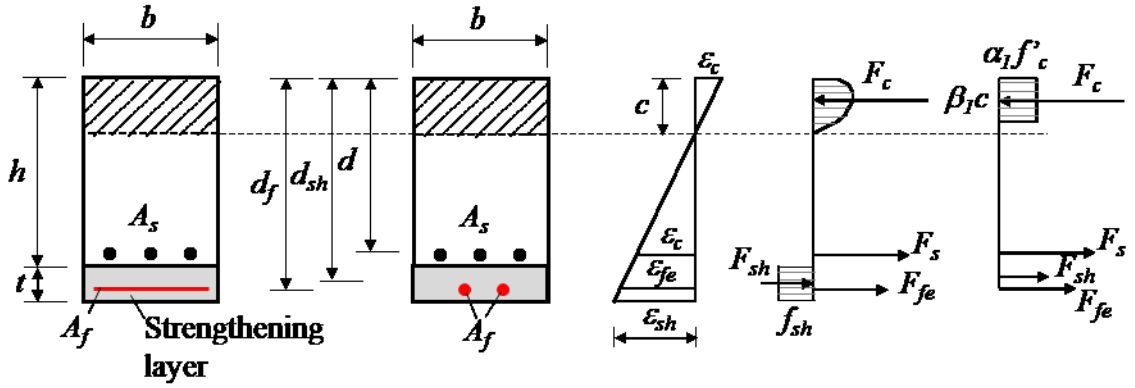

Figure 6.14 – Internal strain and stress distribution for the section of strengthened beams

The ratio of the experimental moment to the nominal moment as presented in Table 6.6 could demonstrate the effectiveness of the strengthening materials in terms of increasing the flexural capacity. It is evident that the effectiveness of FRP and textile Tm was considerably higher compared to that of textile T.

Table 6.5 – Summary of effectiveness factor *k*

Series	Flexural capacity increasing (kNm)	Tensile capacity of FRP/T/Tm reinforcement (kN)	Factor *k* (%)
CON	-	-	-
R-S	1.2	-	0.15
R-S-T	4.5	45.5	0.56
R-S-Tm	4.9	22.8	0.61
R-S-F	8.0	49	1.0
R-P	0.3	-	0.05
R-P-F	5.6	49	-
O-S-T	4.2	45.5	0.48
O-S-F	8.4	49	1.0

Table 6.6 – Comparison between nominal moment and experimental moment

Series	M_n* (kNm)	M_u** (kNm)	M_u/M_n
R-S-T	15.4	16.0	1.04
R-S-Tm	13.6	16.4	1.21
R-S-F	14.8	19.5	1.31
O-S-T	14.8	15.7	1.06
O-S-F	15.1	19.9	1.32

* Nominal moment.
** Ultimate moment obtained experimentally.

6.4. Summary

This study investigated experimentally the performance of TRC and FRP composite in the flexural strengthening of RC beams. Several parameters were examined namely: (a) the strengthening material (TRC and FRP), (b) the strengthening method, (c) the types of mortar (SHCC and PCM), and (d) the textile configuration. The obtained results revealed the following conclusions:

(1) The effectiveness of beams strengthened by the textile was less than that of FRP. The effectiveness factor varied between 0.48 and 0.61. The reason for this low effectiveness might be due to delamination failure at the interface of textile and mortar.

(2) Two types of strengthening methods were investigated, including strengthening overlay and strengthening without section enlargement. The experimental result indicated that the effectiveness factor of both methods was approximately equal.

(3) The two examined mortar seemed to be promising for retrofitting flexural RC members. Both the strengthening FRP-mortar and TRC-mortar system significantly increased the flexural capacity of beams. However SHCC-based composite exhibited more effectiveness.

(4) The textile configuration had a significant effect on the effectiveness factor. The increase of the effective area might prevent debonding between textile, and mortar. As a result, providing better composite behavior and increasing the effectiveness factor.

(5) Different failure modes were observed, including steel yielding together with concrete crushing, rupture of FRP or textile and debonding at the textile-mortar interface. However, the overlay debonding and the intermediate crack-induced debonding (IC debonding) were not observed, demonstrating that satisfactory bond performance between the strengthening layer and substrate concrete was maintained through the loading process.

CHAPTER 7

CONCLUDING REMARKS

7.1. Summary and conclusion

7.1.1. Tensile behavior

Chapter 2 investigated the typical tensile behavior of TRC made of low and high strength ordinary mortar and TR-SHCC through a uniaxial tensile test. The results showed four distinct states of tensile force-displacement relationship, including State I (uncracked concrete), State IIA (crack formation), State IIB (crack stabilization), and State III (failure state). Besides, there are differences between TRC, TR-SHCC, and TRC-LS specimens on the crack pattern, failure mode, and peak load. The results showed that the specimens with the best tensile strength and bond strength (TRC specimens) exhibited the highest peak load. On the contrary, TRC-LS made of the mortar with the lowest tensile strength has the minimum load-bearing capacity. Whereas, a greater number of cracks and finer cracks were observed in TR-SHCC specimens. In terms of failure mode, specimens made of low strength ordinary mortar failed by debonding between textile and matrix, whereas delamination occurred in the case of specimens made of SHCC or high strength ordinary mortar.

7.1.2. Bond behavior

Chapter 3 provided an overview of pull-out tests to determine bond law between textile reinforcement and mortar. The strengths and the weaknesses of each experiment were analyzed and evaluated, therefore, the most suitable and reliable pull-out test was proposed. The research examined four different embedment length, including 25, 50, 100, and 200 mm. The real tests were conducted that give an insightful understanding of the bond behavior of mortar and textile fabric. Three matrixes, including SHCC, low and high strength ordinary mortar were examined. Though the pull-out failure occurred in all specimens, their behavior was significantly different. For TRC specimens made of high strength ordinary mortar, bond strength was not observed in specimens with an embedment length of 25 mm. Whereas, secondary cracks occurred in Series 4. As a result, the embedment length should be in a range of 50 to 100 mm. TRC-SHCC specimens exhibited a weaker bonding between textile and SHCC, especially frictional bonding. To determine the bond strength of TR-SHCC specimens, the embedment length should be greater than 100 mm. For low strength ordinary mortar, the mortar has the smallest tensile strength, the bond strength between the textile and low strength ordinary mortar is the smallest among the examined matrixes. Besides, a bond stress-slip relationship could be defined based on the result of the pull-out test. Additionally, results from experiments gave hints on choosing the anchorage length of TRC.

7.1.3. Lap splice length

a) Lap splice length of members subjected to uniaxial tensile forces

Three examined mortar exhibited the different required lap splice lengths. For specimens made of high strength ordinary mortar, the lap splice length of 300 mm was adequate to deform similar behavior to controlled specimens. On the other hand, the combinations textile-SHCC and textile-low strength ordinary mortar require a lap length greater than 300 mm. The fracture of yarn did not occur in all specimens. It indicates that the examined mortar could not exploit the textile to its full extent. The other conclusions were given:

(1) The load-bearing of the specimens increased with the increase of lap splice length.

(2) The dominant failure of all specimens with a short overlap length of 50 and 100 mm was pull-out.

(3) For TRC specimens made of low strength ordinary mortar, due to the weak bond strength between textile and mortar, the dominant failure mode is pull-out, and lap splice length of 300 mm is inadequate. Delamination failure occurred in specimens with better bond strength (specimens made of SHCC or high strength ordinary mortar). The extent of delamination seems to be more intense in the lap spliced specimens made of lower tensile strength matrix (TR-SHCC specimens). As a result, for Series L300, the load-bearing capacity of TR-SHCC specimens is much lower compared to TRC specimens made of high strength ordinary mortar.

b) Lap splice length of members subjected to bending moment

For ordinary mortar, members under bending moments exhibited some similarity with members subjected to uniaxial tensile forces. The lap splice length must be greater than or equal to 300 mm. In addition, for the short overlap length of 50 and 100 mm, pull-out failure was dominant.

For TR-SHCC specimens, in the case of specimens subjected to tensile forces, the load-bearing capacity of test specimens with lap splice was much smaller than the corresponding value of controlled specimens. In the case of specimens subjected to bending moment, although the peak loads of control series and Series L300 were almost equal, their ductility was markedly different. It indicated that the required lap splice length of TR-SHCC specimens must be greater than 300 mm.

7.1.4. Stress transfer length between textile and rebars

Ten TRC beams with different embedment lengths, including 50, 100, 200, and 300 mm was fabricated and tested until failure. The research aimed at determining the adequate stress transfer length between textiles and rebars in tje pure moment zone. The following conclusions were given:

(1) For the short embedment length of 50 and 100 mm, pull-out failure was dominant.

(2) A mix failure consisted of delamination and pull-out failure occurred in specimens of Series L200.

(3) To ensure the mechanical performance of TRC beams made of high strength ordinary mortar, the stress transfer length of textile reinforcement should be more than or equal to 300 mm.

(4) For TR-SHCC specimens, the average peak loads of series with lap splice were almost equal and were not significantly smaller compared to controlled series.

However, these series exhibited lower ductility, comparing to the control series. It indicated the lap splice lengths of 200 and 300 mm were insufficient to ensure the performance of TR-SHCC specimens.

(5) The fracture of yarn did not occur in all specimens. The reason may be due to the splitting between textile and concrete. Hence, delamination was the most critical failure mode hindering the exploitation of the capacity of textile reinforcement to its full extent. Further experiments and discussions are needed to improve composite performance between textile fabric and concrete.

7.1.5. Effect of mesh size on composite behavior

This chapter investigated the strengthening capacity of different materials, including FRP and two types of textiles. The results showed that the effectiveness of beams strengthened by the textile was less than that of FRP. However, if the tensile capacity of strengthening reinforcement was taken into consideration, textile Tm and FRP exhibited similar effectiveness. Textile Tm was modified based on textile T by removing weft and warp yarns. In each direction, half of the yarns were removed according to the law: remove one every two adjacent yarns. As a result, textile T has a larger mesh size compared to textile Tm. The results indicated that textile Tm has better strengthening effectiveness than textile T. The reason might be the effect of textile configuration. The increase of the effective area might prevent splitting between textile and mortar. As a result, providing better composite behavior and increasing the effectiveness factor.

7.1.6. Mechanism of TRC on lap splice and anchorage zone and factors influence lap splice length

The transmission of bond force between reinforcements and surrounding materials is the fundamental mechanism in lap splice and anchorage zone. The understanding of bond behavior, therefore, is the key importance with regard to the explanation for the mechanism of action as well as failure modes within lap splice and anchorage zone of composite materials.

For ribbed rebars, the composite force transmission can be divided into four-part state (Figure 7.1). Initially, the bond between bar and concrete depends on chemical adhesion and a small amount of friction (1). However, the adhesion and friction resistance is quickly lost even with very small relative displacement between rebars and concrete, hence mechanical interlocking between ribs and surrounding concrete

will take place as a major mechanism in bonding. The ribs of the deformed bars induce large bearing stresses in the concrete, and the first transverse microcracks originate at the tips of the lugs allowing the bar to slip (2). Then, the compressive stresses keep spreading from the rib into surrounding concrete. The wedging action increases and spreads around concrete, which is balanced by circumferential tensile stresses around the reinforcement bar. These circumference tensile stresses will induce longitudinal splitting cracks to propagate along with the reinforcement bar (3). Due to the increment of slip inside the concrete, the concrete between two adjacent ribs is already sheared completely. The stress transfer occurred between the friction of rough concrete surface and reinforcement. As the slip continuing increased, the bond stress declined along with slip increment (4) (Figure 7.2). Two distinct types of bond failure have been observed concerning composite failure: pull-out failure and splitting failure. Bond failure is mostly due to the shearing-off of the concrete keys between adjacent bar deformations, and the failure characterized by local interface collapse between adjacent lugs. In the splitting failure, bond failure mostly occurs due to longitudinal splitting of the concrete cover along the plane of the rebars [Cairns & Jones (1995)], and the bond capacity is completely lost once the radial splitting cracks travel to the outer face of the structural member. By providing sufficient lateral confinement to the concrete, the internal cracking of concrete core, as well as splitting, can be effectively prevented due to natural volumetric expansion, and this confined concrete exhibited higher strength than unconfined concrete.

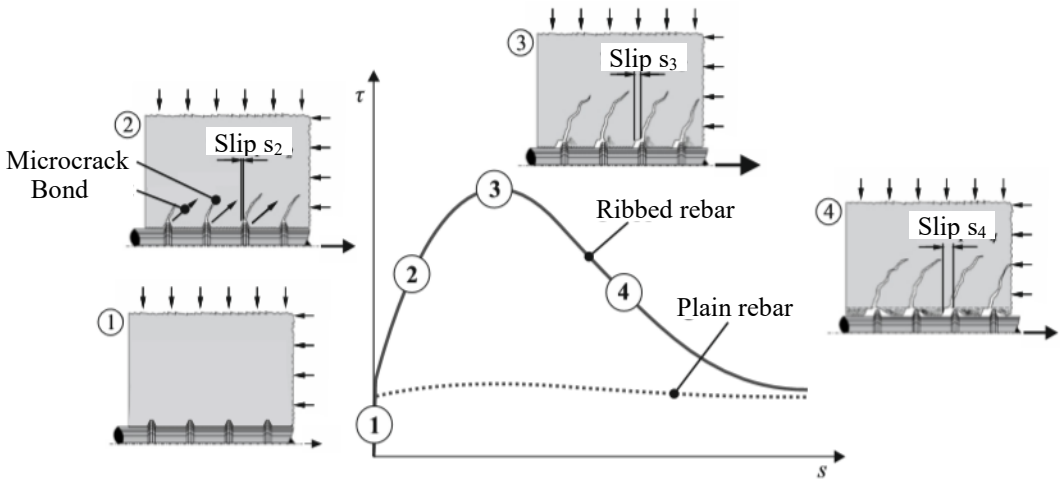

Figure 7.1 - Classification of typical bond stress-slip relationship of rebars [FIB Bulletin (2000)]

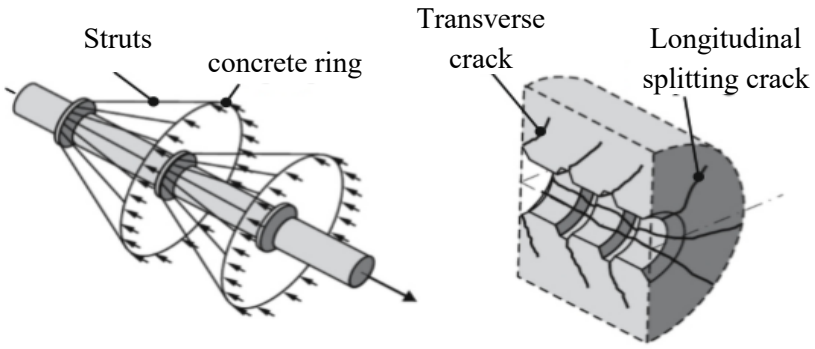

Figure 7. 2 – Failure mechanisms and cracks caused by

The lap splice zone of ribbed rebars usually fails due to the longitudinal crack formation or as a result of the concrete cover splitting in the plane of reinforcements. Schlaich & Schäfer (2001) proposed framework models for the simplified and idealized description of force transmission in the overlap zone. There is a separate distinction between the inner and outer composite parts. The inclination of the compression struts is generally assumed to be 45° (Figure 7.3). The tension struts generate transverse tensile forces within the splice zone, which, if the concrete tensile strength in the plane reinforcement is exceeded, can lead to a transverse tensile failure or cracks of the splice zone.

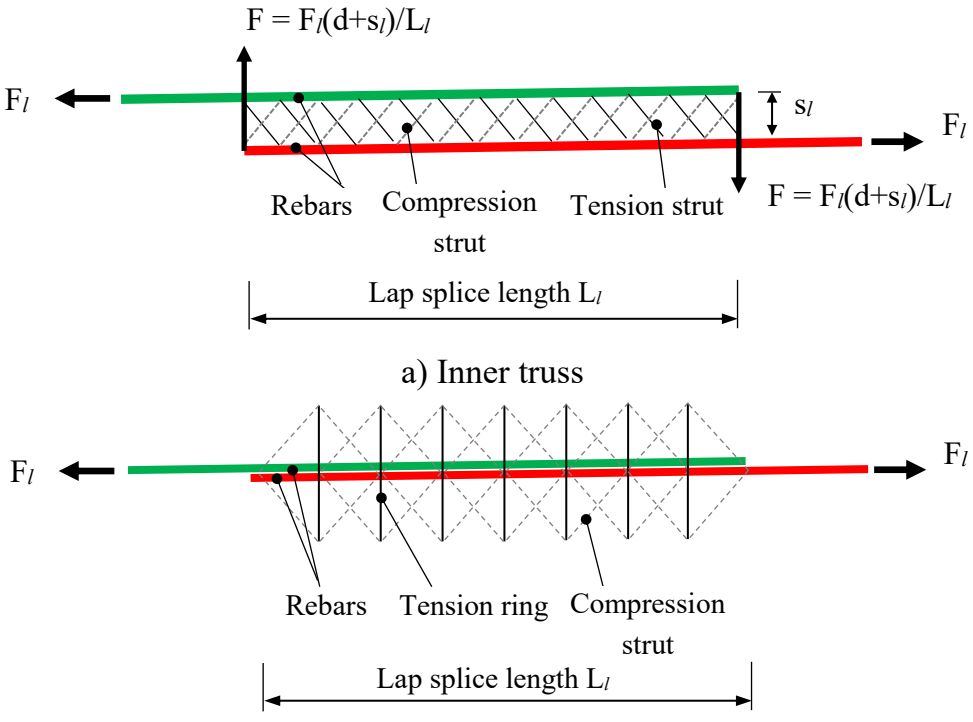

Figure 7.3 – A simplified model of the force transmission in splice zone

For FRP grids, due to rigid intersections of longitudinal bars and transverse bars, the mechanical anchorage at the intersection is one process that should be considered in addition to the other interfacial bonding mechanisms (see Figure 7.4). Currently, there is not much comprehensive research on stress transmission and fracture mechanism within the lap splice zone of RC members reinforced by FRP. Further experiments and discussions are needed.

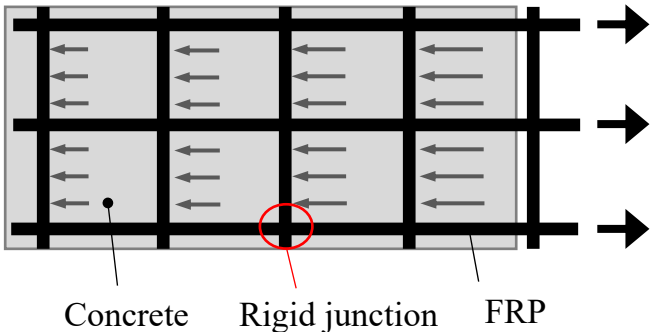

Figure 7.4 – Contribution of transverse bar

For textile fabrics, various investigations showed that the force transmission of textile reinforcements in TRC characterized similarly to the behavior of plain rebars reinforced concrete with a typical three-part sate of the bond stress-slip curve [Bentur & Mindess (1990)]. An example of the classification of the bond stress-slip relationship of textile reinforcements includes: in the first state (1), the chemical adhesion is activated. The acting forces are transferred via adhesion within the interface layers between the reinforcement and the concrete. After the adhesive forces have been exceeded, the chemical bond gradually fails together with the yarn detaching from the concrete (2). As a reason, this is accompanied by a drop in the bond resistance. In the third state (3) the yarn is completely detached from the matrix. In this state, bond resistance is determined by the friction between the yarns and the concrete (refer to section 3.3). The mechanical bond, particularly mechanical interlocking or wedging action generally has a quite minor influence on the bond behavior of TRC. In addition, though the used textile has a grid form with warp and weft yarns, the influence of transverse yarns on bond behavior was also insignificant. The reason was due to weak links between warp and weft yarns. The junctions were easily destroyed when the warp yarn was under tensile force. As a result, weft yarns did not contribute to the bond strength of TRC. Besides, weft yarns might have negative influences. According to Jesse (2004), the contact area

between warp yarns decreased due to the covering of transverse yarns, leads to a local reduction in the transferable bond forces. TRC members are vulnerable to transverse tensile stress. Failure usually occurs at the plane of the textile reinforcement [Lorenz (2014)]. It results from the decrease of concrete cross-section due to the coverage area of the textile. Ortlepp (2009) showed an approximately linear relationship between the effective area and the transverse tensile strength of TRC members (refer to equation 6.1). Therefore, for textiles with small effective area factor (high coverage area and small mesh size), the dominant failure within the lap splice zone, anchorage zone is delamination. Figure 7.5 illustrates the typical delamination failures within the lap splice zone of TRC members.

Although ribbed rebars and FRP grids produce compression stress zone at lap splice parts, the textile fabric can not make a significant compression zone. Lap splice length and embedment length of the textile may be longer than those of ribbed rebars and FRP grids.

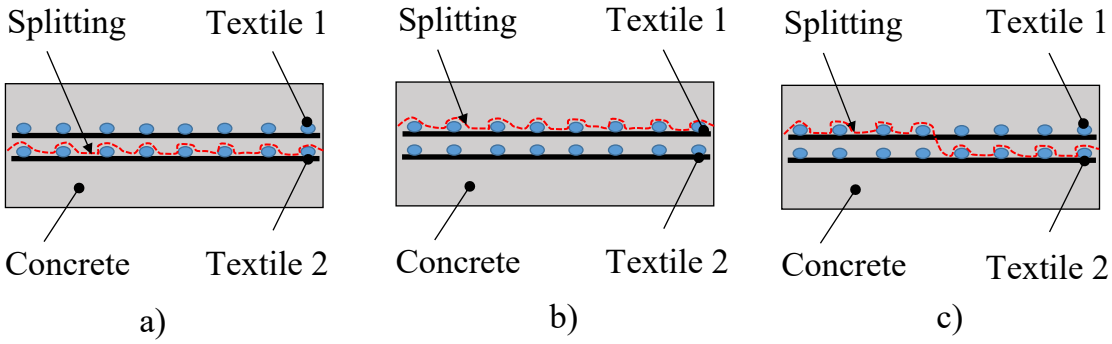

Figure 7.5 – Typical delamination failures within lap splice zone of TRC

a) Splitting within interface layer between two textile fabrics; b) Splitting ouside interface layer; c) Mixed splitting.

The determination of the lap splice lengths governed by the failure in the bond joint and the delamination failure within the lap splice zone. Therefore, the following parameters should be considered:

(1) Bond strength: this parameter directly influences the value of the required lap splice length. If delamination failure is excluded, weaker bond strength requires a greater lap splice length. Even if the delamination forms and propagates, good bond strength can maintain partial composite behavior between textile and mortar, particularly within the lap splice zone.

(2) Tensile strength of mortar: mortar with high tensile strength is capable of eliminating delamination failure, or reduce the extent of delamination area. Therefore, better tensile strength mortars might shorten required lap splice length.

(3) Textile configuration: textile configuration, such as geometry, mesh size, fiber material, etc. strongly influence the determination of lap splice length. However, this study only focuses on the effective area parameter. As mentioned above, delamination resistance is a linear function of an effective area. Hence, the textile fabric needed to attain a suitable effective area by adjusting the mesh size.

7.2. Suggestion for future works

Several points of research related to the structural details of TRC need more studying. In this study, two type of members were examined. More researches are needed to determine the structural details of other members.

- Structural details of TRC members under compression force
- Structural details of TRC members subjected to moment and shear force

In addition, two examined mortar in this research could not exploit the full capacity of textile fabric. Other researches on the combination of textile and high performance mortar are needed.

REFERENCES:

ACI A. 440.3 R-04 Guide Test Methods for Fiber-Reinforced Polymers (FRPs) for Reinforcing or Strengthening Concrete Structures, *American Concrete Institute, Farmington Hills*, USA.

Azzam, A., Richter, M., "Investigation of Stress Transfer Behavior in Textile Reinforced Concrete with Application to Reinforcement Overlapping and Development Lengths", 6th Colloquium on Textile Reinforced Structures (CTRS6), 2011, pp. 103-116.

Banholzer, B., Brockmann, T., and Brameshuber, W., "Material and bonding characteristics for dimensioning and modeling of textile reinforced concrete (TRC) elements", *Materials and Structures*, 39, 2006, pp. 749–763.

Brameshuber, W., "Textile Reinforced Concrete: State of the Art Report*", RILEM TC 201-TRC, RILEM Publications*, Paris, France, 2006.

Brameshuber, W.; Brockmann, T.: Textile Reinforced Concrete (TRC) − Durability aspects of fine grained binder systems, ACI SP-212− In: Durability Concrete. Proceedings of the Sixth International Conference, 2003, pp. 93−111.

Brameshuber, W. (ed.), *International RILEM Conference on Material Science–Second ICTRC–Textile Reinforced Concrete–Theme 1*, Paris, France, 2010.

Bosche, A., Jesse, F., Ortlepp, R., Weiland, S., Curbach, M. 2008. "Textile-reinforced concrete for flexural strengthening of RC-structures-Part 1: structural behavior and design model". In: Aldea C-M, editor. *Design & applications of textile-reinforced concrete, ACI Fall Convention 2007*, pp. 19–40. Fajardo, Puerto Rico.

Brockmann, T.: "Mechanical and Fracture Mechanical Properties of Fine Grained Concrete for Textile Reinforced Composites", Aachen University, Dissertation, 2006.

Butler, M., Hempel, R., and Schorn, H., "Bond behavior of polymer impregnated AR-glass textile reinforcement in concrete", *in ISPIC International Symposium Polymers in Concrete*, University of Minho, Guimaraes, Portugal, 2006, pp. 173–183.

Butler, M.,"Durability of textile reinforced concrete made with AR glass fibre: effect of the matrix composition", *Materials and structures*, Vol. 43, 2010, pp. 1351-1368.

Contamine, R., Si Larbi, A., Hamelin, P.: "Contribution to direct tensile testing of textile reinforced concrete (TRC)", Material Science and Engineering: A, Volume 528, Issues 29-30, 2011, pp.8589-8598.

Curbach, M. and Heeger, J. (eds), *Sachstandbericht zum Einsatz von Textilien im Massivbau (German State of the Art Report for the use of technical textiles in massive structure*, DAfStb, Heft 488, Beuth, Berlin, 1998.

Curbach, M., Ortlepp, R., and Triantafillou, T. C., "TRC for rehabilitation", *Chapter 7, in W. Brameshuber (ed.), Textile Reinforced Concrete: State of the Art Report, RILEM TC 201-TRC, RILEM Publications*, Paris, France, 2006, pp. 221–236.

Donnini, J., Chiappini, G., Lancioni, G., Corialdesi, V.: "Tensile behavior of glass FRCM systems with fabrics' overlap: Experimental results and numerical modelling", Composite structures 212, 2019, pp. 398-411.

Elsanadedy, H.M., Almusallam, T.H., Alsayed, S.H, Al-Salloum, Y.A.: "Flexural strengthening of RC using textile reinforced mortar – Experimental and numerical study". *Composite Structure* Volume 97, 2013, pp.40-55.

Gonzalez-Libreros, J., Sabau, C., Sneed, L.H., Pellegrino, C., Sas, G.: "Shear strengthening of RC beams with FRCM: What do we know so far". In: Teng JG, Dai JG, editors. *Proceedings of 8th international conference on fibre-reinforced (FRP) composites in civil engineering*, Hong Kong, China, 2016, pp.456-461

Hartig, J., Hauslle r-Combe, U., and Schicktanz, K., "Influence of bond properties on the tensile behavior of textile reinforced concrete", *Cement and Concrete Composites*, 30, 2008, pp. 898–906.

Hashemi, S. & Al-Mahaidi, R., "Investigation of bond strength and flexural behaviour of FRP-strengthened reinforced concrete beams using cement-based adhesives", *Aust J Struct Eng* 11(2), 2010, pp.129–39.

Hegger, J., and Voss, S., "Investigations on the bearing behavior and application potential of textile reinforced concrete", *Engineering Structures*, Vol. 30, 2008, pp. 2050-2056.

Jesse, F., and Curbach, M., "Textile reinforced composites— Overview, experimental and theoretical investigations", in V. C. Li, C. K. Y. Leung, K. J. Willam, and S. L. Billington (eds.), Fifth International Conference on Fracture Mechanics of Concrete and Concrete Structures, Ia-FraMCos 204, Vail, CO, 2004, pp. 749-756.

Kang, B. G. and Brameshuber, W.,"Bond behavior of Textile Reinforced Concrete Made of AR-Glass under Glass Cyclic Loading", *Textile Reinforced Concrete-Proceedings of the 1st International RILEM Symposium*, RILEM publications S.A.R.L, 2006, pp. 111-119.

Kong, K., Mesticou, Z., Michel, M., Si Larbi, A., and Junes, A., "Comparative characterization of the durability behaviour of textilereinforced concrete (TRC) under tension and bending", Composite Structures 179, 2017, pp. 107-123.

Krüger, M., "Prestressed textile-reinforced concrete", University of Stuttgart, dissertation, 2004.

Lorenz, E. and Ortlepp, R.,"Basic research on the anchorage of textile reinforcement in cementitious matrix", *Proceedings of the 9th International Symposium on Fiber Reinforced Polymer Reinforcement for Concrete Structure*, Sydney, 2009.

Lorenz, E. and Ortlepp, R.,"Anchoring failure mechanisms of textile reinforced concrete strengthening of RC structures," *Proceedings of the ACI 2010 Fall Convention*, Pittsburgh, 2010.

Lorenz, E., Ortlepp, R., "Investigations to determine the overlap lengths of textile reinforcements made of carbon in textile-reinforced concrete (TRC)", *6th Colloquium on Textile Reinforced Structures (CTRS6)*, 2011, pp. 85-102.

Lorenz, E. and Ortlepp, R.,"Bond Behavior of Textile Reinforcements-Development of a Pull-out Test and Modeling of the Respective Bond versus Slip Relation", *High Performance Fiber Reinforced Cement Composites*, 2012, pp. 479-486.

Mesticou, Z., Bui, L., Junes, A., Si Larbi, A., "Experimental investigation of tensile fatigue behaviour of TextileReinforced Concrete (TRC): Effect of fatigue load and strain rate", *Composite Structures 160*, 2017, pp. 1136-1146.

Ortlepp, R., "The effective area of an adhesive bond of textile reinforced concrete". In CEB-FIP(Hrsg.), JCI(Hrsg.), *Concrete Society (Hrsg.):* Concrete: *21st Century Superhero–Building a Sustainable Future emap Networks–Book of Abstracts and CD-ROM, CEB-FIP*, London, UK, 2009.

Ortlepp, R., Schladitz, F., Curbach, M., "Reinforced concrete columns reinforced with textile concrete", *Concrete and reinforced concrete construction*, 106 (9), 2011, pp. 640–648.

Ortlepp, R., "Efficient Adaptive Test Method for Textile Development Length in TRC", *Advances in Civil Engineering*, 38, 2018, pp. 1-14.

Papanicolaou, C.G., Triantafillou, T.C., Bournas, D.A., Lontou, P.V., "TRM as strengthening and seismic retrofitting material of concrete structures", *In: Proc of 1st international conference on textile reinforced concrete (ICTRC)*, 2006, RWTH Aachen University, Germany, pp. 331-340.

Papanicolaou, C., Triantafillou, T., Papantoniou, I., Balioukos, C., "Strengthening of two-way reinforced concrete slabs with Textile Reinforced Mortars (TRM)". *In: Proc of the 4th colloquium on textile reinforced structures (CTRS4) und zur 1. Anwendertagung*, SFB 528. *Eigenverlag: Technische Universität Dresden*, 2009, pp. 409–420.

Peled, A. and Benter, A.,"Geometrical characteristics and efficiency of textile fabrics for reinforcing cement composite", *Cement and concrete research*, Vol. 30, 2000, pp. 781–790.

Portal, N. W. et al.,"Pull-out of textile reinforcement in concrete*", Construction and Building Materials,* Vol. 71*,* 2014, pp. 63-71.

Raoof, S.M, Koutas, L.N., Bournas, D.A., "Textile-reinforced mortar (TRM) versus fibre-reinforced polymers (FRP) in flexural strengthening of RC beams", *Construction and Building Material,* Volume 15, 2017, pp. 279-291.

Raupach, M., Orlowsky, J., Büttner, T., Dilthey, U., Schleserm, M. "Epoxy-impregnated Textiles in Concrete – Load Bearing Capacity and Durability", *ICTRC*, 2006, pp. 77–88.

Schütze, N.; Lorenz, E. and Curbach, M.,"Test method for textile reinforced concrete", *11th International Symposium on Ferrocement and 3rd ICTRC International Conference On Textile Reinforced Concrete,* 2015, pp. 307-318.

Toutanji, H., Zhao, L., Zhang, Y., "Flexural behavior of reinforced concrete beams externally strengthened with CFRP sheets bonded with an inorganic matrix", *Eng Struct*, Volume 28, issue 4, 2006, pp. 557–566.

Verbruggen, S., Tysmans, T., Wastiels, J., "TRC or CFRP strengthening for reinforced concrete beams: An experimental study of the cracking behavior", *Engineering Structure,* Volume 77, 2014, pp.49-56.

Vogel, F.,"Production and use of the Textile Reinforced Concrete", *Advanced Materials Research*, Vol. 982, 2014, pp. 59-62.

Weiland, S., Ortlepp, R., Brückner, A., and Curbach, M., "Strengthening of RC structures with textile reinforced concrete (TRC)", *in C. M. Aldea (ed.), ACI Spring 2005 Convention New York on Thin Fiber and Textile Reinforced Cementitious Systems*, SP-244-10, 2007, pp. 157–172.

Weiland, S., Ortlepp, R., Hauptenbuchner, B., and Curbach, M., "Textile reinforced concrete for flexural strengthening of RC-structures—Part 2: Application on a concrete shell", *ACI SP, Design & Applications of Textile-Reinforced Concrete*, 251(3), 41–58, 2008.

Xu, Y. & Ke-Quan, Y., "Flexural strengthening of RC beams with CFRP grid-reinforced ECC matrix", *Composite Structure* Volume 189, 2018, pp. 9-26.

Zastrau, B., Richter, M., and Lepenies, I., "On the analytical solution of pullout phenomena in textile reinforced concrete", *Journal of Engineering Materials and Technology*, Volume 125, 2003, pp. 38–43.